7-2020

Investigation of the Role of Heparin-binding Pocket in Amyloid Fibrils Formation of FGF-1

I Gusti Ayu Agung Septiari
University of Arkansas, Fayetteville

Investigation of the Role
of Heparin-binding Pocket in Amyloid Fibrils Formation of FGF-1

A thesis submitted in partial fulfillment
of the requirements for the degree of
Master of Science in Cell and Molecular Biology

by

I Gusti Ayu Agung Septiari
Universitas Udayana, Indonesia
Bachelor of Science in Pharmacy, 2014

July 2020
University of Arkansas

This thesis is approved for recommendation to the Graduate Council.

_____
Suresh Kumar Thallapuranam, Ph.D.
Thesis Chair

_____
Navam S. Hettiarachchy, Ph.D.
Committee Member

_____
Mahmoud Moradi, Ph.D.
Committee Member

_____
Paul Adams, Ph.D.
Committee Member

ABSTRACT

Human acidic fibroblast growth factor (aFGF/hFGF-1) is one of the promising molecules to be investigated to generate an in-depth understanding of the pathological mechanism of Alzheimer's disease (AD) neurodegenerative disorder characterized by the presence of amyloid fibrils. Some *in vivo* and human brain tissue studies proved the correlation of high-level expression of FGF-1-induced neuroinflammation and the occurrence of AD. The presence of amyloid fibrils as a hallmark of AD can be related to the generic property of the proteins to form amyloid fibrils; High level of FGF-1, in this case, may contribute to the formation of amyloid fibrils. As a heparin-binding protein, hFGF-1 requires heparin to bind in the heparin-binding pocket to provide protection from proteolysis and heat inactivation and potentiate the mitogenic activity of FGF-1. Due to the importance of heparin-binding pocket to the native structural stability of the FGF-1, we hypothesized that destabilization of heparin-binding pocket might facilitate amyloid fibrils formation in FGF-1.

We carried out in vitro studies by using sodium dodecyl sulfate (SDS) as an amyloid fibril inducer and sucrose octasulfate (SOS) to mimic the activity of heparin to prove our hypothesis. Our study can be a preliminary step to understand the significant role of heparin-binding pocket in amyloid fibrils formation and explore its potential as a druggable site in search of the cure of AD. Fluorescence spectroscopy, limited trypsin digestion, transmission electron microscopy, and mass spectrometry were performed to achieve the objective of this research project. The results of this study suggest that 0.2mM is the optimum concentration of SDS to induce amyloid-like fibrils formation in hFGF-1 (wild-type FGF-1). The presence of SOS is found to protect hFGF-1 from fibrillation induced by SDS, reduce, and disaggregate fibrils

formation in hFGF-1. Stabilization of the heparin-binding pocket renders the ability of hFGF-1 to protect and reduce the chance of amyloid fibrils formation.

Keywords: Alzheimer's disease, amyloid-fibrils, FGF-1, sodium dodecyl sulfate (SDS), sucrose octa sulfate (SOS), heparin-binding pocket.

ACKNOWLEDGEMENTS

I would like to thank Dr. T.K.S. Kumar for his supervision, guidance, and patience. Thank you so much for the knowledge and encouragements. I treasure all of these. Thank you so much for the help, guidance, and friendship to Zeina Al Raawi. Thank you for Dr. Sanhita Maity, Patience, Dr. Ravi Kumar Gundampati, Shilpi Agrawal, and Musaab Al-Ameer for being excellent mentors during my time in the Kumar Lab. I would also like to extend my thanks to the rest of the members of Kumar's group for their support and encouragement.

Moreover, I would like to thank Dr. Douglas Rhoads and CEMB program for helping me to finish my thesis. Thank you for Gloria Ann Passmore, who gave her support during my study. My friends Mrs. Connie Satzler in Kansas, Mrs. Elizabeth C. English, and Mrs. Diane Ungar, Mbak Keukeu, and family who always provide their support during my study. I would also like to thank my Fulbright friends Gema, Tika, Ami, Dodi, Harumi, Meutia, PJ, Sergio, Ametepe, Ai-Ling, Sarah, and Rian for the friendship, support, and good times. Thank you for my parents, who always pray and support me during my stay in the US.

TABLE OF CONTENTS

LIST OF FIGURES

LIST OF TABLES

CHAPTER 1

INTRODUCTION

Accumulation of aggregated intracellular and extracellular protein is a major pathological hallmark of neurodegeneration associated with misfolded proteins such as Alzheimer's disease (AD), Parkinson's disease (PD), and Huntington's disease (HD)[1, 2]. The prevalence of these highly debilitating diseases fuels extensive research in the field of protein aggregation as a part of the relentless pursuit of the cure of the diseases.

Regarding its structural features, there are two different types of protein aggregates: amyloid fibrils and amorphous aggregates. Amorphous aggregates comprise mostly disordered polypeptide chains, despite its molecular assembly containing high content of β-sheet structure in particular regions. Amyloid fibrils are highly ordered and repetitive structures that share common features, such as canonical cross-β structure and the frequent presence of repetitive hydrophobic or polar interactions along the fibrillar axis. All polypeptides, regardless of its sequence, display the similar fold and share common morphologies (long, unbranched, and often twisted structures a few nanometres in diameter)[1-3].

It is suggested that polypeptide chains' capability to adopt amyloid-like conformations is a fundamental feature of polypeptide chains; however, the tendency of the structure formation cis significantly varied with the sequence. The reaction rate of the amyloid fibrillogenesis is concentration-dependent and can increase by the addition of homologous pre-aggregated polypeptides that perform as seeds/templates[1-3].

One of the notorious diseases inflicting the aging population associated with the amyloid fibrils (amyloid-β) is Alzheimer's disease. Alzheimer's disease is related to the alteration of the brain biochemical environment, accumulation of both protein fragment amyloid-β (Aβ) outside

neurons, and an abnormal form of the protein tau (tau tangles) inside neurons, are two of several brain changes related to Alzheimer's disease. There are 5.8 million people in the United States who have Alzheimer's disease. This number is predicted to increase to almost fourteen million by 2050. The national economic burden in 2019 because of Alzheimer's and other dementia is two hundred ninety billion dollars. These costs could increase in the future (2019 Alzheimer's Disease Facts and Figures, 2019). In the past twenty years, most of the drugs under trial, e.g., Crenezumab, Gantenerumab, Solanezumab, and Bapineuzumab) for AD have focused on tackling Aβ peptide accumulation; the majority of Alzheimer's drugs development based on the concept of debatable amyloid cascade hypothesis.

Nevertheless, most of the drugs could not produce clinically beneficial results [4]. Surprisingly, Aducanumab, the drug that is decreasing the size of amyloid-β plaque [4] and its phase III trial was halted in March 2019 made its reversal in October 2019. It shows that amyloid-β is still a relevant drug target. More research devoted to unraveling the molecular mechanism of AD should pursue to aid acceleration in the field of Alzheimer's drug development.

Human acidic fibroblast growth factor (aFGF-1 or FGF-1) is one of the promising molecules to be explored to gain an in-depth understanding of Alzheimer's disease. This growth factor originates from neural tissue, where it is found to be highly concentrated. The proliferation and differentiation of various cell types in vitro are affected by FGF-1. FGF-1 activates the neuron survival mechanism. It is delivered from the ependymal cells of the cerebral third ventricle into the cerebrospinal fluid (CSF)[5, 6]. FGF-1 is a heparin-binding protein; heparin renders protection from proteolysis (trypsin digestion) and heat inactivation and potentiates the

mitogenic activity of FGF-1[7]. Under oxidizing conditions, binding to heparin increases FGF stability[8].

Some previous studies link the presence of a high level of FGF-1 and the occurrence of Alzheimer's disease[5, 6, 9, 10]. FGF-1 may play a significant role in AD not only because of its potency in mediating neuroinflammation but also the property of FGF-1 as polypeptide chains to form amyloid-like conformations that the concentration of the protein itself can influence its reaction rate. In addition to that, human FGF-1 tends to unfold at physiological temperature in the absence of sugar poly anions[11, 12].

Therefore, exploring the role of destabilization of heparin-binding pocket in amyloid fibrils formation can lead to an understanding of the mechanism of amyloid fibrils formation in FGF-1. Subsequently, we can also obtain more in-depth knowledge of the role of heparin-binding pocket in protein aggregation, especially for the heparin-binding protein family. Presumably, it also provides a novel drug target to prevent protein aggregation that can aid future research in exploring a new avenue of Alzheimer's drug development.

1. Protein Folding, Misfolding, and Aggregation

Endoplasmic reticulum (ER) is an organelle that is specialized for protein folding[13]. In this compartment, proper protein folding of a newly synthesized polypeptide is achieved through the interaction with the molecular chaperones and folding enzymes (such as protein disulfide isomerase and prolyl peptidyl cis-trans isomerases)[13]. Molecular chaperones are proteins that assist other proteins in accomplishing their native active conformation but are not part of the final protein structure[14]. ER contains two major chaperones system: the classical chaperones (such as Hsp70 and Hsp90 families) and the carbohydrate-binding chaperone system (lectin chaperones)[13]. Protein disulfide isomerase (PDI) is the most abundant foldase and best-characterized oxidoreductase in

ER[15]. Oxidoreductase plays a critical role in achieving a decent rate of protein folding, otherwise ample aggregation and degradation will occur[13]. Prolyl peptidyl cis-trans isomerases (PPIases) is a folding enzyme that catalyzes the isomerization between the cis and trans forms of peptide bonds[13].

Trafficking of the protein from the ER and its degradation via endoplasmic reticulum-associated degradation (ERAD) is closely related to the folding of the protein in the ER[16]. The faith of the protein after the entry to the ER is the formation of folding intermediates[16]. Some of these folding intermediates fold properly, and others are targeted for degradation[16]. The proteins that fold correctly will exit the ER[16]. Whereas, the intermediates that do not fold correctly will be hampered from secretion by their aggregation or interaction with ER folding factors, or by a combination of the two[16].

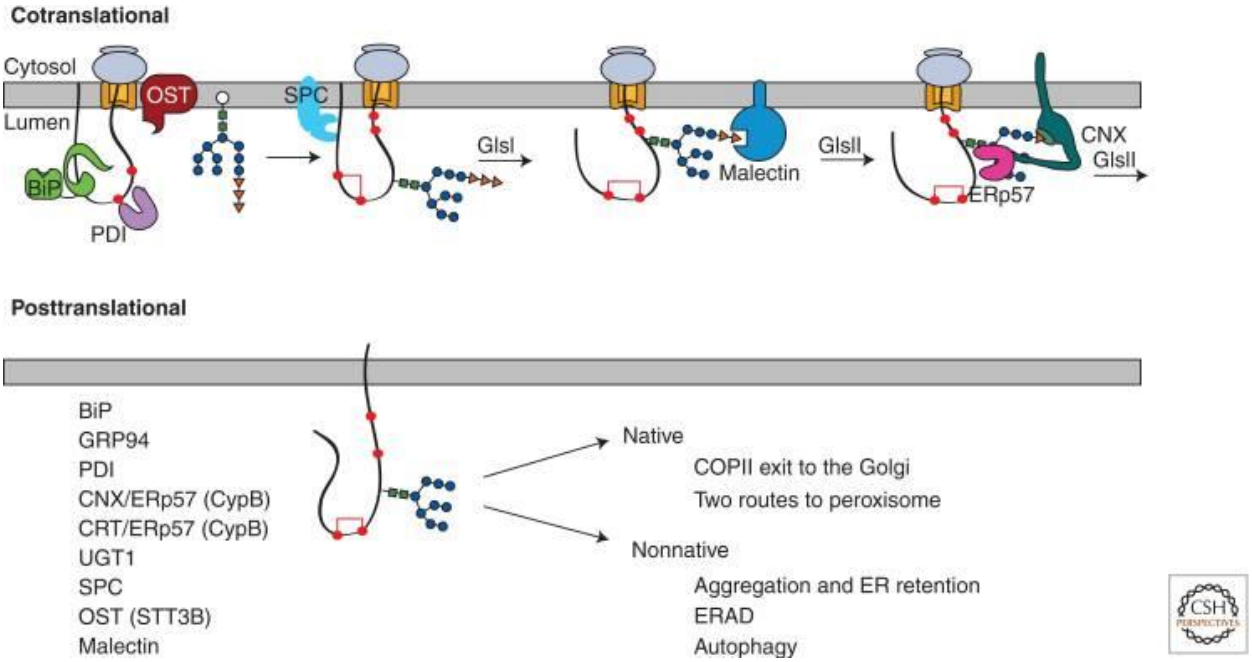

Figure 1 Co- and post-translational protein folding in the lumen of the Endoplasmic Reticulum

Top panel, the ribosome (grey), sits on the Sec61 translocon (orange) to support cotranslational translocation of the nascent chain into the ER lumen. The oligosaccharyltransferase (OST) attaches preassembled glycans (tree structure) to Asn on the nascent chain. BiP (green) and PDI (purple) are positioned for early assistance. Disulfide bonds start to form. The signal sequence peptidase complex (SPC, light blue) cleaves the amino-terminal signal sequence. Glucosidase I (GIsI) removes the terminal glucose residue (orange triangle) from the N-linked glycan. The diglucosylated glycan can bind to the membrane-associated lectin, malectin (dark blue). Glucosidase II (GIsII) removes second glucose to generate a monoglucosylated glycan structure that is bound to calnexin (CNX, green), a lectin chaperone associated with the oxidoreductase ERp57 (pink). Lectin chaperone binding continues until GIsII removes the final glucose residue[13].

Bottom panel, the listed factors interact co- and posttranslationally, after the nascent chain's translation has been completed. These factors help with maturation and the sorting of the native or nonnative protein for its various fates[13].

2. Alzheimer's Disease

Amyloid β peptide (Aβ) and tau protein have an important role in the occurrence of Alzheimer's disease (AD). Two different features marked the brains of AD patients: (1) formation of the extracellular amyloid plaques from the amyloid plaques formed by the proteolytic product (Aβ) of the amyloid precursor protein (APP), a cell surface receptor processed by β-secretase **(**β-amyloid cleavage enzyme, BACE1) and γ-secretase; (2) formation of neurofibrillary tangles

(NFTs) by hyperphosphorylated forms of the neuronal microtubule-associated protein tau [17]. Even though neuronal toxicity in AD is correlated to Aβ and tau; it remains vague which molecular interplay occurs between these two proteins[1].

α-secretase process APP in a healthy brain via non-amyloidogenic pathway, resulting in a secreted fragment and a C-terminal part, which is subsequently cleaved by γ-secretase into smaller peptides. The cell will remove these smaller peptides eventually. Meanwhile, in the amyloidogenic pathway, APP cleavage is processed by β-secretase, and afterward, γ-secretase action will produce Aβ peptide[17].

Metal ions play roles in AD, and it showed by the evidence that APP processing can be shifted towards the amyloid pathway in the presence of metal ions. It is also found that a high concentration of trace metals exists in amyloid plaques. α-secretase activity is affected by Zn^{2+} and $Fe^{2+/3+}$, while β-secretase activity is influenced by the Cu^{2+} [18]. Aβ is found to be phosphorylated in vivo that is linked to the increase in toxicity. Therefore, trace metals, Fe presumably a pivotal player in the Aβ aggregation pathway because the phosphate group considerably increases the peptide ability to bind Fe[1, 19]. This finding supports other evidence that showed Fe impedes the turnover of toxic oligomeric Aβ metastable species into ordered fibrils[20]. Furthermore, it is known that binding of Aβ to oxidized forms of Fe or Zn^{2+} generates hydrogen peroxide that could involve in the general toxicity initiated by APP misprocessing[21]. In healthy conditions, Aβ is localized in the interstitial fluid of the brain, but AD amyloid plaques are found in particular brain areas, which turn out to be the most compromised/affected by the disease [1].

3. The structure of amyloid fibrils

The modern biophysical definition of amyloid fibrils is an unbranched protein fiber whose repeating substructure contains β strands that run perpendicular to the fiber axis, creating a cross-

β sheet of indeterminate/indefinite length. Therefore, an ordered arrangement of many (usually thousands) copies of a peptide or protein is constituent of amyloids[22]. Electron microscopy (EM) analysis shows that amyloids exhibit long, nonbranched filaments with diameters 6-12 nm[22]. Characteristic of X-ray fiber diffraction patterns is found in amyloid structure due to the repeating cross-β sheet motif[22]. Frequently, fibrils contain multiple protofilaments twisted around the fibril axis [1, 2].

X-ray fiber diffraction revealed that amyloid fibrils generate extended β-sheets stabilized fundamentally by intermolecular hydrogen bonds entailing mainly back-bone atoms running parallel to the axis of the fibril in a structure defined as cross-β[23]. Moreover, it found that one face of these extended β-sheets contains exposure to water. In contrast, the other one is tightly packed against another such β-sheet with a dry interface stabilized by van der Waals and hydrophobic interactions between interdigitated side chains [23].

In contrast with the conventional protein structures, amyloid fibrils exhibit the polymorphic characteristic. Determined by the environmental condition of the incubation of the monomeric protein, such as ionic strength, pH, temperature, concentration, type, and degree of stirring of the aggregating solution, different amyloid morphologies can be generated. This property of amyloid fibrils implies that the dependent factor of the structural features of the fibrils formed by a particular protein can be related to the milieu where amyloid formation takes place[23].

4. Molecular mechanisms of fibril formation

Amyloidogenesis is a biochemical process that converts a soluble and innocuous/native protein into insoluble and fibrillar protein aggregates, called amyloid fibrils [24]. It is suggested that the capability of polypeptide chains to adopt amyloid-like conformations is a fundamental feature of polypeptide chains; however, the tendency of the structure formation is significantly varied with

the sequence. The reaction rate of the amyloid fibrillogenesis is concentration-dependent and can increase by the addition of homologous pre-aggregated polypeptides that perform as seeds/templates[1-3].

The dependent factor of the reaction rate of the amyloid fibrillogenesis is the protein concentration. This process can be hastened by the incorporation of homologous pre-aggregated polypeptides, acting as seeds/templates. Interaction between the monomers — acting as 'active' growing unit — and the templates will promote the monomers' structural transformation to the amyloidogenic conformation. There are two models of amyloid fibrillogenesis: nucleation-elongation polymerization and double-concerted fibrillation[1, 2, 24, 25]. Based on the nucleation-elongation polymerization model, there are three main steps of amyloid fibril formation/aggregation[1]:

1. The lag phase is a thermodynamically unfavorable reaction of nuclei formation. It occurs through the association of soluble species (usually monomers) where prolonged incubation of the amyloidogenic proteins is necessary. Overall, the kinetics of the amyloid reaction is affected by the formation of the nuclei (rate-determining step). The lag phase involves transformation steps from the soluble, native structure of the protein to the generation of the first species exhibiting β-sheet conformation, subsequently forming nucleus as a template. Pre-existing aggregates can act as a catalyst of the nucleation step. The initiation of globular protein aggregation requires the thermodynamic destabilization of the native monomer. In protein exhibiting a quarternary native structure, the functional oligomer dissociation into monomeric subunits is required[1].
2. Exponential phase, monomeric proteins coalesce to the template through conformational transition, immediately after the nucleus (seed) is formed. Conformational transition cause

polymerization and fibril growth in this stage. There are some different mechanism responsible for the increase in structural order found at this stage: initially ordered β-sheet oligomers cause the direct growth of fibrils, before fibril formation and elongation, the transformation of these oligomers into β-sheet enriched non-fibrillar assemblies occur or formation of large amorphous aggregates from initially disordered oligomers and subsequent structural reorganization, first to nonfibrillar β-sheet rich assemblies and eventually to fibrils[1].

3. The stationary phase (under supersaturated condition) is a condition in which no more association of soluble species to the ends of preformed fibrils. Furthermore, it includes deceleration of the growth phase lead to the saturation phase and eventually fibril maturation[1].

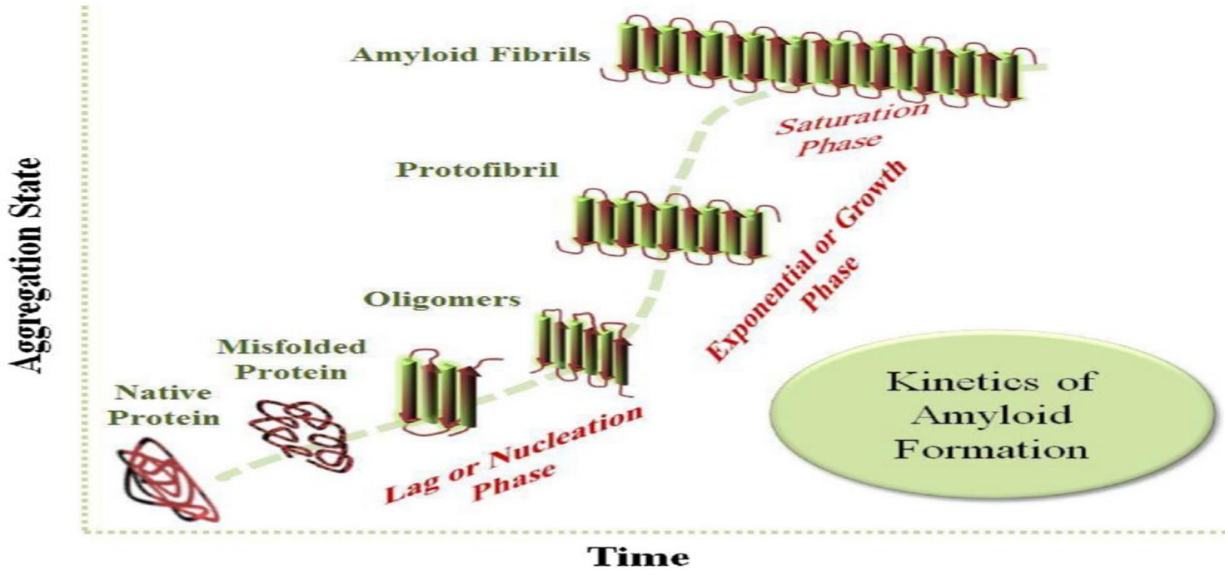

Figure 2 **Cartoon depiction of the kinetics of amyloid formation[26]**
A partial destabilization of the native state is required in amyloidogenesis. The formation of amyloid fibril is a nucleation dependent manner. It consists of three steps: lag or nucleation phase, elongation or exponential phase, and stationary phase or saturation phase[26]

Regarding the double-concerted fibrillation model, two consecutive, concerted associations of monomers are required to form amyloid fibrils. Associations of the monomers will subsequently generate oligomeric granular species that perform its function as a growing unit for the fibril formation, in the absence of template[24]. The major driving force for the supra structures formation is structural rearrangement within the oligomeric species. The final fibril is generated through the interactions switch from intra-oligomeric to inter-oligomeric interactions since the oligomers already consisted of interactive regions between constituting monomers [24].

5. Inhibitors of Amyloid Fibril formation

There are four class of well-documented amyloid fibril inhibitors (drugs and nutraceuticals) used in the status quo or under investigation: anthracyclines and tetracyclines, sterols, peptide and engineered antibodies, polyphenols, and nanoparticles[27].

a) Anthracyclines and tetracyclines

4'-iodo-4' deoxydoxorubicin (IDOX), the anthracyclines anticancer drug is found to generate clinical benefits in five patients who suffered from immunoglobulin light-chain amyloidosis by inhibiting the progression of amyloidosis[28]. Moreover, in vitro studies showed that IDOX was able to strongly bind to five natural amyloid fibrils but native amyloid precursor[28]. However, the cardiotoxicity effect of IDOX requires a structurally similar agent with a better toxicological profile[28]. The similarity of the structure between the polycyclic conjugated structure of tetracyclines (TCs) and the aglycone moiety of IDOX combined with the clinical benefits and well-characterized pharmacological, pharmacokinetic, and toxicological profile made it a proper candidate to replace IDOX[28]. A positive result of TCs' fibrillogenesis inhibitory effect on human prion protein (PrP), human amylin (IAPP), huntingtin, W7FW14F, apomyoglobin, poly-(A) binding protein nuclear 1, α-synuclein, β2M, and immunoglobulin light chain (LC) was obtained

from the in vitro and in vivo studies[28]. To date, no clear data is available to explain the relationship between the structures of TCs and their anti-amyloidogenic activity[28]. Information derived from molecular mechanics investigation demonstrated that the observed activity on TCs was linked to the flexibility between the extended and folded conformations of TCs[28].

b) Sterols

Sterols such as squalamine and its derivative, trodusquemine show the ability to prevent the aggregation of the protein α-syn[29, 30]. Protein α-syn can form deposits known as Lewy bodies, a hallmark of Parkinson's disease (PD)[29]. Both squalamine and trodusquemine can displace α-syn monomers from the membranes required for the aggregation of the α-syn[29, 30]. Furthermore, trodusquemine also shows an inhibitory effect on the secondary nucleation of aggregation through direct interaction with α-syn[27, 29, 30].

Small peptides, also known as β-breakers are soluble short sequence portions of amyloidogenic proteins. Administration of β-breakers prevents the formation of protein aggregation or promoting the disaggregation of existing fibrils. A positive result was gained from an in vitro study regarding the effect of small peptides on Aβ. Despite some drawbacks of the small peptides such as poor stability, susceptibility to proteolytic degradation, and short half-life, attempts have been made to overcome these challenges through chemical modification such as N-methylation and cyclization [31-35].

c) Peptides and Engineered Antibodies

To date, a recombinant human IgG1 antibody, Aducanumab, showed the most favorable result in which it showed the decline of brain amyloid burden coupled with a positive effect on cognition and global clinical status, with dose-dependent trends[4]. Aducanumab binds to soluble Aβ aggregates and insoluble fibrils with more than 10,000-fold selectivity over monomers[4].

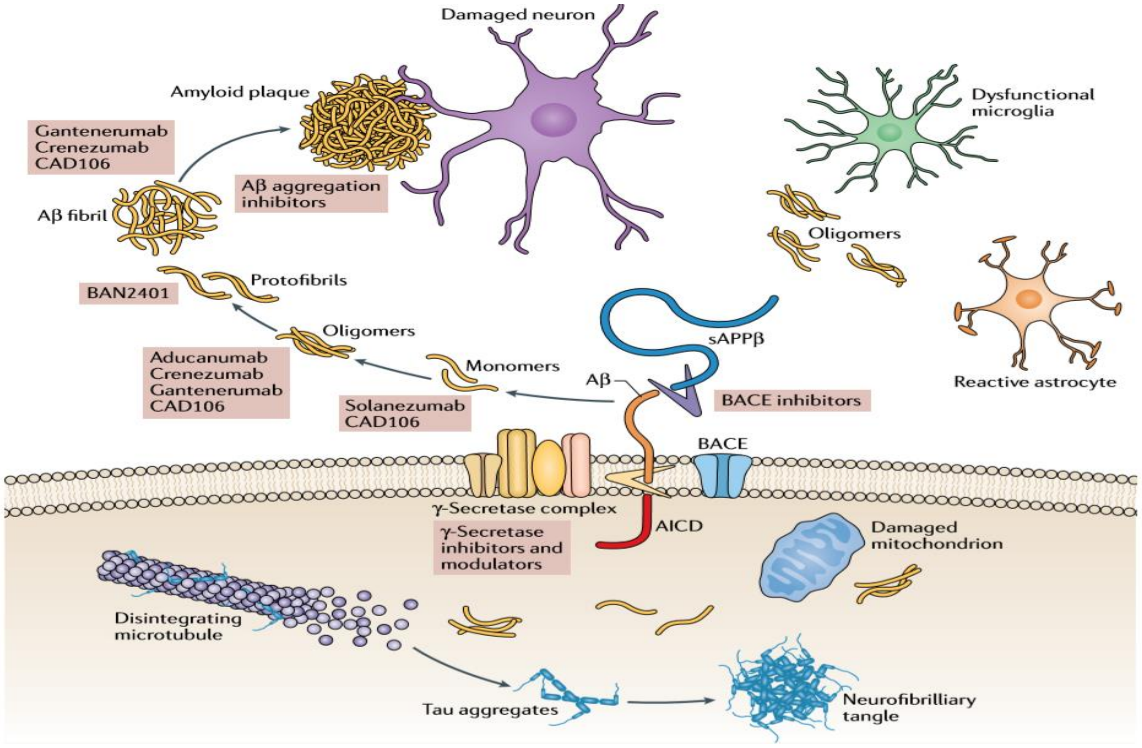

Figure 3 Cellular targets for anti-Aβ drugs
Anti-amyloid-β (Aβ) drugs in phase III clinical development for the treatment of Alzheimer's disease and their mechanisms of action. AICD, amyloid precursor protein intracellular domain; BACE, β-secretase; sAPPβ, soluble amyloid precursor protein-β[4].

d) Polyphenols

Polyphenols are well-known for the antioxidant property. Moreover, they also render the inhibitory effect of amyloid aggregation[27]. Epigallocatechin-gallate (EGCG), the major catechin found in the leaves of green tea, demonstrates its activity to inhibit the formation of aggregates from several potentially amyloidogenic proteins or peptides, such as Aβ, α-syn[36], IAPP[37], huntingtin[38], ATX3[39]. EGCG form interaction with both monomeric protein and oligomeric aggregates. EGCG mechanism of action is affected by the difference in protein target[38, 40]. Generally, EGCG can redirect the aggregation towards off-pathway, non-toxic, β-sheet-poor aggregates, and/or remodeling the aggregates after their formation[38, 40]. Polyphenols commonly found in grapes, berries, red wine, resveratrol demonstrates a well-characterized effect on Aβ

amyloid aggregation[27, 41]. It can retard fibril formation and disaggregate preformed fibrils but not inhibiting oligomer formation[27]. Curcumin exhibits its capability to prevent oligomerization in Aβ and tau[27, 42, 43], redirect the aggregation towards non-toxic oligomers (Aβ and α-syn)[27, 44, 45], and disaggregate preformed fibrils (Aβ, tau, and α-syn)[27, 42, 43, 45]. Oleuropein — the main phenolic compound of olive oil — possesses the capability to inhibit the formation of toxic amyloid aggregates[27]. Predominantly, it can redirect the aggregation towards non-toxic, off- pathways. Moreover, oleuropein also thwarts protein binding to the plasma membrane[27].

e) Nanoparticles

Nanoparticles exhibit potency to inhibit amyloid aggregation[27]. According to their composition, nanoparticles possess a particular degree of specificity towards amyloid deposit[27]. For example, polytrehalose nanoparticles demonstrate their potential to inhibit the aggregation of poly-Q proteins[46]. Gold nanoparticles effectively inhibit aggregation of insulin[47], and Aβ[48] and silver and iron oxide nanoparticles can hinder the aggregation of amylin[49]. Furthermore, their ability to cross the blood-brain barrier at low concentration is a benefit of nanoparticles as an inhibitor of amyloid aggregation[27].

6. Fibroblast Growth Factors Family

Growth factors play an important role in regulating cellular functions, including adhesion, proliferation, migration, and differentiation in the epithelium, bone, and soft connective tissue[50]. A wide array of biological functions such as cellular proliferation, survival, migration, and differentiation are modulated by fibroblast growth factors (FGFs) that signal through FGF receptors (FGFRs)[50]. There are 23 members of the FGF family with only 18 FGFR ligands; four family members are FGF homologous factors (FGF-11, FGF-12, FGF-13, and FGF-14), which do not bind with FGFR[51]. Phylogenetic analysis reveals that there are seven subfamilies of the human

FGF gene family: FGF-1, FGF4, FGF7, FGF8, FGF9, FGF-11, and FGF-19 (Figure 4)[52]. FGF-1 and 2; FGF4, 5, and 6; FGF 3, 7, 10, and 22; FGF8, 17, and 18; FGF9, 16, and 20; FGF-11, 12, 13, and 14; and FGF-19, 21, and 23 are clustered as the FGF-1, FGF4, FGF7, FGF8, FGF9, FGF-11, and FGF-19 subfamily, respectively[52]. In vertebrates, the variation of the molecular weight of FGFs is found from 17-34kDa, while the FGF in Drosophila is 84kDa[53]. Sequence identity of 16%-65% is shown by all members of the family that share a conserved sequence of 120 amino acids[53]. Acidic fibroblast growth factor (aFGF/FGF-1) and basic fibroblast growth factor (bFGF/FGF-2) are the two best-characterized members of the FGFs family[54]. FGF-1 and FGF-2 show 55% sequence identity with a different isoelectric point, 5-6 and 9.6, respectively[54]. Moreover, the two FGFs can be distinguished by the necessity of FGF-1 to bind heparin to stimulate its mitogenic activity, unlike FGF-2 that does not require binding to heparin[54].

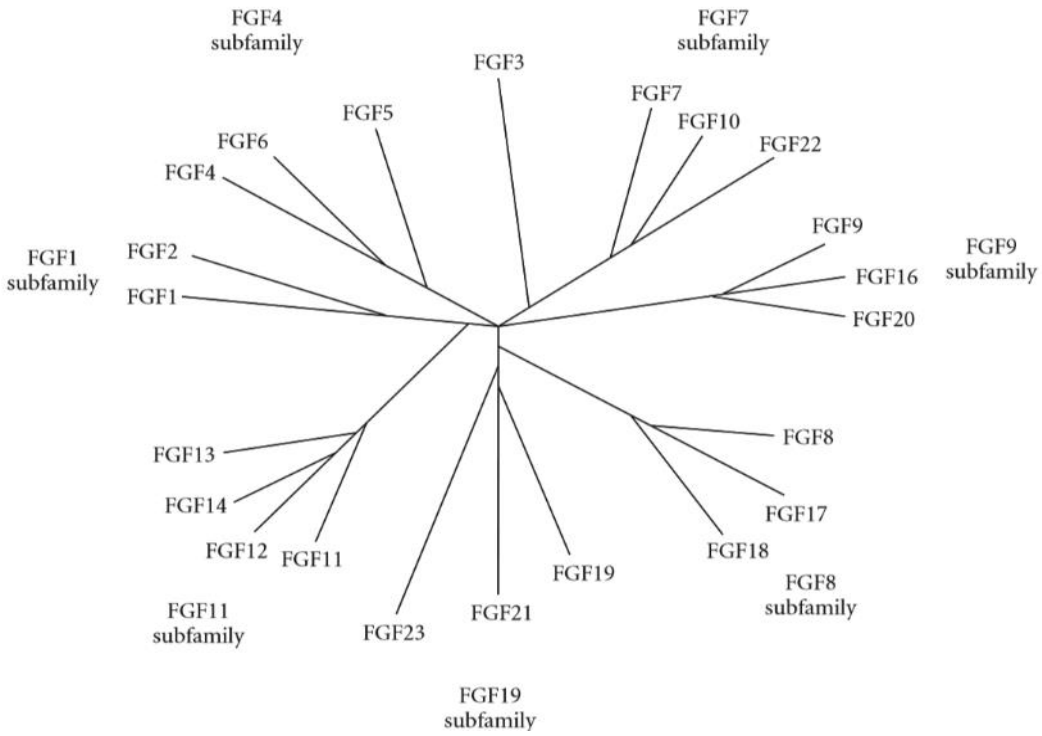

Figure 4 Phylogenetic tree of human FGF family[52]
The Human FGF gene family consists of seven subfamilies containing two until four members for each subfamily. The lengths of the branch are proportional to the evolutionary distance between each gene[50]

.

7. Fibroblast Growth Factors Signaling Pathway

The pathway of FGFs metabolism is mediated by the association of FGFs with a specific tyrosine kinase receptor (FGFR) and heparin sulfate proteoglycans (HSPG) to assemble a ternary complex on the cell surface. Ligand binding causes FGFRs to undergo a dimerization process that causes tyrosine autophosphorylation[55]. These phosphorylated tyrosines perform their function as high-affinity binding sites for proteins containing Src-homology 2 (SH2) domains or phosphotyrosine binding (PTB)[55]. Binding of these intracellular proteins and phosphorylated tyrosines initiates several signaling pathways (e.g., RAS/MAP Kinase pathway, PI3 Kinase/AKT pathway, and PLCγ pathway) that leads to specific cellular responses[50, 55]. The membrane-associated docking protein, fibroblast growth factor receptor substrate 2 (FRS2) binds to the FGFR

juxtamembrane domain through its PTB domain and undergoes phosphorylation by the receptor[55]. A variety of adaptor proteins — growth factor receptor-bound protein 2 (Grb2), the guanine nucleotide exchange factor Son of sevenless (Sos) — are recruited by the FRS2[55]. G-protein Ras is then activated by the recruitment of these adaptor proteins, which leads to the stimulation of the mitogen-activated protein kinase (MAPK) pathway[55]. The MAPK pathway outcomes are DNA synthesis, proliferation, and/or differentiation that vary depending on the cell type or state. FRS2 signaling complex also causes activation of PI3 (phosphoinositide 3) kinase/AKT pathway, which leads to cell survival (Figure 3)[55]. FGF-1 exhibits a unique feature among the FGF family through its ability to stimulate all FGFRs. As a result, FGF-1 is a broad specificity human mitogen that is designated/entitled as "universal FGFR ligand." Plasticity in the N terminus region plays an essential role in its broad specificity[56-58].

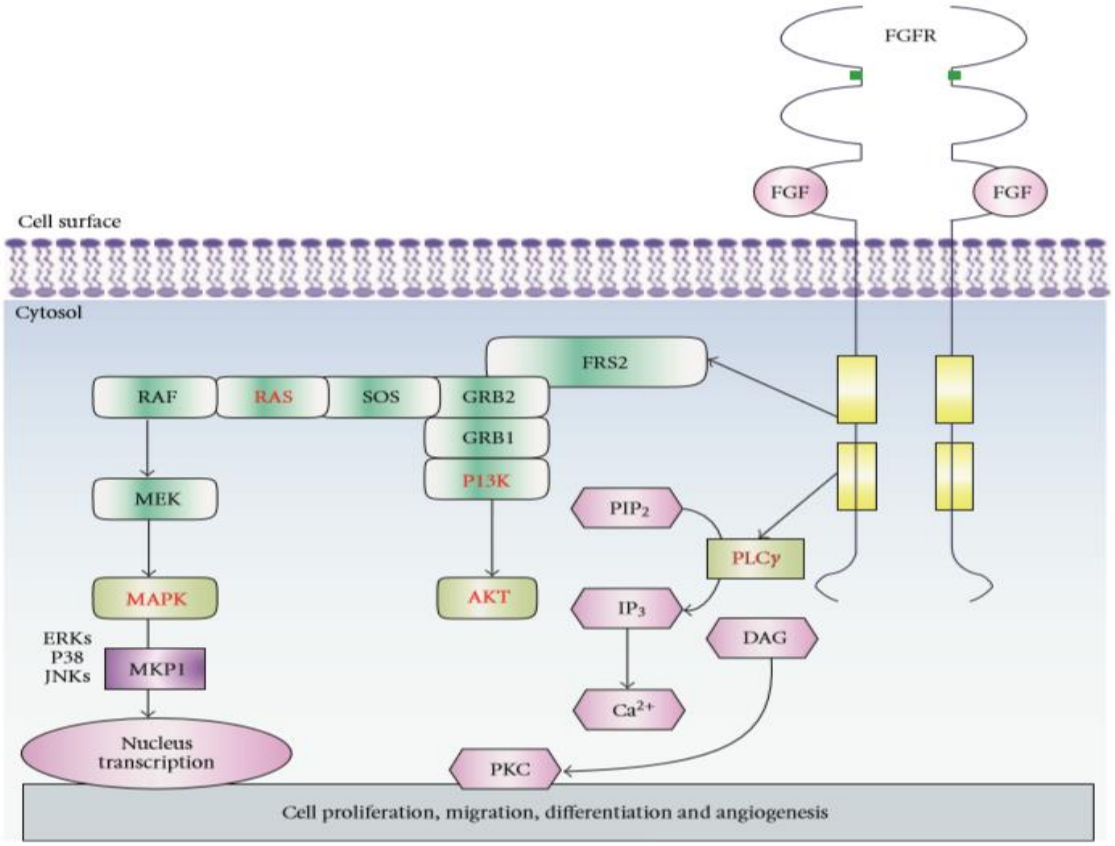

Figure 5 FGFs signaling pathway[50]
FGFs promote the stimulation of tyrosine phosphorylation of the docking protein FRS. This process is followed by the formation of GRB2-SHP2-GAB-1 complex resulting in activation of RAS-MAP kinase pathway and PI3 kinase/AKT pathway. In another pathway, PLCγ pathway, phosphatidylinositol is hydrolyzed by the activated PLCγ, generating IP3 and DAG and results in PKC activation. FRS2: fibroblast growth factor receptor substrate 2, GRB: guanine nucleotide exchange factor, SOS: son of sevenless, RAS: monomeric G-protein, RAF: kinase, MEK: kinase, MKP1: MAP kinase phosphatase, PIP2: phosphatidylinositol (4,5)-biphosphate, IP3: inositol triphosphate, DAG: diacylglycerol, PKC: protein kinase C[50]

8. Structure of the human fibroblast growth factor

FGF-1 is identified by the pseudo-threefold rotational symmetry as a member of the β-trefoil family of proteins[59, 60]. The overall structure of FGF-1 contains three repeating "trefoil-fold" structural motifs[61]. Each motif is around 42 amino acids (with some variation in length between the three motifs)[61]. Each motif comprises four β-strands: two β-strands of each motif involve in

the overall six-stranded β-barrel architecture, and two β-strands of each motif contain a β-hairpin[61]. The three β-hairpins create a triangular arrangement that packs against the bottom of the β-barrel[61]. The x-ray crystal structure of human FGF-1/hFGF-1 (the mature 140 amino acid form) with 2.0 Å resolution (PDB ID: 2AFG) has been established (Figure 6)[12]. The general arrangement of the primary and secondary structure is displayed in Figure 5[61]. The predominant native structure of FGF-1 is β-sheet that contains eight tyrosine, one tryptophan, and three cysteine residues[61]. Unlike other extracellular proteins that contain cysteine residues forming disulfide bonds; Only free cysteine residues are found in FGF-1[61]. Furthermore, in native FGF-1, seven of eight tyrosine residues are exposed to the solvent, whereas the single tryptophan shows a partial solvent accessibility[59-61].

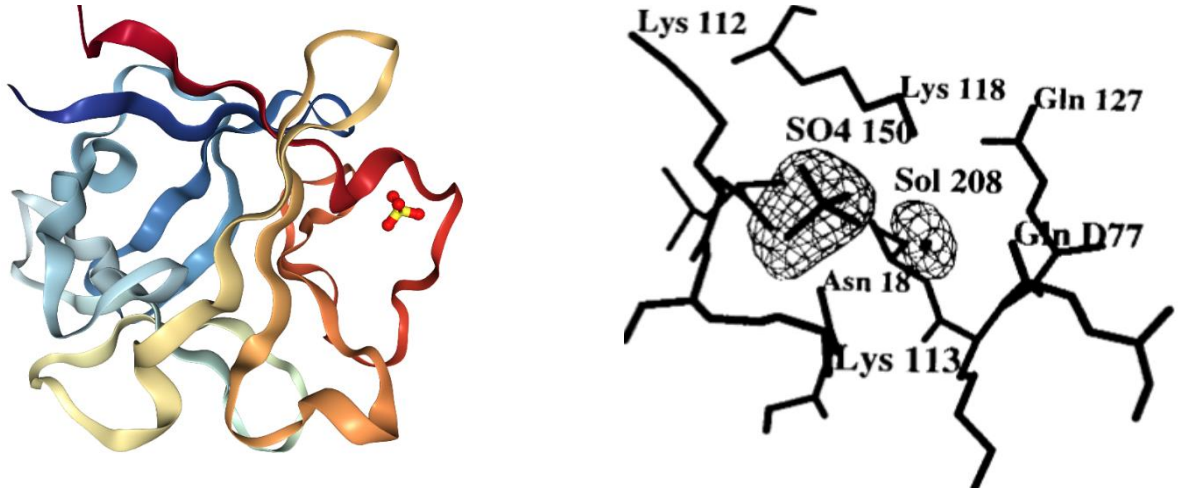

(a) (b)

Figure 6 Ribbon Diagram of Human FGF-1 (hFGF-1) (PDB ID 2AFG) and Structure of Human FGF-1 in the region of residues Asn 18, Lys 113, and Lys 118.
Structure of human FGF-1 depicted as a ribbon diagram. The ribbon diagram shows that hFGF-1 interacts with a sulfate ion (a). The sulfate ion interacts mainly with the Nδ2 atom of Asn 18, the main chain amide of Lys 113, and the Nζ atom of Lys 118 (b)[12].

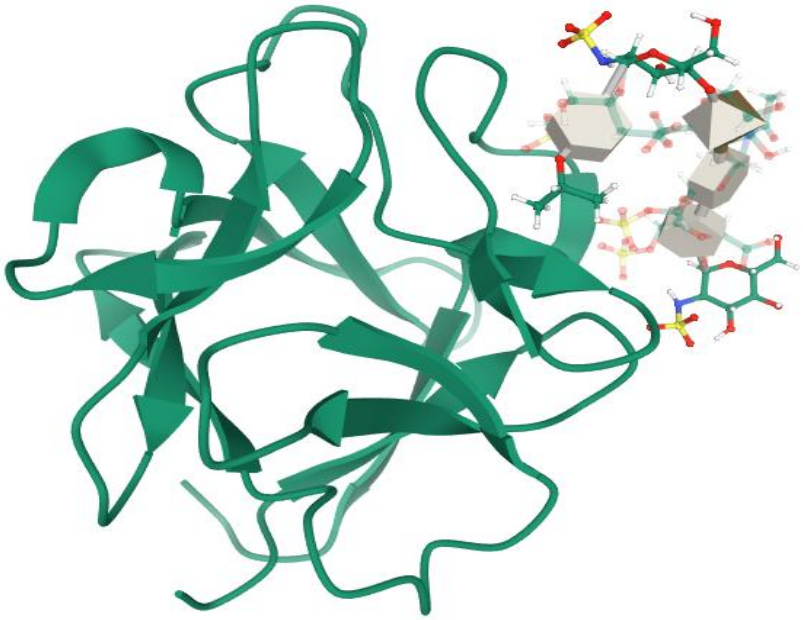

Figure 7 Structure of a human FGF-1 monomer complexed to a hexasaccharide heparin-analogue[62]
The amino acids sequence of the monomeric FGF-1 is
NLPPGNYKKPKLLYCSNGGHFLRILPDGTVDGTRDRSDQHIQLQLSAESVGEVYIKST
ETGQYLAMDTDGLLYGSQTPNEECLFLERLEENHYNTYISKKHAEKNWFVGLKKNGS
CKRGPRTHYGQKAILFLPLPVSSD

9. The Heparin-binding affinity of the human acidic Fibroblast Growth Factor (hFGF-1)

Heparin-binding capacity is one of the essential physical properties of FGFs. The study has revealed that heparin comprising of at least four monosaccharide units is mandatory to stabilize FGF-1 from thermal unfolding[61]. Upon binding with heparin, FGFs are unsusceptible to denaturation by acid or heat and proteases such as thrombin, trypsin, plasmin, subtilisin, papain, and thermolysin[54, 63]. Crystallographic studies have shown that interaction between a high negative charge density HS with positively charged amino acids in the N-terminus (residue 18) and C-terminus region (residues 112-128) exist[64, 65]. Another crystal structure (PDB ID: 1E0O) shown that the C-terminal region of FGF-1 is a dominant heparin-binding site. Seven residues of FGF-1:

K126, K127, N128, K132, R133, R136, and K142 promote heparin-binding in this crystal structure[64]. This study also revealed that van der Waals has a significant contribution to the binding of heparin and FGF-1[64].

Binding of heparin analog to FGF-1 causes an overall reduction in flexibility of FGF-1 (except for a few residues), as revealed by NMR studies. Nevertheless, the flexibility of FGF-1 in strand 12 was not considerably altered by the heparin-binding due to the presence of Leu133 and Leu135, residues located in the receptor-binding regions of FGF-1[61]. The unaffected flexibility of the amino acid residues that are responsible for the receptor binding of FGF-1 may contribute to the broad-specificity of FGF-1 towards FGFRs[61]. Another study revealed that residue K132, located in the base of the pocket toward the protein core, contribute to form interaction with critical N-sulfate and 2 O-sulfate groups on the heparin iduronic acid sugar[66].

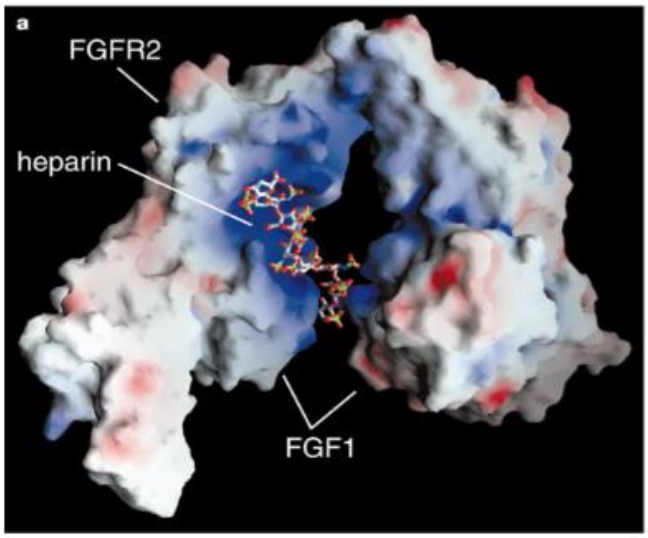

Figure 8 Complex of the FGF-1-FGFR2-Heparin[64]
The heparin is drawn as a stick model. Regions of positive charge are represented in blue that surrounds the heparin decasaccharide[64].

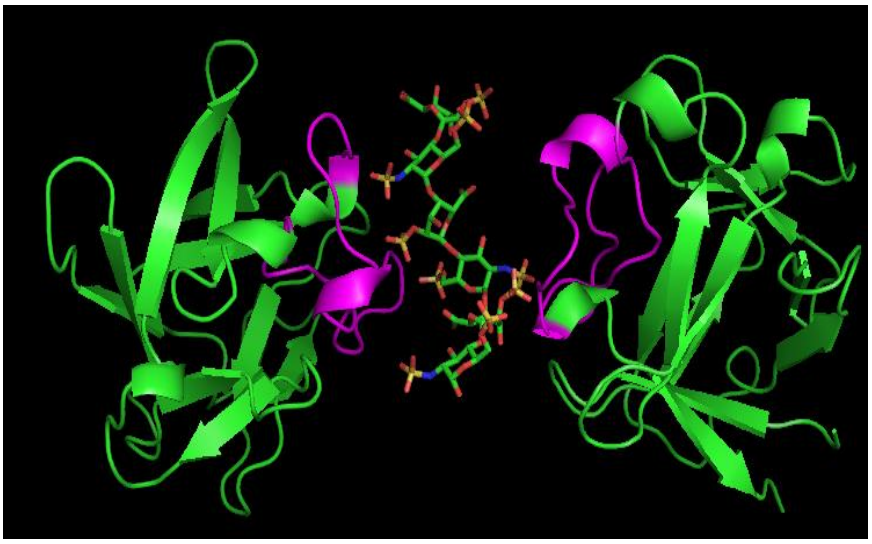

Figure 9 Complex of Heparin-FGF-1 generated by Pymol[65]
Dimer of FGF-1 is linked by heparin. FGF-1 dimer is drawn as a green cartoon model and heparin is represented as a stick model. The heparin-binding pocket of FGF-1 is represented in magenta with sequence GSNWFVGLKKNGSCKRGPRTHYGQK: PDB ID: 2AXM[65].

10. Interaction of SOS and Heparin-Binding Pocket

Sucrose octasulfate (SOS), low-molecular-weight sulfated sugar is capable of binding and stabilizing FGFs[11]. Therefore, it is deemed to stimulate fibroblast growth factor (FGF) signaling[11]. Previous studies have shown that SOS imitates heparin action in supporting FGF-induced neoangiogenesis and cell proliferation in vitro[11]. Extending the half-life of FGF is suggested as the mechanism in which SOS strengthens FGF signaling. Upon binding to SOS, FGFs are protected against high temperatures and low pH11.

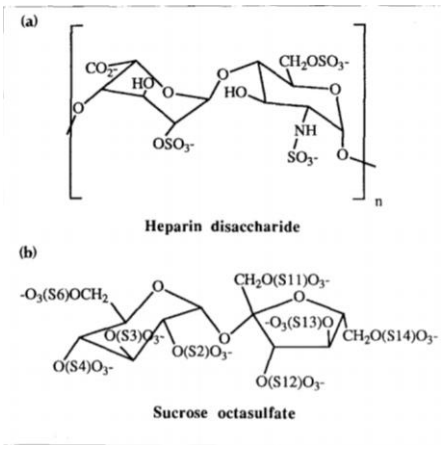

Figure 10 Structure of Heparin Disaccharide (a) and ucrose Octasulfate (b)[67]

SOS, heparin, and other proteoglycans have the same binding site. The crystal structure of a 1:1 complex between FGF-1 and SOS at 2.7Å resolution showed that SOS binds to a positively charged region of FGF-1[67]. This region contains residues 112-127 where SOS mainly interacts with Lys112, Arg116, Lys118, and Arg122[67]. Moreover, this region is also crucial for heparin-binding site. Binding of SOS and FGF-1 allows the neutralization of several positively charged residues that can destabilize the native structure of FGF-1 by electrostatic repulsion[67].

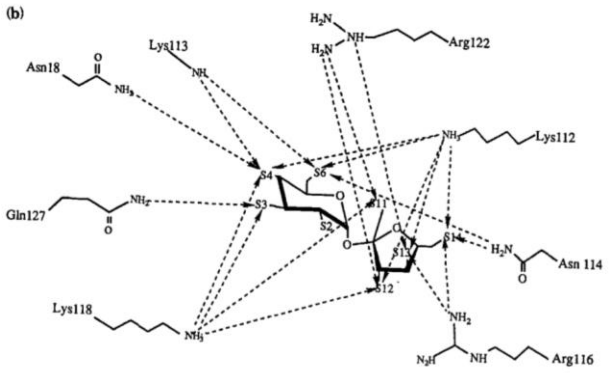

Figure 11 Schematic Representation of SOS binding to FGF-1[67]

11. Plausible role of the Fibroblast Growth Factors in Amyloid Diseases

Acidic fibroblast growth factor (aFGF-1 or FGF-1) is one of the promising molecules to be explored to gain an in-depth understanding of Alzheimer's disease. The origin of this growth

factor is from neural tissue, where it is found to be highly concentrated[5]. The proliferation and differentiation of various cell types in vitro are affected by FGF-1. FGF-1 activates the neuron survival mechanism. It is delivered from the cerebral third ventricle's ependymal cells into the cerebrospinal fluid (CSF) [5, 6].

Some previous studies link the presence of high levels of FGF-1 and the occurrence of Alzheimer's disease. The first study observed that astrocytes containing high levels of FGF-1 presented around senile plaques in seven Alzheimer's patients' postmortem brain tissue[6]. The examination was conducted by immunohistochemistry employing a specific antiserum against FGF-1[6]. The diagnosis of Alzheimer's disease was established in every case by the presence of a large amount of plaques and tangles[6]. The promoting factor of the astrocytes assembly around the plaques was presumed due to the high binding affinity between FGF-1 and heparan sulfate proteoglycan[6]. This presumption is strengthened by the fact that the mitogenic activity of FGF-1 is increased more than 100-fold by heparin and heparin sulfate [6].

The result from in vivo observation showed that high levels of secreted FGF-1 upregulated apolipoprotein E (apoE) production in astrocytes of the brain injury lesion by autocrine mechanism[9]. Therefore, it was presumed that stress conditions (e.g., heat shock, oxidation, and long-term culture) trigger astrocytes to generate FGF-1 to induce the production of apoE-HDL (apolipoprotein E-high-density lipoproteins), an important compound for the healing process in the postinjury brain[9]. ApoE synthesis is triggered by FGF-1 via the PI3K/Akt (phosphoinositide 3-kinases/ protein kinase B) pathway rather than Ras/MEK/Erk (mitogen-activated protein kinase kinase/ extracellular signal-regulated kinase) pathway [9].

Another study found that the level of FGF-1 in the cerebrospinal fluid and serum of thirty-two Alzheimer's patients were higher than those thirty-two patients without Alzheimer's disease

(normal controls)[5]. Western blotting and enzyme-linked immunosorbent assay (ELISA) was carried out to measure the level of the FGF-1[5]. This study was based on the fact that FGF-1 is one of the most pivotal central nervous system (CNS) growth factors and a powerful mitogen[5]. Moreover, it was assumed that biochemical brain abnormalities could be manifested in cerebrospinal fluid (CSF) because of CSF proximity to the extracellular space of the brain [5]. It was found that FGF-1 plays an essential role in enhancing microglial and astrocyte-mediated neuroinflammation[10]. Neuroinflammation, the hallmark of Alzheimer's disease progression, can be a potential drug target in Alzheimer's drug development[10]. It can be pursued by blocking the expression and release of FGF-1 because inhibition of FGF-1 can prevent the expression of neuroinflammatory molecules[10].

It can be concluded from these in vivo and human brain tissue studies that astrocytes express a high level of FGF-1 that leads to apoE-HDL production in Alzheimer's disease; astrocytes activity in enhancing FGF-1 production promotes neuroinflammation, a hallmark of AD. FGF-1 may play a significant role in AD, not only because of its potency in mediating neuroinflammation but also the property of a FGF-1 as polypetide chains to form amyloid-like conformations. The reaction rate of amyloid formation can be influenced by the concentration of the protein itself **[1-3]**.

12. <u>Methods for Assessing Amyloid Fibrils Formation</u>

a) Transmission electron microscopy (TEM)

Fibrillar characteristic is showed by the amyloid fibrils when investigated under electron microscope[26]. The TEM27 can analyze amyloid aggregates extracted from tissue or synthesized in vitro while the non-fibrillar aggregates are lost during the extraction process and are not present in in vitro experiments[2628]. Observation through TEM showed that amyloid aggregates possess a wavy

or rod-like or twisted structure with a diameter ranging from 5-25 nm[26]. Information about the variations of the degree of twisting, the number of protofilaments forming a fibril, and mature fibrils diameter can be obtained from the TEM images[26]. Various TEM images showed that regardless of their biochemical form, amyloid deposits from different tissue consist of a bundle of not branched, straight fibrils, ranging from 6 nm to 13 nm in diameter (average 7.5-10 nm) and 100-1600 nm in length [26].

b) Circular Dichroism (CD)

Circular dichroism (CD) is based on the distinctive absorption of left-handed and right-handed circularly polarized light of molecules in the absence of a magnetic field[68]. The difference in absorbance for left-handed and right-handed circularly polarized light, ΔA ($= A_L - A_R$) is the experimentally measured parameter in CD[68]. CD is an absorption phenomenon in which the chromophores that produce the CD spectrum are precisely like those generating a conventional absorption spectrum[68]. Either chirality of the chromophore or location of the chromophore in an asymmetric environment must be fulfilled to exhibit a CD signal[68]. The asymmetry of the polypeptide chain and the asymmetry at the α-carbon atoms in the amino acid residues are two factors that cause the optical activity of proteins[68].

There are two types of protein circular dichroism (CD) spectroscopy: far UV or back-bone with data collection using wavelength from 190 to 250 nm and near UV or aromatic with data collection using wavelength from 250 to 300 nm[69]. The near-UV CD bands of proteins (310-255 nm) are generated by Trp, Tyr, Phe, and cystine[68, 69]. Near-UV CD bands can be used to derive information regarding the tertiary, and occasionally quaternary structure of the protein[68]. The far-UV CD bands of proteins can provide information regarding the secondary structure of the protein (α-helix, β-sheet, β-turn, and unordered content)[68].

Circular dichroism provides a powerful qualitative characterization of the secondary structure content of amyloid fibrils when the fibrils are soluble[68]. In general, the characteristic of the far-UV spectra of different protein classes are[68]:

- All-α proteins show an intense negative band with two peaks (at 208 and 222 nm) and a strong positive band (at 191-193 nm)[68]. The intensities of these bands reflect α-helical content. Δεmrw values for a totally helical protein would be of the order of -11 M^{-1} cm^{-1} (at 208 and 222 nm) and +21 M^{-1} cm^{-1} (at 191-193 nm)[68].
- The spectra of regular all-β proteins are significantly weaker than those of all-α proteins. These spectra usually have a negative band (at 210-225 nm, $\Delta\varepsilon_{mrw}$: -1 to -35 M^{-1} cm^{-1}) and a stronger positive band (at 190-200 nm, $\Delta\varepsilon_{mrw}$: 2-6 M^{-1} cm^{-1})[68].
- Unordered peptides and denatured proteins generate a strong negative band (at 195-200 nm, Δεmrw: -4 to -8M^{-1} cm^{-1}) and a much weaker band (which can be either positive or negative) between 215 and 230 nm ($\Delta\varepsilon_{mrw}$: +0.5 to -2.5 M^{-1} cm^{-1})[68].

c) Fluorescence Spectroscopy

A molecule's ability to absorb a photon of appropriate energy promotes an electronic transition from the ground state to an excited state[70]. To return to its ground state, a molecule in an electronically excited state must emit the energy[70]. These processes are described by a Jablonski diagram (Figure 12).

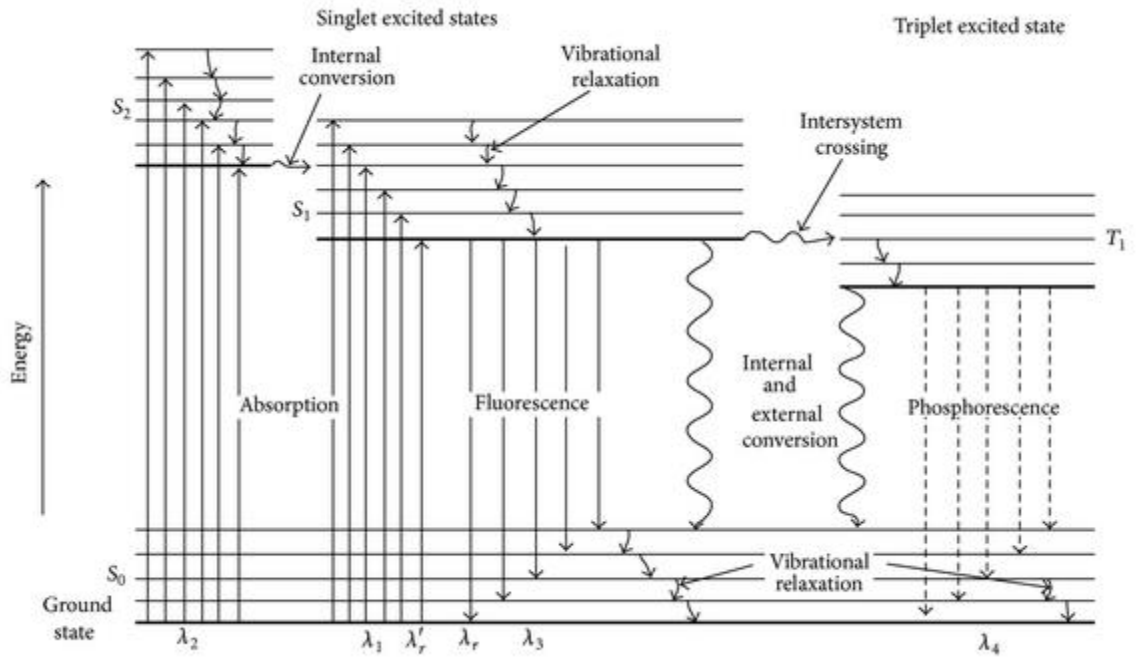

Figure 12 Jablonski diagram
Illustration of the electronic levels of common organic molecules and possible transitions between different singlet and triplet states[70].

The absorption of a photon happens very rapidly (~ 10^{-15} sec) from the lowest vibrational level of the ground state (S_0) to the higher electronic and vibrational states (e.g., S_1, S_2)[71]. Relaxation of the electron from higher energy states to the lowest vibrational level of the first excited state (S1) occurs quickly (~10^{-10} sec to 10^{-12} sec); This phenomenon known as internal conversion[71]. Radiative and nonradiative are two general pathways for the dissipation of excited-state energy in the absence of photochemical reactions. Photon release occurs during the loss of energy in a radiative pathway[71]. Fluorescence is the light liberated when the photon comes from the first excited singlet state to the ground state[71].

Moreover, an electron can move from the excited singlet state to an excited triplet state, known as intersystem crossing[71]. Presumably, the release of a photon accompanies the return of

the electron from the triplet state to the ground state[71]. The emission during this process is called phosphorescence [71].

There are two types of protein fluorescence, intrinsic protein fluorescence and extrinsic protein fluorescence. Intrinsic protein fluorescence relies on the signal from the naturally fluorescent amino acid tryptophan and limitedly from tyrosine. While extrinsic fluorescence use dyes that can form covalent and noncovalent bonding with the proteins[72].

Tryptophan fluorescence is almost always associated with the term "natural protein fluorescence" because it is the most highly fluorescent amino acid in proteins. Tyrosine is the second most fluorescent amino acid in protein; Application of tyrosine fluorescence is mostly limited to tryptophan-free proteins. Whereas, because of the weakness of phenylalanine fluorescence, it is never used in protein studies[72, 73].

The sensitivity of tryptophan emission to polarity and mobility of the environment makes tryptophan fluorescence a pivotal tool in studies of protein structure and dynamics. Nearly all polar protein groups can quench tryptophan fluorescence. There are some dynamic quenchers of tryptophan fluorescence: aspartic and glutamic acid residues (effective dynamic quenchers in their neutral form); lysine and arginine (are more effective in their charged forms); histidine; disulfide; amide and peptide groups. At low pH, histidine shows its quenching effect through the formation of a stacking complex with the indole ring. Even though single cysteine can be an effective quencher, one of the strongest quenchers of tryptophan fluorescence is disulfide[73].

Extrinsic fluorescent dyes, for example, Thioflavin T (ThT), Congo Red (CR) and 1-anilino-8-naphthalenesulfonate (ANS) (Figure 3.) are used for the aim of protein characterization, such as for aggregates characterization and identification, to monitor refolding and unfolding processes, to examine amyloid fibril, molten globule intermediates, to access the degree of exposed

surface hydrophobicity of the conformationally altered protein, etc. The interaction between the dye and protein molecule could give alteration to the fluorescence emission through the alteration of relaxation pathway which is the basic principle of the use of extrinsic dyes for protein characterization[74].

Interaction of ANS with protein molecules dictates ANS's fluorescence properties, which result in alterations of polarity and viscosity of the environment[72]. The binding mechanism of ANS to protein involves hydrophobic interactions, electrostatic interactions, and complementary interactions such as van der Waals interactions[72]. In electrostatic interaction, the predominant interaction is the ion-pairing between the negatively charged sulfonate groups of ANS with positively charged amino acids, e.g., histidine, lysine, or arginine[72].

ThT is among the most widely used dye to selectively stain and identify amyloid fibrils *in vivo* and *in vitro*[74]. The result from the molecular dynamics simulations shows that ThT bind parallel to the long axis of the fibril surface in grooves formed by side-chain ladders (Figure 13a and 13b)[74]. ThT displays an additional absorption peak at 450 nm and becomes highly fluorescent with an emission maximum at 480 nm[74].

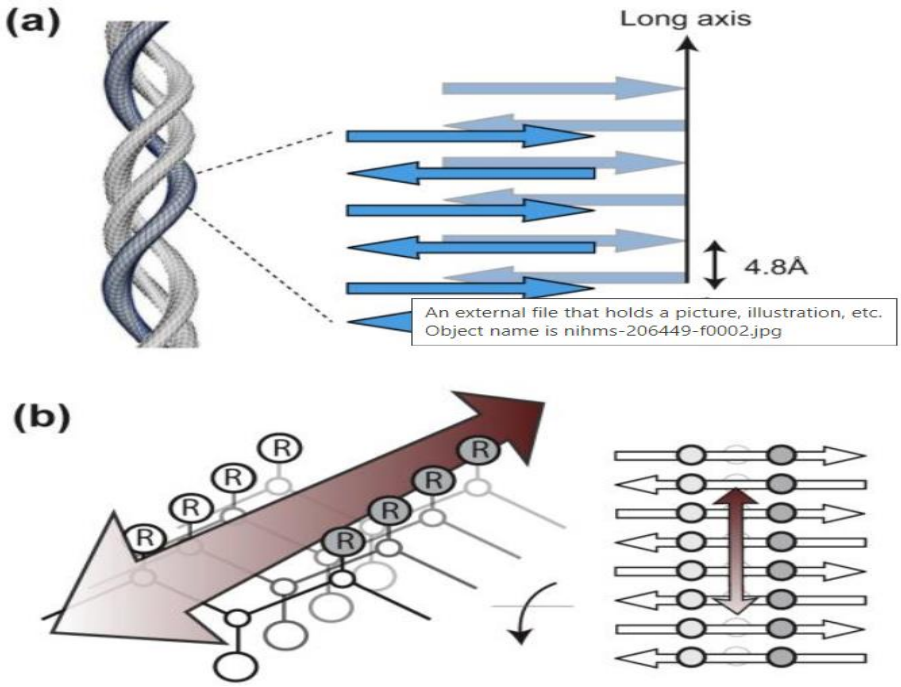

Figure 13 (a) Cross-β structure of amyloid fibrils (b) ThT is proposed to bind along surface side-chain grooves running parallel to the long axis of the β-sheet[74].

AIMS OF THE STUDY

Some previous studies link the presence of a high level of FGF-1 and the occurrence of Alzheimer's disease[5, 6, 9, 10]. FGF-1 may play a significant role in AD not only because of its potency in mediating neuroinflammation but also the property of FGF-1 as polypeptide chains to form amyloid-like conformations that the concentration of the protein itself1-3 can influence reaction rate of the [1-3]formation of amyloid-like structures[1-3]. In addition to that, human FGF-1 tends to unfold at physiological temperature in the absence of sugar poly anions[11, 12].

Therefore, exploring the role of destabilization of heparin-binding pocket in amyloid fibrils formation can lead to an understanding of the mechanism of amyloid fibrils formation in FGF-1. Subsequently, we can also obtain more in-depth knowledge of the role of heparin-binding pocket in protein aggregation, especially for the heparin-binding protein family.

Presumably, it also provides a novel drug target to prevent protein aggregation that can aid future research in exploring a new avenue of Alzheimer's drug development.

In this project, we conducted some experiments using different techniques such as fluorescence spectroscopy, limited trypsin digestion, transmission electron microscope (TEM), and mass spectrometry to induce fibrils formation in hFGF-1, characterize the sodium dodecyl sulphate (SDS)-induced fibrils formation in hFGF-1, and understand the molecular mechanism of fibril formation in hFGF-1.

CHAPTER 2

MATERIALS AND METHODS

1g of Ampicillin salt was dissolved in 10ml ethanol 50% to make a 0.1% Ampicillin stock solution. The stock solution was stored at -20℃. 1M IPTG was prepared by dissolving 2.38g IPTG in 10ml distilled, di-ionized water (ddH_2O). IPTG binds to and inactivates the lac repressor. It leads to the activation of the lac operon and induction of protein expression. Three sodium dodecyl sulphate (SDS) stock solutions were prepared: 10% (SDS-PAGE), 2mM (Fluorescence Spectroscopy, Trypsin Digestion, Transmission Electron Microscopy, Mass Spectrophotometry), and 15mM (Fluorescence Spectroscopy). 10%, 2mM, 15mM SDS were prepared by dissolving 1g, 0.006g, and 0.043g SDS in 10ml ddH_2O, respectively. 0.005g SOS stock solution was dissolved in buffer pH 7.2 (10mM phosphate buffer + 100mM NaCl) to make 2mM SOS stock solution. The stock solution was stored at -20℃. Trypsin stock solution was prepared by dissolving 3mg Bovine Trypsin in 1ml ddH_2O. 8M Urea was prepared by dissolving 240.24g Urea in 500ml ddH_2O. 1mg/ml ThT stock solution was prepared by dissolving 1mg ThT in 1ml ddH_2O .

1. Bacterial Transformation

1µl plasmid DNA (pET20b-pentaFGF-1 plasmid) was transformed into BL-21 (DE3) pLysS competent *E. coli* cells. The incubation was conducted on ice for 30 minutes. The cells were heat-shocked at 42℃ for 1 minute and immediately shifted to the ice for 3 minutes. 800µl of sterile lysogen broth (LB) media was added to the cells inside the laminar hood. The mixture was incubated in an orbital shaker at 37℃ for 45 minutes at 250rpm. 100µl of the mixture was plated on separate labeled Ampicillin (Amp) Agar plates (containing 25µg/µl Amp) using sterile steel spreader inside the laminar hood. The ampicillin (Amp) was used because FGF-1 plasmid

possesses a gene resistant to Amp. As a result, only BL-21 (DE3) pLysS competent *E. coli* cells carried the FGF-1 plasmid can survive. Agar plates were stored upside down and incubated overnight (12-14 hours) at 37℃.

2. Protein Expression

a. Small-Scale Expression (SSE)

Small scale expression was carried out before large scale expression to examine the presence of the protein of interest. It was conducted by inoculating one or more colonies from the Agar plate into 10ml of LB broth containing 10µl Amp and incubated overnight (14-15 hours). The next morning, 5%/1 ml of the overnight culture was inoculated into 10mL of LB containing 10µL of Amp and incubated at 37℃ for 2.15 hours at 250rpm. Optical density (OD) of the culture was measured by UV visible spectrometer at wavelength 600 nm after 2.15 hours. 9µl IPTG was added to the culture as an inducer when it reached the required OD (between 0.6 to 0.8). The chemical structure of IPTG is analogous to allolactose. IPTG binds to and inactivates the lac repressor. It leads to the activation of the lac operon and induction of protein expression of BL-21 (DE3) pLysS competent *E. coli* cells. After 3.5 hours, the bacterial cells were collected, sonicated, then centrifuged for 3 minutes at 13,000rpm to derive the protein of interest. Four samples were applied in SDS-PAGE: uninduced (without IPTG addition), induced (IPTG addition), pellet, and supernatant.

b. Trichloroacetic acid (TCA) Precipitation

TCA precipitation was conducted before SDS-PAGE. TCA is an acidic compound and contains ester and salt. This procedure aims to obtain complete denatured protein due to the disruption of non-covalent bonds such as the hydrogen-bonded water molecules surrounding a protein and the addition of a reducing agent (2-mercaptoethanol) that can reduce disulfide bonds.

A particular amount of TCA (10% of the protein volume) was added to the protein samples. The mixture was vortexed and centrifuged at 13000rpm for 3 mins, and the supernatant was discarded. 100% Acetone was added to wash the pellet and centrifugation was conducted again at 13000 rpm for 3 min and the supernatant was discarded again. The pellets were air-dried. 8M Urea was added to dissolve the pellets and 10µl loading dye was added into the dissolved pellet.

i. Sodium-Dodecyl Sulfate-Polyacrylamide Agarose Gel Electrophoresis (SDS-PAGE)

The protein sample was applied in 15% Resolving gel and stacking gel. Composition of the 15% resolving gel (2 gels) was 1.1ml ddH2O, 5ml 30% acrylamide, 3.75mL 1M Tris.HCl pH 8.8, 100 ul 10% SDS, 100 ul 10% APS, and 10 ul TEMED. While composition for the 15% stacking gel (2 gels) was 3.75ml ddH2O, 0.83ml 30% acrylamide, 0.62mL 1M Tris.HCl pH 6.8, 50 ul 10% SDS, 50 ul 10% APS, and 10 ul TEMED. The gel was run at 200V, 100mA. Then, the gel was stained by Coomassie Brilliant Blue for 3-5 min, rinsed with water, and put in the destainer solution (contains methanol and acetic acid) overnight with KimWipes overlaid at the top to absorb the dye. The gel was scanned the next day.

d) Large-Scale Expression (LSE)

Large quantities of hFGF-1 protein were generated through large-scale expression. The procedure was the same as SSE, except 200ml of primary culture was inoculated, and 2 liters of secondary culture was inoculated using 25ml of the inoculated and overnight incubated primary culture. 50mg/ml ampicillin and 500µl of 1M IPTG were added. The 2 liters culture volumes yielded two falcons tube containing 1liter pellets/each and was stored at -20℃.

e) Protein Purification

35ml of 10mM Phosphate Buffer (PB) pH 7.2 was used to dissolve the pellet obtained from LSE. Ultrasonication was conducted to lyse the cells, and the lysate was separated from the

cell debris by centrifugation at 19000 rpm for 25 min at 4℃. The supernatant was transferred to a new falcon tube to be loaded onto the heparin sepharose column.

The column was pre-equilibrated with 2 column volumes (30ml) of 10mM PB pH 7.2. The supernatant was then loaded onto the column. The flow-through/unbound protein was collected if a peak was observed. Next, the peak was then base lined with 10mM PB pH 7.2. Serial elution buffers containing 10mM PB and 100mM, 300mM, 500mM, 800mM, and 1500mM NaCl pH 7.2 were used in hFGF-1 protein purification. All the fractions were collected and applied for TCA precipitation procedure before SDS-PAGE was run. hFGF-1 was eluted in PB containing 1500mM NaCl. A thick band at ~16kDa verified the presence of pure hFGF-1 protein. The column was regenerated using 25ml 8M Urea, 50ml 10mM PB and 20ml 20% ethanol. The column was stored at -20℃.

The pure hFGF-1 protein was concentrated by using a 10kDa concentrator in buffer containing 25mM $(NH_4)_2SO_4$, 100mM NaCl, and 10mM PBS. It was centrifuged at 4500rpm, 4℃ until reaching the desired volume. Then, concentrated hFGF-1 was stored at -80℃ for further application in biophysical and biochemical characterizations.

3. <u>Intrinsic Fluorescence Spectroscopy</u>

The fluorescence emission spectrum of FGF-1 was conducted using Hitachi F-2500 spectrofluorometer at 25℃ (2.5nm resolution) and a quartz cell with a 1.0cm path length, in a single beam mode. The samples for this experiment was prepared using 10μM FGF-1 in buffer containing 100mM NaCl and 10mM PBS (pH 7.2); 0.01-10mM (0.2mM to induce fibril formation); ratio of FGF-1 and SOS is 1:1-1:20. There are some sets of samples for this experiment: FGF-1+SOS (1:1-1:20)+SDS (0.2mM); FGF-1+SDS (0.2mM)+SOS (1:1-1:20); FGF-1+SOS (1:15)+SDS (0.01-10mM); and FGF-1+SOS (1:15)+ SDS (0.01-10mM). Each

sample was triplicated, and incubation was performed at 37℃ for 6-7mins after the addition of SOS and 10mins after the addition of SDS. The samples were excited at a wavelength of 280nm, and the data was collected between 300nm and 450nm. Intrinsic fluorescence at these wavelengths examined changes in tyrosine (308nm) and tryptophan (350nm) in FGF-1 when the addition of SOS, SDS, the combination of SOS and SDS were performed. The aims of the intrinsic fluorescence in this experiment were to assess alteration in the three-dimensional structure and folding manner of FGF-1 when combined with SOS and SDS.

4) **Extrinsic Fluorescence Spectroscopy**

The fluorescence emission spectrum of FGF-1 was conducted using Hitachi F-2500 spectrofluorometer at 25℃ (2.5nm resolution) and a quartz cell with a 1.0cm path length, in a single beam mode. The sample for this experiment was prepared using a protein concentration of 10μM in buffer containing 100mM NaCl and 10mM PBS (pH 7.2), 0.01-10mM (0.2mM to induce fibril formation); ratio of FGF-1 and SOS is (1:1)-(1:20), and 50mg/ml ThT (Sigma-Aldrich). There are some sets of samples for this experiment: FGF-1+SOS+SDS (0.2mM)+ThT; FGF-1+SOS+SDS+ThT; FGF-1+SDS+SOS+ThT; FGF-1+SDS+SOS (1:15); and FGF-1+SDS+ThT. Each sample was triplicated, and incubation was performed at 37℃ for 6-7mins after the addition of SOS and 10mins after the addition of SDS. The samples were excited at a wavelength of 440nm, and the data was collected between 455nm and 600nm. Fluorescence intensity at 485nm was recorded.

5) Limited Trypsin Digestion

Both concentration and time-dependent limited trypsin digestion were conducted in 100mM NaCl and 10mM PBS (pH 7.2) with a total volume of 100μl. The concentration of trypsin stock solution, FGF-1, SDS, and the ratio of FGF-1 and SOS were 3mg/ml; 10μM; 0.2mM;

1:1,1:10,1:15, respectively. The concentration of trypsin used for the concentration-dependent limited trypsin digestion was 0.02-0.5mg/ml (30mins incubation at 37℃) while the concentration for the time-dependent, limited trypsin digestion was 0.04mg/ml. Some sets of samples were applied for time-dependent limited trypsin digestion: FGF-1+trypsin; FGF-1+SDS+trypsin; FGF-1+SOS(1:15)+trypsin; FGF-1+SOS(1:1)+trypsin; FGF-1+SOS(1:10)+trypsin; FGF-1+SDS+SOS(1:1); FGF-1+SDS+SOS(1:10); and FGF-1+SOS(1:15)+SDS. Each sample was triplicated, and incubation was performed at 37℃ for 6-7mins after the addition of SOS and 10mins after the addition of SDS. Pellet generated after incubation of FGF-1 and SDS were washed three times with 100mM NaCl and 10mM PBS (pH 7.2) to remove excess SDS and centrifuged for 10 minutes at 13000 r.p.m. After the addition of trypsin, all the samples were incubated at 37℃ for 1-30mins. Next, all samples were subjected to TCA precipitation and applied for 15% SDS-PAGE. Gels were stained using Coomassie Brilliant Blue (Sigma Aldrich) and analyzed using UN-SCAN IT software densitometric by plotting the average pixel intensity versus time intervals.

6) <u>Transmission Electron Microscope (TEM)</u>

The samples for this experiment were prepared using 40μM FGF-1, 0.2mM SDS, and the ratio of FGF-1, and SOS is 1:10 in the total volume of 100μl. There were five sets of samples for this experiment: FGF-1; SDS; FGF-1+0.2Mm SDS; FGF-1+0.2mM SDS+SOS (1:10); FGF-1+SOS(1:10)+0.2mM SDS. All samples were incubated at 37℃ for 24 hours. Pellets generated after incubation with SDS were washed with ddH_2O and dissolved with 40μl ddH_2O. 10μl of each sample were pipetted and applied in a separate grid. The samples were air-dried and stored inside the petri dish. The morphology and size of the aggregates were investigated by high-resolution Transmission electron microscopy (Jeol-HRTEM-2011, USA) with an accelerating voltage of 80–100 kV. TEM images were taken at different magnifications.

7) Mass Spectrometry

There were seven samples that are subjected to mass spectrometry: FGF-1+trypsin; FGF-1+SOS (1:1); FGF-1+0.2mM SDS+trypsin; FGF-1+0.2mM SDS+SOS (1:1)+trypsin; FGF-1+SOS (1:1)+0.2mM SDS+trypsin; FGF-1+SOS (1:10)+0.2mM SDS+trypsin; trypsin. The concentration of FGF-1 and trypsin that were used in this experiment are 10μM and 0.04 mg/mL, respectively. After trypsin addition, all samples were incubated at 37℃ for 30 minutes. 10μL of TCA was added to each sample that contains trypsin and centrifuged for 3 minutes at 13.000 rpm. The supernatant of each sample was transferred to the new Eppendorf tubes. All samples were sent to mass spectrometry facility in Poultry Science.

CHAPTER 3

RESULTS

The predominant native structure of FGF-1 is β-sheet that contains eight tyrosine, a single tryptophan residue quenched in the native state, and three buried reduced cysteine residues[61,75, 76]. Positive charges from the nearby histidine and lysine residues quench the fluorescence of the single tryptophan at position 121 in hFGF-1[8, 77, 78]. This quenching effect corresponds to the presence of imidazole and pyrrole groups in the vicinity of the indole ring of the tryptophan[79]. In native FGF-1, seven of eight tyrosine residues are exposed to the solvent, whereas the single tryptophan shows a partial solvent accessibility[59-61]. Consequently, the fluorescence behavior of FGF-1 is defined by eight tyrosine residues[80]. In the native state, FGF-1 shows a prominent peak at 305nm, which corresponds to the emission of tyrosine residues. Upon disruption to the protein structure, a substantial amount of tryptophan fluorescence is observed because the positively charged residues moved away from the indole ring and relieved the quenching effect[75].

FGFs are heparin-binding protein [61]. Upon binding with heparin, FGFs are unsusceptible to denaturation by acid or heat and proteases such as thrombin, trypsin, plasmin, subtilisin, papain, and thermolysin[54, 63]. Crystallographic studies have shown that interaction between a high negative charge density HS with positively charged amino acids in the N-terminus (residue 18) and C-terminus region (residues 112-128) exist[64, 65]. Another crystal structure (PDB ID: 1E0O) shown that the C-terminal region of FGF-1 is a dominant heparin-binding site. Seven residues of FGF-1: K126, K127, N128, K132, R133, R136, and K142 promote heparin-binding in this crystal structure[64]. This study also revealed that van der Waals has a significant contribution to the binding of heparin and FGF-1[64].

a) Structural Changes Induced by SDS

Eight tyrosine and one tryptophan comprise the primary sequence of FGF-1. Measuring the intrinsic fluorescence of these aromatic residues can provide information regarding alteration in the tertiary structure of the protein. In the native state, hFGF-1 shows a prominent peak at 305nm, which corresponds to the emission of tyrosine residues. Upon disruption to the protein structure, a substantial amount of tryptophan fluorescence is observed because the positively charged residues moved away from the indole ring and relieved the quenching effect[75]. This observed fluorescence is attributed to an emission maximum at around 350 nm. As a result, the ratio of the fluorescence intensity at 305nm and 350nm (I_{305}/I_{350}) can be used to monitor the change in the tertiary structure of hFGF-1.

The fluorescence emission spectrum of hFGF-1 is dominated by a single peak near 305nm upon excitation at 280nm (orange line in figure 17), and the tryptophan fluorescence is substantially quenched at pH 7.2 at 25°C. At 37°C, a red shift is observed because FGF-1 is in a partially unfolded state with the peak around 310 nm. In the presence of 0.02-0.04mM SDS, blue shift in λ_{max} is observed relative to hFGF-1 only. The observed shift is from 310nm (hFGF-1 only at 37°C) to around 305nm due to the hydrophobic environment but without any significant change in fluorescence emission intensities. A drastic change of the λ_{max} occurs at the concentration of SDS from 0.08mM to 0.2mM relative to hFGF-1 only at 37°C, from 310nm to around 325nm (bathochromic shift) (figure 17). The spectrum of hFGF-1 in the presence of 0.08mM-0.2mM shows significant broad shoulder at 350nm, which corresponds to the emission of the previously quenched tryptophan residues. These changes are not found when hFGF-1 interacts with 0.02-0.04mM SDS due to a quenched tryptophan residue in the native state when protein is still properly folded. At 0.2-0.6mM of SDS, fluorescence intensity is decreased with

shift of λ_{max} by ~10nm (from 325nm to around 315nm) (figure 17) and this region is attributed for partial unfolding of tryptophan residue. This result indicates that perturbation occurs in the tertiary structures of protein due to the presence of SDS in this concentration. hFGF-1 in the presence of 1-10mM SDS results in the peak centered at ~314nm with a broad shoulder at ~340nm. It suggests that this range concentration of SDS induces a partial degree of the unfolding of tryptophan residue in hFGF-1. A significant reduction of the ratio of 305nm to 350nm (I_{305}/I_{350}) (figure 16) is observed at 0.07mM-10mM SDS with the lowest point at 0.1mM SDS and 0.2mM SDS (Figure 16). It indicates that at this range of concentration, the tertiary structure of the hFGF-1 is significantly altered due to the alteration in the microenvironment of the tryptophan residue. Whereas, a higher value of I_{305}/I_{350} indicates a more native-like, properly folded structure[75].

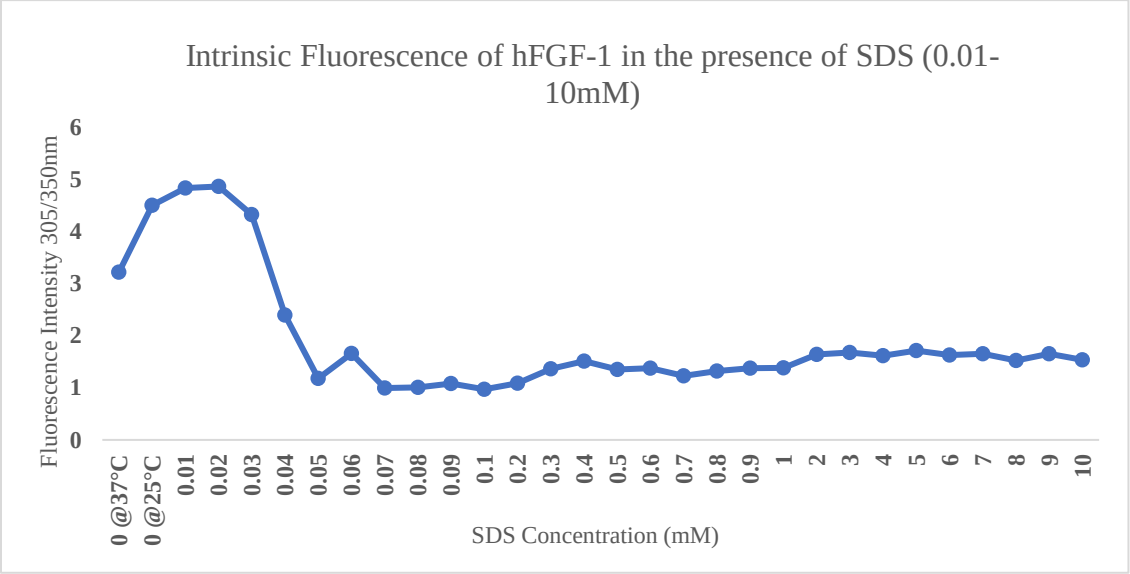

Figure 14 Intrinsic Fluorescence Analysis of hFGF-1 in the Presence of SDS
Fluorescence intensity ratio (I_{305}/I_{350}) as measured as a function of different concentration of SDS in PB buffer in 100mM NaCl (pH 7.2) after 10 minutes of incubation 37°C.

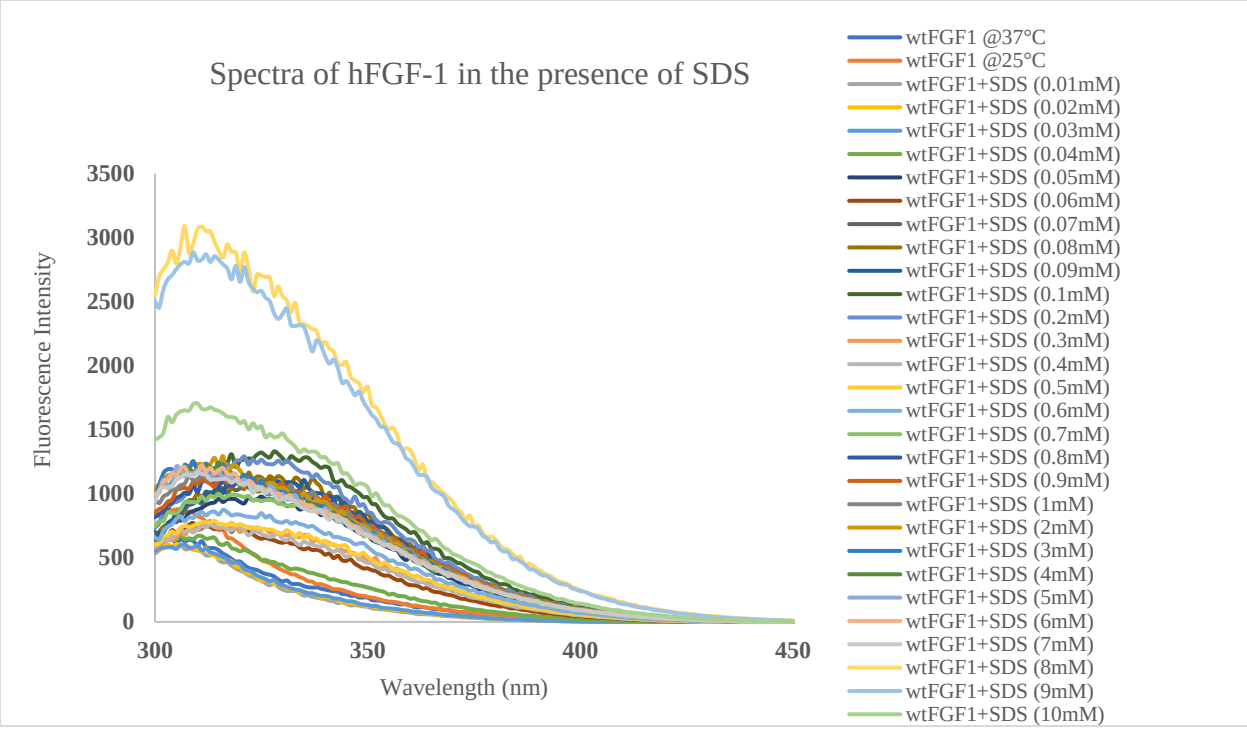

Figure 15 Intrinsic Fluorescence Spectra of hFGF-1 in the presence of SDS
Spectra of hFGF-1 in the presence of different concentration of SDS in PB buffer in 100mM NaCl (pH 7.2) after 10 minutes of incubation at 37℃.

hFGF-1 is incubated together with different ratios of SOS to hFGF-1 and 0.2mM SDS to observe the ability of SOS to protect the tertiary structure of the protein from SDS. A Comparison of the spectrum of hFGF-1 in the presence of 0.2mM SDS and the spectra of hFGF-1, different ratio of SOS to hFGF-1, and 0.2mM SDS shows a blue shift from ~317nm (hFGF-1 and 0.2mM SDS) to ~309nm (hFGF-1, 0.2mM SDS, different ratio of SOS to hFGF-1). The spectra also show a reduction in the fluorescence intensity relative to the hFGF-1 in the presence of 0.2mM SDS. The spectra of hFGF-1 in the presence of different ratios of SOS to hFGF-1 and 0.2mM SDS compare to hFGF-1 and 0.2mM SDS show diminished broad shoulders at 340nm. The emission of quenched tryptophan residues in the nonpolar environment inside the protein globule (in hFGF-1 and 0.2mM SDS tryptophan quenching is relieved) is attributable to this event. The result of I_{305}/I_{350} shows the highest value (around 5) at the ratio of hFGF-1 to SOS

(1:10), (1:15), and (1:20) (Figure 17). It indicates a more native-like, properly folded structure of the protein in the presence of SOS. Furthermore, this finding suggests that SOS binds first to stabilize and protect native conformation of hFGF-1 so that SDS cannot perturb and induce alteration in the tertiary structure of the protein.

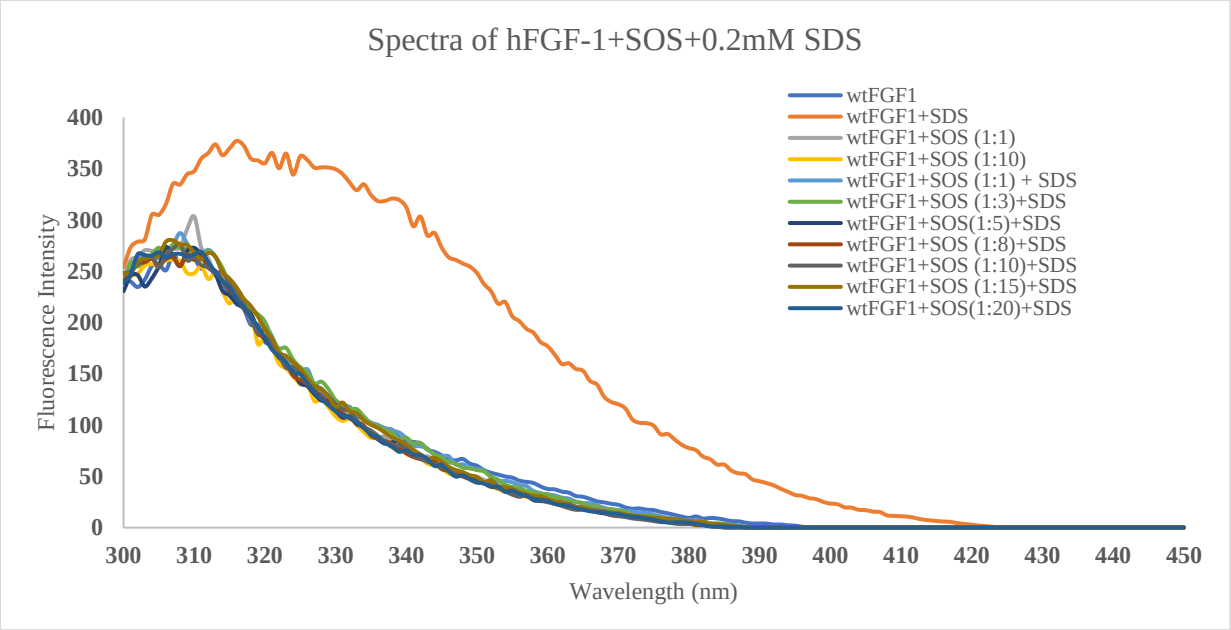

Figure 16 Intrinsic Fluorescence Spectra of hFGF-1+SOS+0.2mM SDS
Spectra of hFGF-1 in the presence of different ratio of hFGF-1 to SOS and 0.2mM SDS in PB buffer in 100mM NaCl (pH 7.2) after 10 minutes of incubation at 37℃.

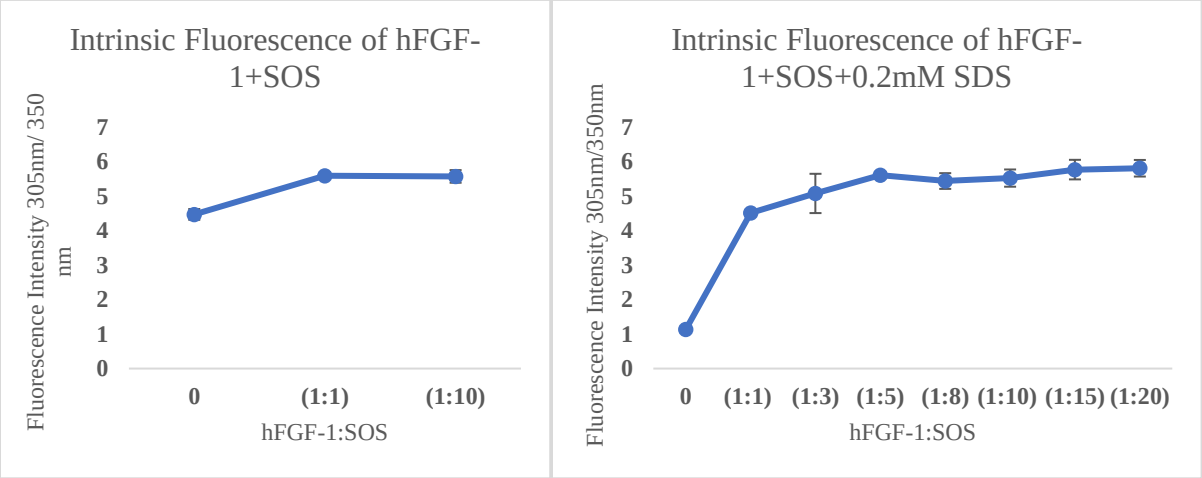

Figure 17 Intrinsic Fluorescence of wtGF-1+SOS+0.2mM SDS
Fluorescence intensity ratio (I_{305}/I_{350}) measured as a function of different ratio of hFGF-1 to SOS in PB buffer in 100mM NaCl (pH 7.2) after 10 minutes of incubation at 37℃. The error bars show the standard deviation of triplicate samples.

The control samples, hFGF-1 at 25℃, 37℃, in the presence of SOS (1:1), and (1:10) show peak at ~308 nm. Red shift (from~308nm to ~314nm) with the increase in fluorescence intensity is observed in λ_{max} when hFGF-1 is incubated with 0.2mM SDS and a different ratio of

hFGF-1 to SOS relative to the control samples (figure 18). Another comparison of the spectrum of hFGF-1 in the presence of 0.2mM SDS and hFGF-1 incubated with 0.2mM SDS and different ratio of hFGF-1 to SOS, a blue shift is detected, from ~328nm to ~314nm. The broad shoulder at 350nm with the lower fluorescence intensity compared to hFGF-1 in the presence of 0.2mM SDS is also observed in these spectra. The decline of the broadness of the shoulder at 350 nm in these spectra indicates that tryptophan residue is partially refolded to some extent from the solvent-exposed region to the hydrophobic interior of the protein. This result is also confirmed by the intrinsic fluorescence in which at the ratio of hFGF-1 to SOS (1:10), (1:15), (1:20), the I_{305}/I_{350} shows the highest value (around 2) (figure 19). Even though this value is less than the I_{305}/I_{350} of hFGF-1 only (about 5) but greater than the SDS-induced amyloid-like fibrils (hFGF-1 and 0.2mM SDS) (around 1), this finding indicates that the structural alteration occurred in the fibrils in the presence of SOS that can cause a refolding process to some extent.

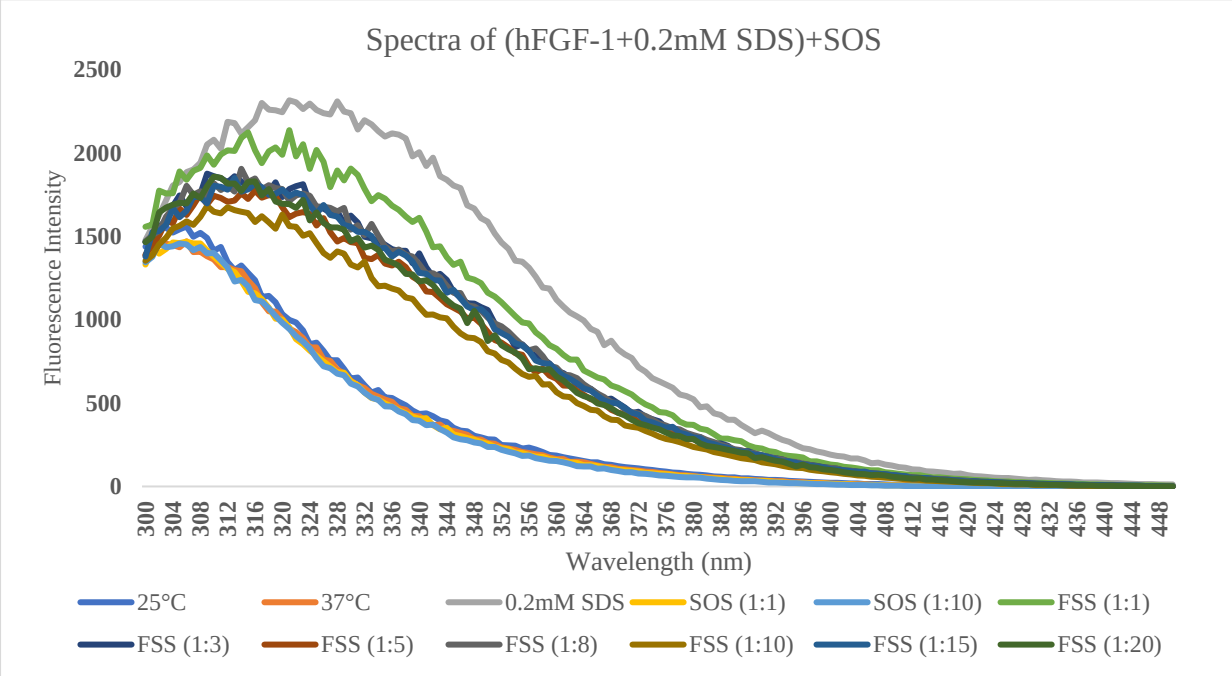

Figure 18 Intrinsic Fluorescence Spectra of (hFGF-1+0.2mM SDS)+SOS
Spectra of hFGF-1 in the presence of different ratios of hFGF-1 to SOS and 0.2mM SDS in PB buffer in 100mM NaCl (pH 7.2) after 10 minutes of incubation at 37℃ then SOS is added and incubated for 6-7 minutes. FSS is stand for a sample containing hFGF-1, different ratio of hFGF-1 to SOS and 0.2mM SDS.*FSS is hFGF-1, 0.2mM SDS, and SOS.

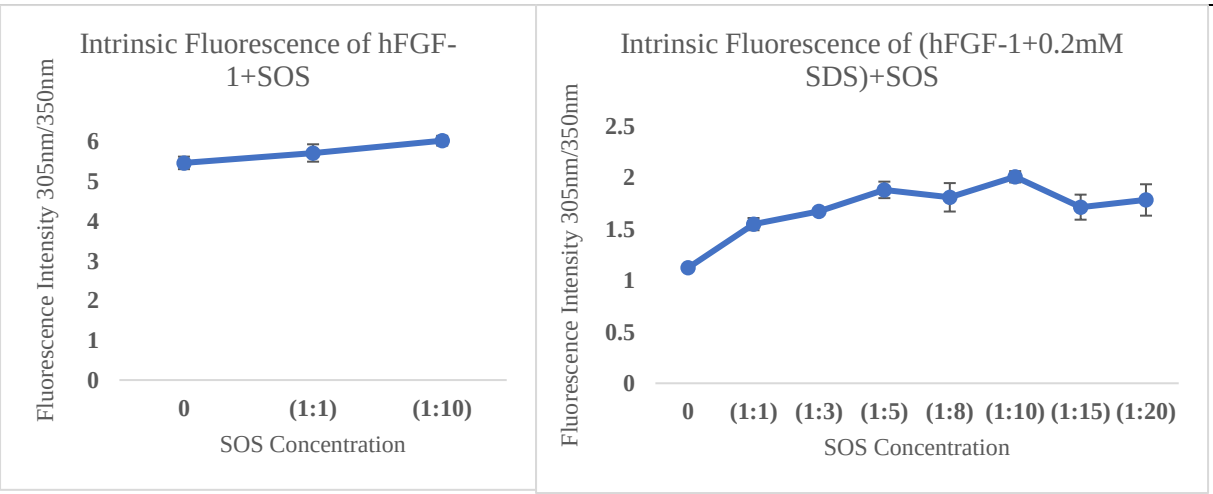

Figure 19 Intrinsic Fluorescence of (hFGF-1+0.2mM SDS) +SOS
Fluorescence intensity ratio (I_{305}/I_{350}) measured as a function of different ratios of hFGF-1 to SOS in PB buffer in 100mM NaCl. The error bars show the standard deviation of triplicate samples.

b) SDS-induced Fibrils Formation in FGF-1

Thioflavin-T (ThT), a cationic benzothiazole dye, is used as a fluorescent probe to monitor the formation and growth of amyloid fibrils. It can be used to quantify fibrillation through enhancement of emission intensity at 485nm by several orders of magnitude upon binding to the linear arrangement of β-sheets of the amyloid fibrils[74]. When the compound specifically binds to the highly ordered β-sheet structure of amyloid fibrils, the fluorescence intensity of ThT increases significantly[81].

Figure 20 showed that the relative fluorescence intensity at 485nm increases from 0.05mM and significantly exhibiting maximum intensity at 0.2mM with 40-fold increased fluorescence intensity compared to the sample containing hFGF-1 only. Furthermore, the spectrum of hFGF-1 in the presence of 0.2mM SDS shows the highest fluorescence intensity (green line in figure 21). When the concentration of SDS increase (more than 0.2mM), a decrease in fluorescence intensities are observed (0.3mM-3mM). In particular, the obvious decrease in fluorescence intensity can be observed at 2-10mM of SDS. After the concentration of SDS reached 3mM until 10mM, a plateau is observed in the fluorescence intensity. This result exhibits that at a low concentration of SDS (below the CMC), the surface-accessible grooves lined with aromatic amino acids or hydrophobic sides-chains are available for ThT binding as protein exists as a partially structured state. In addition, below the CMC, SDS can form an amyloid-like fibril structure in hFGF-1 in which ThT will specifically bind. Whereas, with increasing concentrations of SDS (above the CMC) due to conformational changes of protein, less amyloid-like fibrils structure, ThT intensity is decreased (Unpublished work by Dr. Sanhita Maity and Zeina Al Raawi in Kumar group). We can derive a conclusion that 0.2mM SDS is the concentration inducing amyloid fibril-like structure in hFGF-1. Result obtained from intrinsic

fluorescence also confirms this finding that 0.2mM of SDS cause the most significant alteration in the tertiary structure of the hFGF-1.

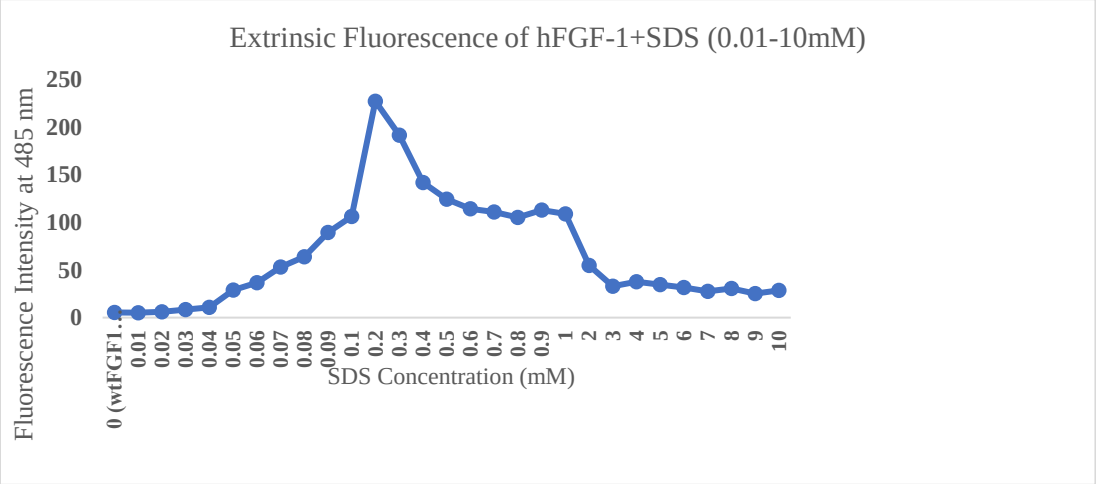

Figure 20 ThT-related growth curves of hFGF-1 in the presence of SDS
ThT-related growth curves of hFGF-1 in the presence of a different concentration of SDS (0-10mM) in 10 mM PB buffer containing 100mM NaCl (pH 7.2) at 485nm.

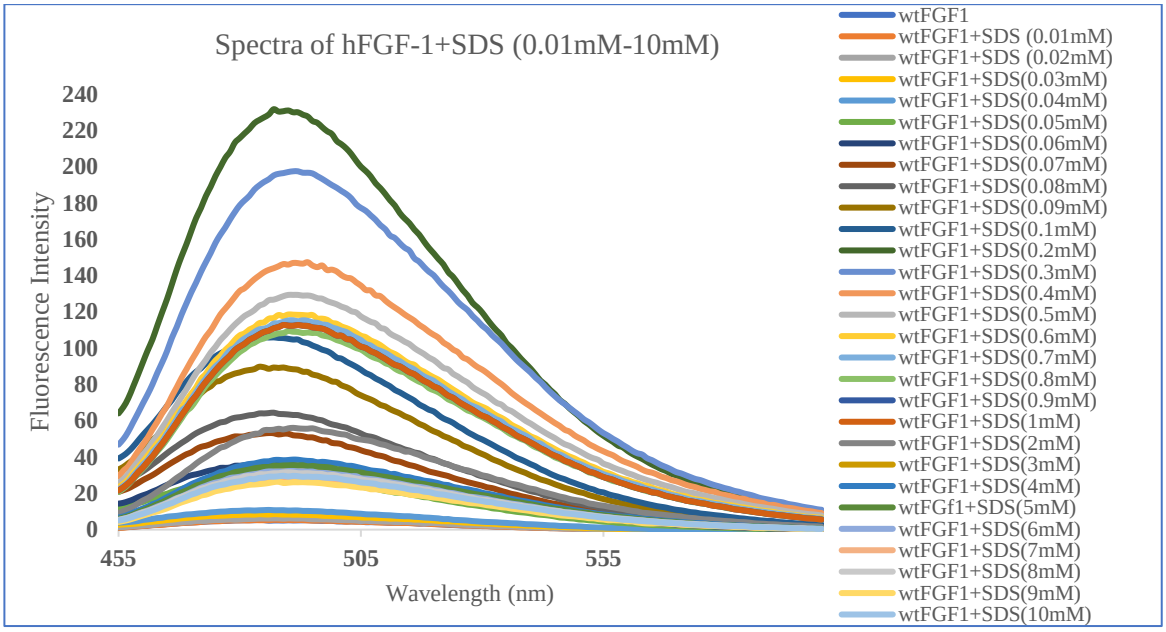

Figure 21 ThT Spectra of hFGF-1 in the presence of SDS
Spectra with the highest fluorescence intensity is shown in green. This spectrum is referred to the sample containing hFGF-1 and 0.2mM SDS. The highest intensity of the ThT spectra in sample containing hFGF-1 and 0.2mM SDS shows that this sample contains the highest magnitude of fibrillation.

In the presence of different ratios of hFGF-1 to SOS and SDS, we conduct two separate ThT assay to quantify amyloid-like fibril formation. In the first experiment, the addition of hFGF-1, SOS, 0.2mM SDS is done in simultaneous manner. Extrinsic fluorescence shows that the decrease in the fluorescence intensity at 485nm as the ratio of protein to SOS increase (figure 22). The significant reduction of fluorescence intensity is shown at a ratio of hFGF-1 to SOS at (1:10), (1:15), and (1:20). It indicates fewer fibrils are formed in these samples (less ThT binding) and SOS can protect the tertiary structure of the protein from the perturbation of SDS compare to the sample containing hFGF-1 and 0.2mM SDS only. Furthermore, it is found that the ratio of hFGF-1 to SOS (1:1) is the least effective in decreasing amyloid-like fibrils in hFGF-1.

While in the second experiment, hFGF-1 and 0.2mM SDS are first incubated for 10 minutes to allow amyloid-like fibril formation, then SOS is added, then incubation for the 6-7 minutes. ThT binding assay shows that in the presence of SOS, the fluorescence intensity at 485nm decrease as the ratio of hFGF-1 to SOS increase (figure 24). This decrease is related to the reduction of the formation of the fibrils. The significant decrease is observed at the ratio between hFGF-1 to SOS (1:15) and (1:20) relative to the sample in the absence of SOS. It suggests that SOS can reduce the formation of the amyloid-like fibrils in hFGF-1. The result from the intrinsic and ThT extrinsic fluorescence indicates that SOS can protect the tertiary structure of the hFGF-1 from the perturbation of 0.2mM SDS and reduced the fibril formation.

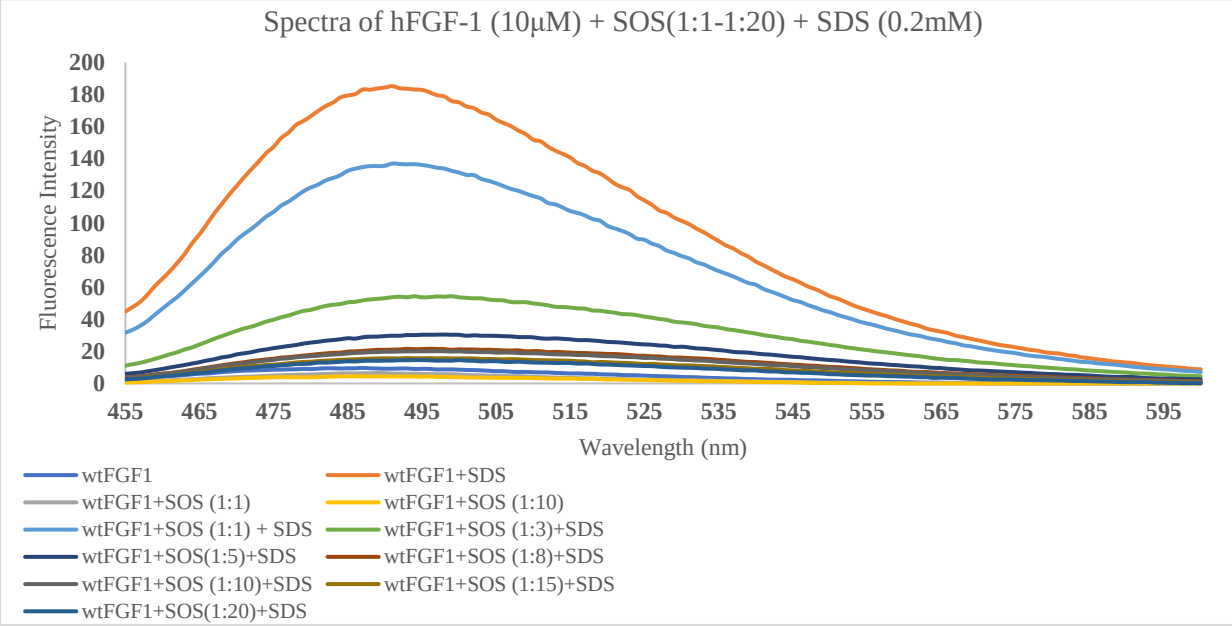

Figure 22 ThT Spectra of hFGF-1+SOS+0.2mM SDS

Spectra with the highest fluorescence intensity is shown in orange. This spectrum is referred to the sample containing hFGF-1 and 0.2mM SDS. As the concentration of SOS increases, the fluorescence intensity decreases. It indicates less fibrils bind to the ThT.

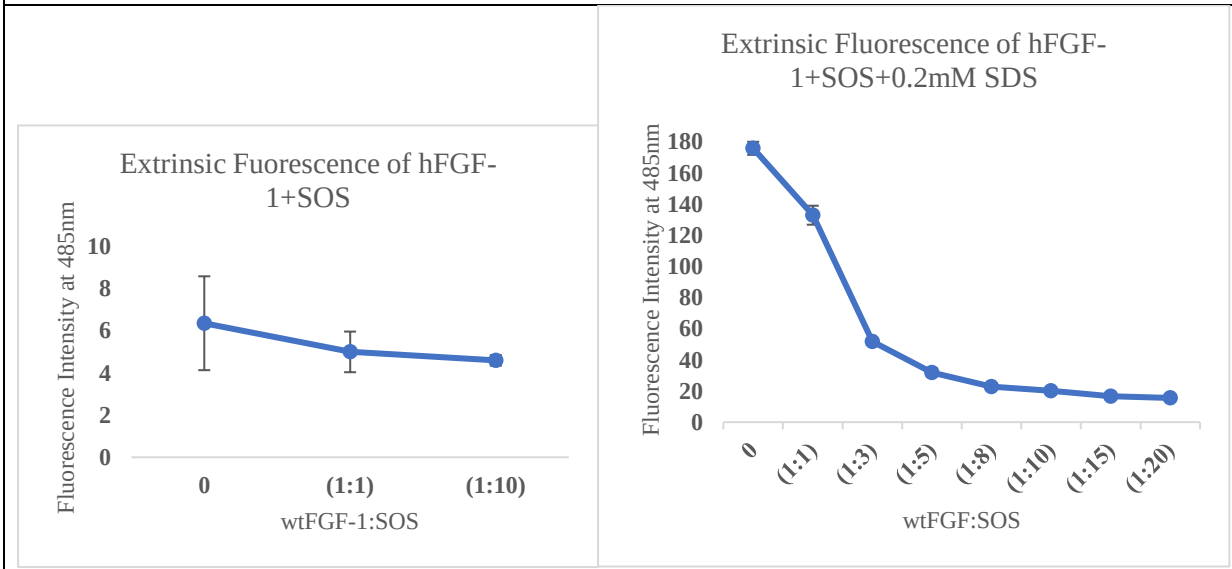

Figure 23 ThT-related growth curves of hFGF-1 in the presence of SOS and 0.2mM SDS

ThT-related growth curves of hFGF-1 in the presence of a different ratio of hFGF-1 to SOS and 0.2mM SDS in 10 mM PB buffer containing 100mM NaCl (pH 7.2) at 485nm.

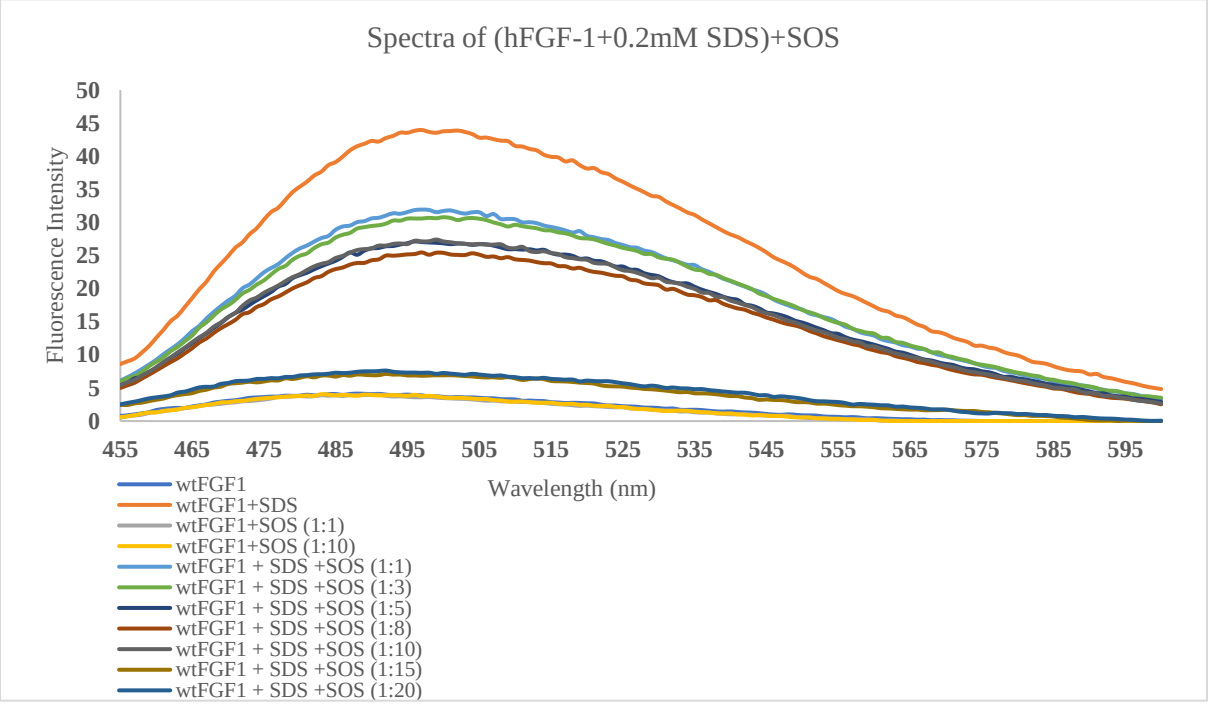

Figure 24 ThT Spectra of (hFGF-1+ 0.2mM SDS)+SOS
Spectra with the highest fluorescence intensity is shown in orange. This spectrum is referred to the sample containing hFGF-1 and 0.2mM SDS. As the concentration of SOS increases, the fluorescence intensity decreases. It indicates less fibrils binds to ThT

.

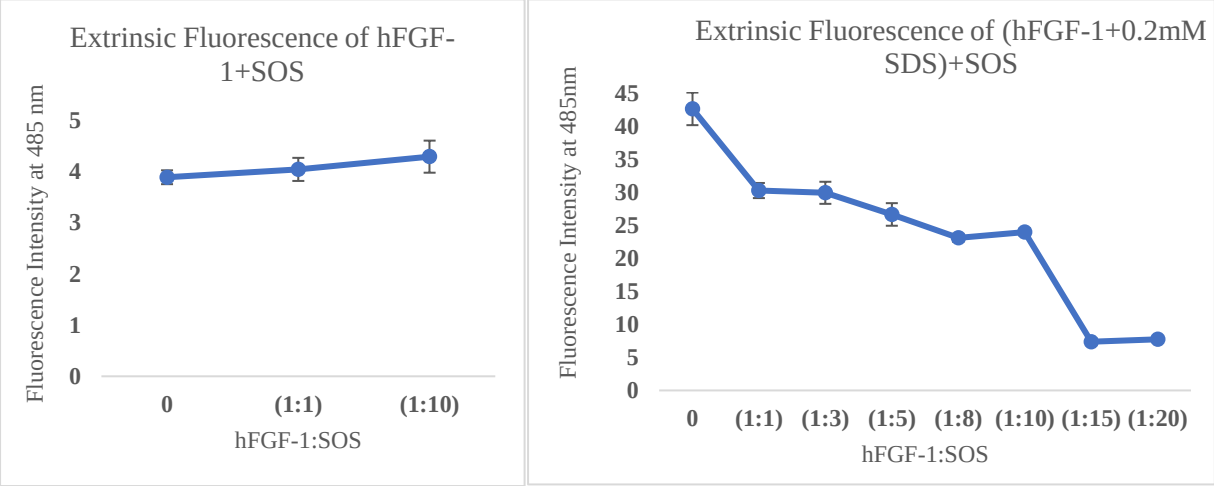

Figure 25 ThT-related growth curves of hFGF-1 in the presence of 0.2mM SDS and SOS
ThT-related growth curves of hFGF-1 in the presence of a different ratio of hFGF-1 to SOS and 0.2mM SDS in 10 mM PB buffer containing 100mM NaCl (pH 7.2) at 485nm.

c) Structure of SDS-induced Fibrils Formation in FGF-1

The morphological changes of 0.2mM SDS-induced amyloid-like fibril in hFGF-1 in the presence of SOS is examined by transmission electron microscope (TEM). TEM result in figure 33 (a) depicts the individual spherical-like aggregates which formed upon incubation of merely hFGF-1 for 24 hours at 37℃ in buffer containing 100mM NaCl in 10 mM phosphate buffer (pH 7.2). In the presence of 0.2mM SDS (figure 33 (b)), aggregates showed thicker, longer, fibrillar assemblies.

When hFGF-1 is incubated with 0.2mM SDS and hFGF-1:SOS (1:10) for 24 hours at 37℃ (Figure 33 (c)), the thick fibrillar assemblies are disaggregated, shown by a significant decrease in the length and density of the fibrillar assemblies. This data indicates that SOS could destabilize the fibrillar assemblies of hFGF-1 induced by 0.2mM SDS. Incubation of hFGF-1 with hFGF-1:SOS (1:10) and 0.2mM SDS (figure 33 (d)) shows spherical-like aggregates (the same structure was also observed in the incubation of hFGF-1 only in figure 33 (a)), less dense, and branched aggregates compare with hFGF-1 in the presence of 0.2mM SDS only. It can be suggested that the addition of SOS before 0.2mM SDS can prevent the formation of fibrillar assemblies of hFGF-1. SOS is capable of binding and stabilizing FGFs. Upon binding to SOS, FGFs are protected against high temperatures and low pH[11]. SOS binds to a positively charged region of FGF-1. This region contains residues 112-127 where SOS mainly interacts with Lys112, Arg116, Lys118, and Arg122 (heparin-binding site). Binding of SOS and FGF-1 allows the neutralization of several positively charged residues that can destabilize the native structure of FGF-1 by electrostatic repulsion[67]. Stabilization of hFGF-1 by SOS presumably protects hFGF-1 from the denaturant activity of SDS at a certain level.

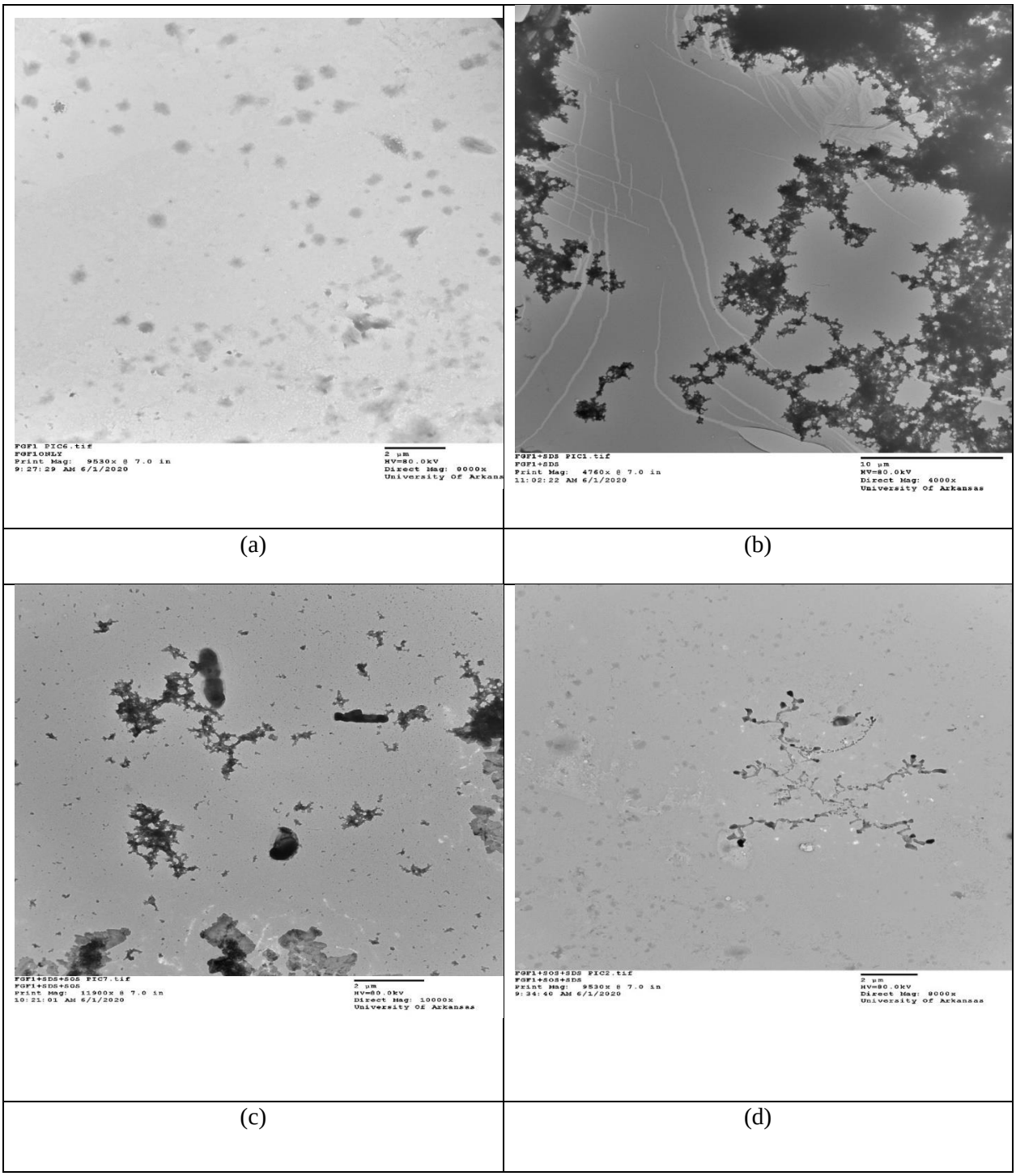

Figure 26 TEM Images

(a) hFGF-1; (b) hFGF-1 in the presence of 0.2mM SDS; (c) hFGF-1 in the presence of 0.2mM SDS and SOS (1:10); (d) hFGF-1 in the presence of SOS (1:10) and 0.2mM SDS. The reaction mixture containing 40 µM hFGF-1, hFGF-1:SOS (1:10), 0.2mM SDS, and 100 mM NaCl in 10mM phosphate buffer (pH 7.2), incubation at 37℃ for 24 hours.

d) The Flexibility of the Backbone of FGF-1 is Diminished in SDS-induced Fibrils Formation in FGF-1

Limited proteolytic digestion has been applied to map surface-exposed, flexible, or weakly structured areas of folded, globular, monomeric, and oligomeric proteins, and to assess protein folding dynamics[82]. This technique is based on the proteolytic digestion that is governed by the presence of an appropriate protease recognition sequence in the protein substrate, the availability of that sequence for cleavage, and the specificity of the proteolytic enzyme[82, 83]. In this study, limited proteolysis experiment was performed to assess the stability of SDS-induced amyloid-like fibrils towards proteolytic degradation. Trypsin was used in this experiment because hFGF-1 contains many lysine and arginine residues (a constituent of the putative heparin binding site) in its sequence, and most of them are concentrated in the C-terminal segment (residues 105-140)[83].

We carried out concentration-dependent trypsin digestion to find out the concentration of trypsin in which 80% of the hFGF-1 will be digested in 30 minutes incubation. Figure 27 depicts the result of the SDS-PAGE of concentration-dependent limited trypsin digestion of hFGF-1 and figure 28 shows the result of the densitometric analysis. We applied 0.04mg/mL (around 95% of the protein is digested) of trypsin for the time-dependent limited trypsin digestion for the hFGF-1 only, hFGF-1 in the presence of 0.2mM SDS, hFGF-1 in the presence of SOS, and hFGF-1 in the presence of both 0.2mM SDS and SOS. This trypsin concentration was chosen because it gave the highest percentage of undigested protein compare to the other concentration; even though it did not reach 80% of undigested protein in 30 minutes of incubation (figure 28). We carried out time-dependent limited trypsin digestion of hFGF-1 only with the concentration of trypsin 0.04mg/mL. This sample acts as a control that the densitometric analysis will be compared with

hFGF-1 in the presence of 0.2mM SDS, different ratio of hFGF-1 to SOS, and a combination of 0.2mM SDS and different ratio of hFGF-1 to SOS. Both the result of the SDS-PAGE and the densitometric analysis in (figure 29 and 30) show that in 5-10 minutes almost all of the protein is digested.

Figure 27 The SDS-PAGE analysis of hFGF-1 concentration-dependent limited trypsin digestion.
Lane 1: hFGF-1 only. Lane 2: hFGF-1+0.02mg/mL trypsin. Lane 3: hFGF-1+0.04mg/mL trypsin. Lane 4: hFGF-1+0.06mg/mL trypsin. Lane 5: hFGF-1+0.08 mg/mL trypsin. Lane 6: hFGF-1+0.1 mg/mL trypsin. Lane 7: hFGF-1+0.2 mg/mL trypsin. Lane 8: hFGF-1+0.4 mg/mL trypsin. Lane 9: hFGF-1+0.5 mg/mL trypsin. Lane 10: trypsin only. All samples are incubated for 30 minutes.

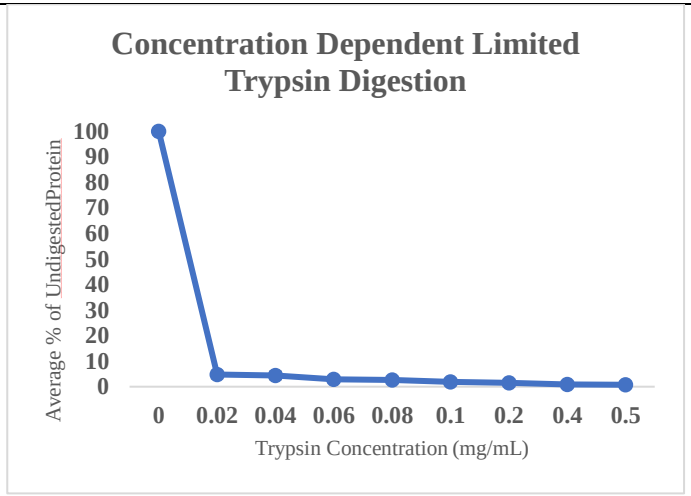

Figure 28 Densitometric analysis of concentration-dependent limited trypsin digestion of hFGF-1

Figure 29 The SDS-PAGE analysis of hFGF-1 time-dependent limited trypsin digestion (0.04mg/mL).
All samples contain hFGF-1 and trypsin 0.04 mg/mL. Lane 1: hFGF-1 only. Lane 2: 1 minute incubation. Lane 3: 2 minutes incubation. Lane 4: 4 minutes incubation. Lane 5: 5 minutes incubation. Lane 6: 6 minutes incubation. Lane 7: 8 minutes incubation. Lane 8: 10 minutes incubation. Lane 9: hFGF-1. Lane 10: 12 minutes incubation. Lane 11: 15 minutes incubation. Lane 12: 18 minutes incubation. Lane 13: 21 minutes incubation. Lane 14: 24 minutes incubation. Lane 15: 27 minutes incubation. Lane 16: 30 minutes incubation

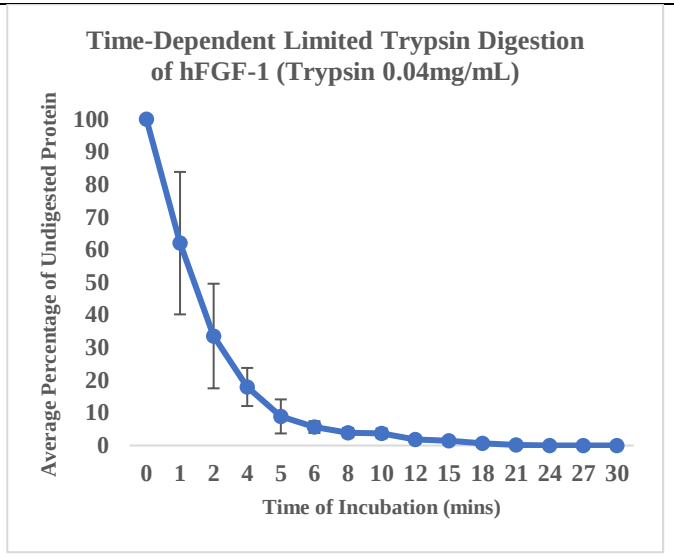

Figure 18 Densitometric analysis of time-dependent limited trypsin digestion of hFGF-1

SDS-PAGE result from the trypsin digestion of SDS-induced amyloid-like fibrils in hFGF-1 (figure 31) showed that SDS-induced fibrils are not totally digested after 30 minutes of incubation (figure 31). It is also observed that trypsin digestion is slower in SDS-induced amyloid-like fibrils (figure 32) compared to the digestion of native hFGF-1. This result shows that SDS-induced amyloid-like fibrils in hFGF-1 are resistant to proteolytic degradation, one of the peculiar characteristics of amyloid fibrils[84]. In the presence of different ratios of hFGF-1 to SOS (1:1 and 1:10), the SDS-PAGE results show that hFGF-1 is resistant to proteolytic degradation where the bands of the hFGF-1 are still intact until 30 minutes of incubation with trypsin (figure 33 and 35). The densitometric analysis shows that in the presence of SOS (1:10) (figure 36), the degree of insusceptibility of hFGF-1 to the proteolytic degradation increase in which around 20% of the protein is digested. Whereas, approximately 40% of the protein is digested in the presence of SOS (1:1) (figure 34). Upon binding of SOS, hFGF-1 is stabilized by the elimination of electrostatic repulsion so that it is resistant towards proteolytic degradation. Moreover, it indicates that upon binding of SOS, hFGF-1 is less dynamic/mobile; in many cases, limited proteolysis was observed to take place at sites of the polypeptide chain exhibiting high segmental mobility[84].

In the presence of SOS (1:1 and 1:10), SDS-induced amyloid-like fibrils in hFGF-1 are resistant to proteolytic degradation shown by the SDS-PAGE result in which the bands are still intact until 30 minutes of incubation with trypsin (figure 37 and figure 39). The densitometric analysis shows that SDS- induced fibril is digested to around 70% after exposure to SOS (1:1) (figure 38). While, after exposure to SOS (1:10), densitometric analysis (figure 40) shows that SDS- induced fibril is digested to approximately 80%.

Figure 31 The SDS-PAGE analysis of time-dependent limited trypsin digestion of hFGF-1, SDS 0.2mM, and trypsin 0.04mg/mL.

All samples contain hFGF-1, 0.2mM SDS, and 0.04mg/mL trypsin. Lane 1: hFGF-1+0.2mM SDS (0 minute). Lane 2: 1 minute incubation. Lane 3: 2 minutes incubation. Lane 4: 4 minutes incubation. Lane 5: 5 minutes incubation. Lane 6: 6 minutes incubation. Lane 7: 8 minutes incubation. Lane 8: 10 minutes incubation. Lane 9: 12 minutes incubation. Lane 10: 15 minutes incubation. Lane 11: 18 minutes incubation. Lane 12: 21 minutes incubation. Lane 13: 24 minutes incubation. Lane 14: 27 minutes incubation. Lane 15: 30 minutes incubation.

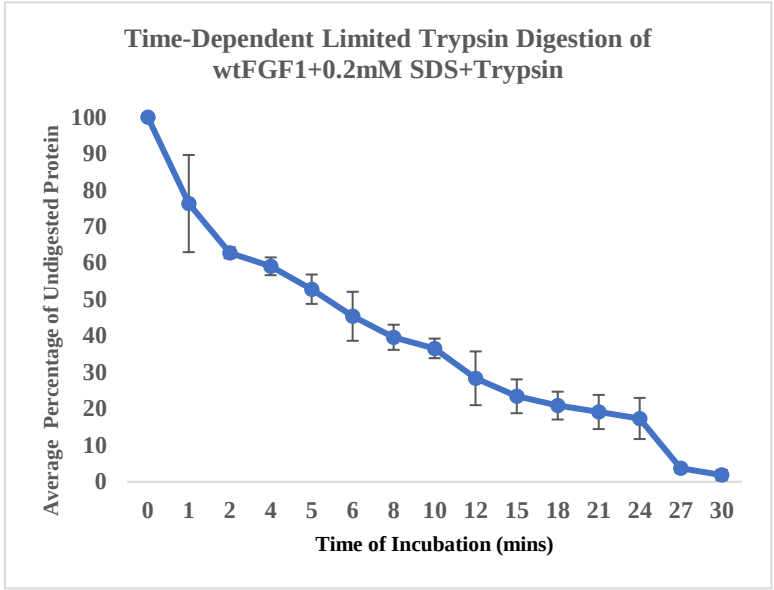

Figure 32 Densitometric analysis of time-dependent limited trypsin digestion of hFGF-1, SDS 0.2mM, and trypsin 0.04mg/mL.

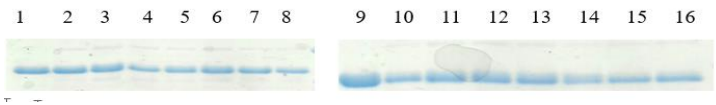

Figure 33 The SDS-PAGE analysis of time-dependent limited trypsin digestion of hFGF-1, hFGF-1:SOS (1:1), and 0.04mg/mL trypsin.

All samples contain hFGF-1, hFGF-1:SOS (1:1), and 0.04mg/mL trypsin. Lane 1: hFGF-1+SOS (1:1). Lane 2: 1 minute incubation. Lane 3: 2 minutes incubation. Lane 4: 4 minutes incubation. Lane 5: 5 minutes incubation. Lane 6: 6 minutes incubation. Lane 7: 8 minutes incubation. Lane 8: 10 minutes incubation. Lane 9: hFGF-1+SOS (1:1). Lane 10: 12 minutes incubation. Lane 11: 15 minutes incubation. Lane 12: 18 minutes incubation. Lane 13: 21 minutes incubation. Lane 14: 24 minutes incubation. Lane 15: 27 minutes incubation. Lane 16: 30 minutes incubation.

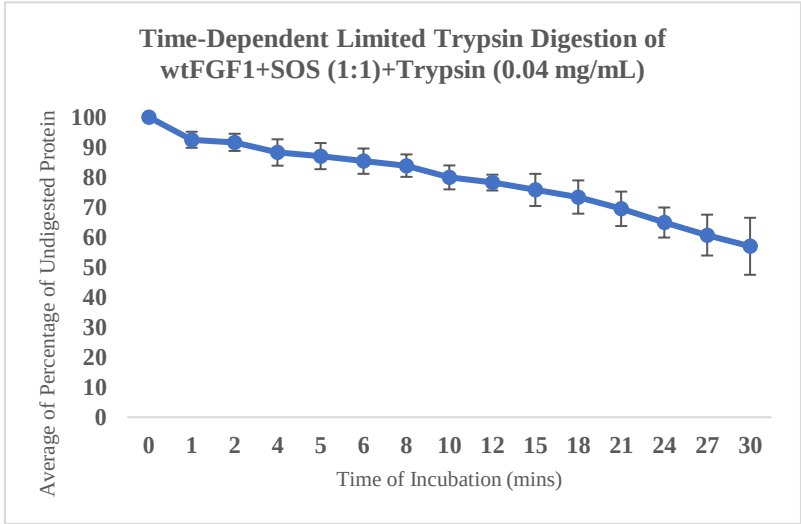

Figure 34 Densitometric analysis of time-dependent limited trypsin digestion of hFGF-1, hFGF-1:SOS (1:1), and trypsin 0.04mg/mL.

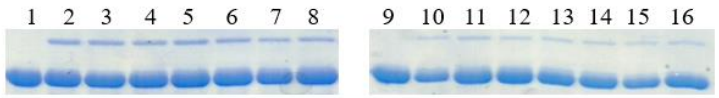

Figure 35 The SDS-PAGE analysis of time-dependent limited trypsin digestion hFGF-1, SOS (1:10), trypsin 0.04mg/mL.

All samples contain hFGF-1, hFGF-1:SOS (1:10), and trypsin 0.04mg/mL. Lane 1: hFGF-1+SOS (1:10). Lane 2: 1 minute incubation. Lane 3: 2 minutes incubation. Lane 4: 4 minutes incubation. Lane 5: 5 minutes incubation. Lane 6: 6 minutes incubation. Lane 7: 8 minutes incubation. Lane 8: 10 minutes incubation. Lane 9: hFGF-1+SOS (1:10). Lane 10: 12 minutes incubation. Lane 11: 15 minutes incubation. Lane 12: 18 minutes incubation. Lane 13: 21 minutes incubation. Lane 14: 24 minutes incubation. Lane 15: 27 minutes incubation. Lane 16: 30 minutes incubation.

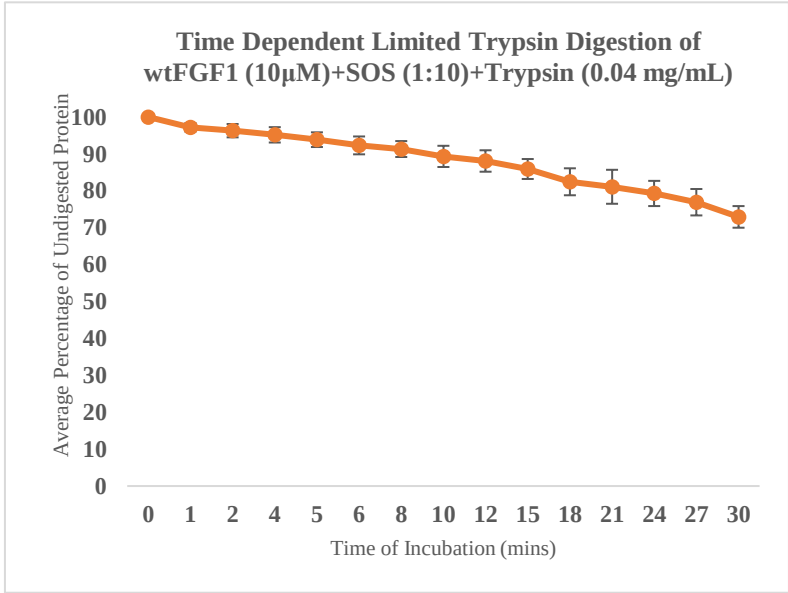

Figure 36 Densitometric analysis of time-dependent limited trypsin digestion of hFGF-1, SOS (1:10), and trypsin 0.04mg/mL.

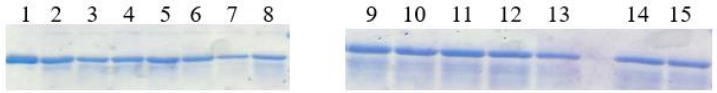

Figure 37 The SDS-PAGE analysis of time-dependent limited trypsin digestion hFGF-1, SDS 0.2mM, SOS (1:1), and trypsin 0.04mg/mL.

All samples contain hFGF-1, SDS 0.2mM, and hFGF-1:SOS (1:1), and trypsin 0.04mg/mL. Lane 1: hFGF-1+SDS 0.2mM+SOS (1:1). Lane 2: 1 minute incubation. Lane 3: 2 minutes incubation. Lane 4: 4 minutes incubation. Lane 5: 5 minutes incubation. Lane 6: 6 minutes incubation. Lane 7: 8 minutes incubation. Lane 8: 10 minutes incubation. Lane 9: 12 minutes incubation. Lane 10: 15 minutes incubation. Lane 11: 18 minutes incubation. Lane 12: 21 minutes incubation. Lane 13: 24 minutes incubation. Lane 14: 27 minutes incubation. Lane 15: 30 minutes incubation.

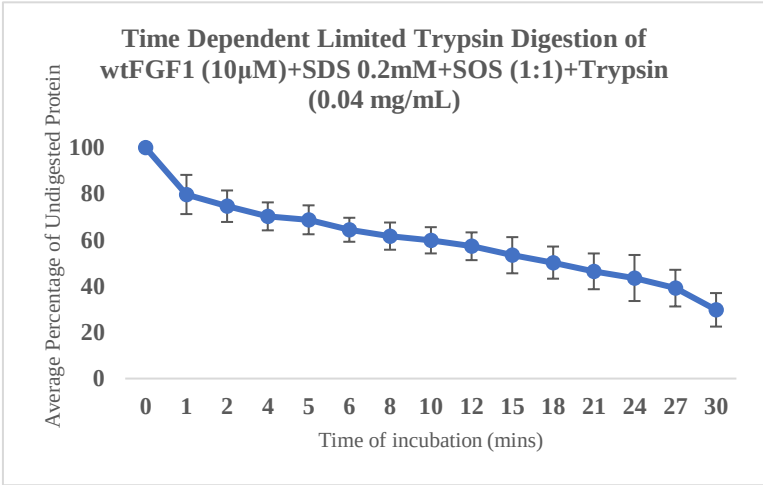

Figure 38 Densitometric analysis of time-dependent limited trypsin digestion of hFGF-1, SDS 0.2mM, SOS (1:1), trypsin 0.04mg/mL.

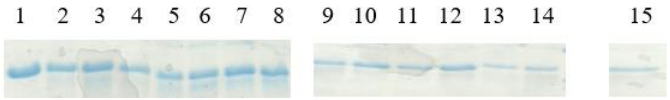

Figure 39 The SDS-PAGE analysis of time-dependent limited trypsin digestion of hFGF-1, SDS 0.2mM, SOS (1:10), and trypsin 0.04mg/mL.

All samples contain hFGF-1, SDS 0.2mM, and hFGF-1:SOS (1:10), and trypsin 0.04mg/mL. Lane 1: hFGF-1+SDS 0.2mM+SOS (1:10). Lane 2: 1 minute incubation. Lane 3: 2 minutes incubation. Lane 4: 4 minutes incubation. Lane 5: 5 minutes incubation. Lane 6: 6 minutes incubation. Lane 7: 8 minutes incubation. Lane 8: 10 minutes incubation. Lane 9: 12 minutes incubation. Lane 10: 15 minutes incubation. Lane 11: 18 minutes incubation. Lane 12: 24 minutes incubation. Lane 13: 27 minutes incubation. Lane 14: 30 minutes incubation. Lane 15: 21 minutes incubation.

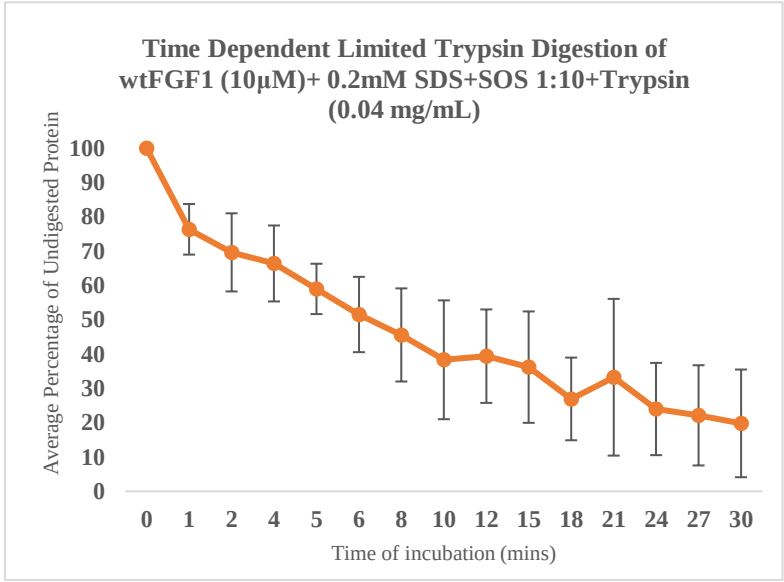

Figure 40 Densitometric analysis of time-dependent limited trypsin digestion of hFGF-1, SDS 0.2mM, SOS (1:10), and trypsin 0.04 mg/mL

When hFGF-1 was incubated for 6-7 minutes with SOS (1:15) and followed by the addition of 0.2mM SDS with 10 minutes incubation, the densitometric analysis profile is almost the same with the samples containing hFGF-1 and SOS (1:10) (figure 43). The same result was also found in samples that contain SOS (1:15), 0.2mM SDS, and hFGF-1 (figure 44). It can be suggested that this resistant property is due to the stabilization effect of the SOS that reduces the flexibility of hFGF-1 so that SDS cannot access the protein and perturb its structure.

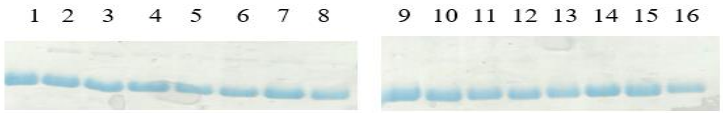

Figure 41The SDS-PAGE analysis of hFGF-1 time-dependent limited trypsin digestion of hFGF-1, SOS (1:15), SDS 0.2mM, and trypsin 0.04mg/mL.
All samples contain hFGF-1, hFGF-1:SOS (1:10), and SDS 0.2mM, and trypsin 0.04mg/mL. Lane 1: hFGF-1+ SOS (1:15)+SDS 0.2mM. Lane 2: 1 minute incubation. Lane 3: 2 minutes incubation. Lane 4: 4 minutes incubation. Lane 5: 5 minutes incubation. Lane 6: 6 minutes incubation. Lane 7: 8 minutes incubation. Lane 8: 10 minutes incubation. Lane 9: hFGF-1+ SOS (1:15)+SDS 0.2mM. Lane 10: 12 minutes incubation. Lane 11: 15 minutes incubation. Lane 12: 18 minutes incubation. Lane 13: 21 minutes incubation. Lane 14: 24 minutes incubation. Lane 15: 27 minutes incubation. Lane 16: 30 minutes incubation.

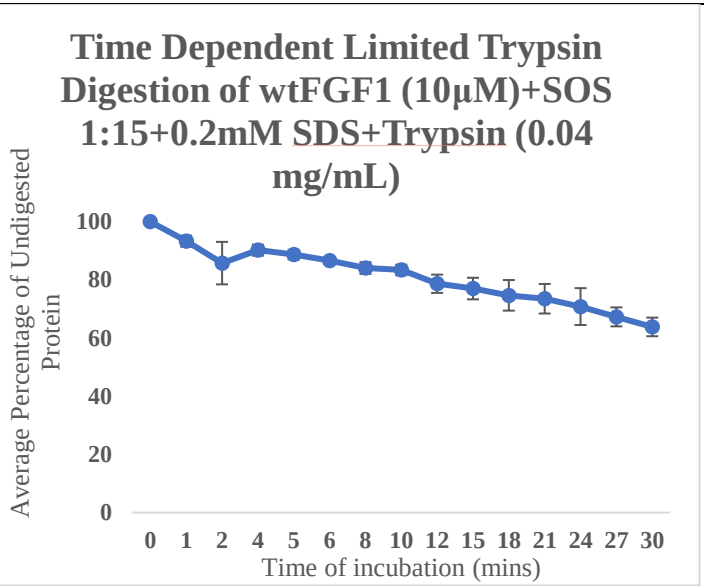

Figure 42 Densitometric analysis of time-dependent limited trypsin digestion of hFGF-1, SOS (1:15), SDS 0.2mM SDS, and trypsin 0.04mg/mL

Overall, these experiments show that hFGF-1 in the presence of 0.2mM SDS (SDS-induced amyloid-like fibrils) and SOS (in different order of addition) are resistant to proteolytic degradation in different degree compare to native hFGF-1 (figure 45). If SOS can disrupt the fibrils (green line in figure 45), fragments of the fibrils show more resistance to proteolytic degradation compare to the SDS-induced amyloid-like fibrils itself (orange line in figure 45). Since the profile of the densitometric analysis of a sample containing hFGF-1 and SOS (1:10) is almost the same as the sample containing hFGF-1, SOS (1:15), and 0.2 mM SDS. It can be suggested that SOS stabilizes the protein and reduce its mobility so that trypsin could not digest the protein, and SDS could not fully perturb the structure of hFGF-1. Presumably, stabilization of the heparin-binding pocket renders the ability of hFGF-1 to protect and reduce the chance of amyloid fibrils formation induced by 0.2mM SDS.

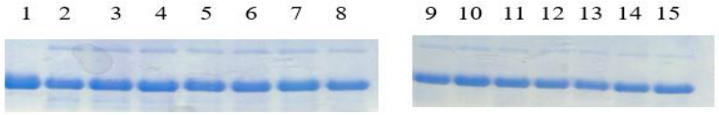

Figure 43 The SDS-PAGE analysis of hFGF-1 time-dependent limited trypsin digestion of SOS (1:15), SDS 0.2mM, and hFGF-1.

All samples contain SOS (1:15), SDS 0.2mM, and hFGF-1, and trypsin 0.04mg/mL. Lane 1: SOS (1:15)+ SDS 0.2mM+hFGF-1. Lane 2: 1 minute incubation. Lane 3: 2 minutes incubation. Lane 4: 4 minutes incubation. Lane 5: 5 minutes incubation. Lane 6: 6 minutes incubation. Lane 7: 8 minutes incubation. Lane 8: 10 minutes incubation. Lane 9: 12 minutes incubation. Lane 10: 15 minutes incubation. Lane 11: 18 minutes incubation. Lane 12: 21 minutes incubation. Lane 13: 24 minutes incubation. Lane 14: 27 minutes incubation. Lane 15: 30 minutes incubation.

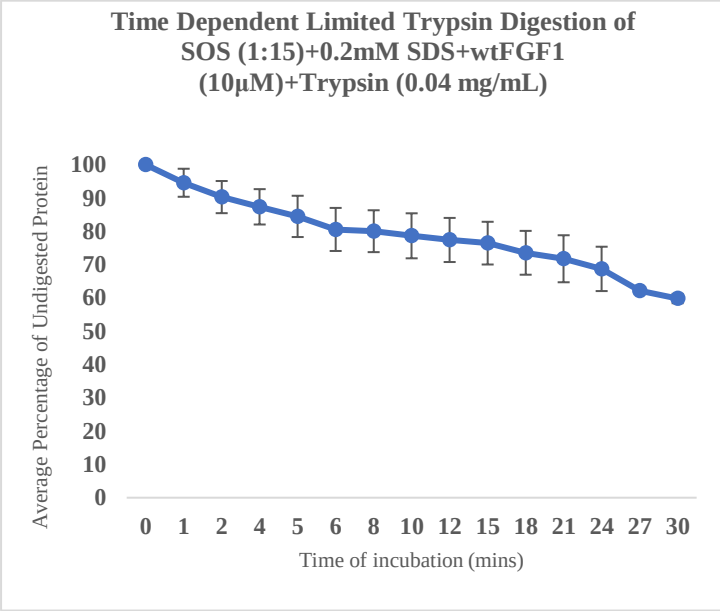

Figure 44 Densitometric analysis of hFGF-1 time-dependent limited trypsin digestion of SOS (1:15), SDS 0.2mM, and trypsin 0.04mg/mL

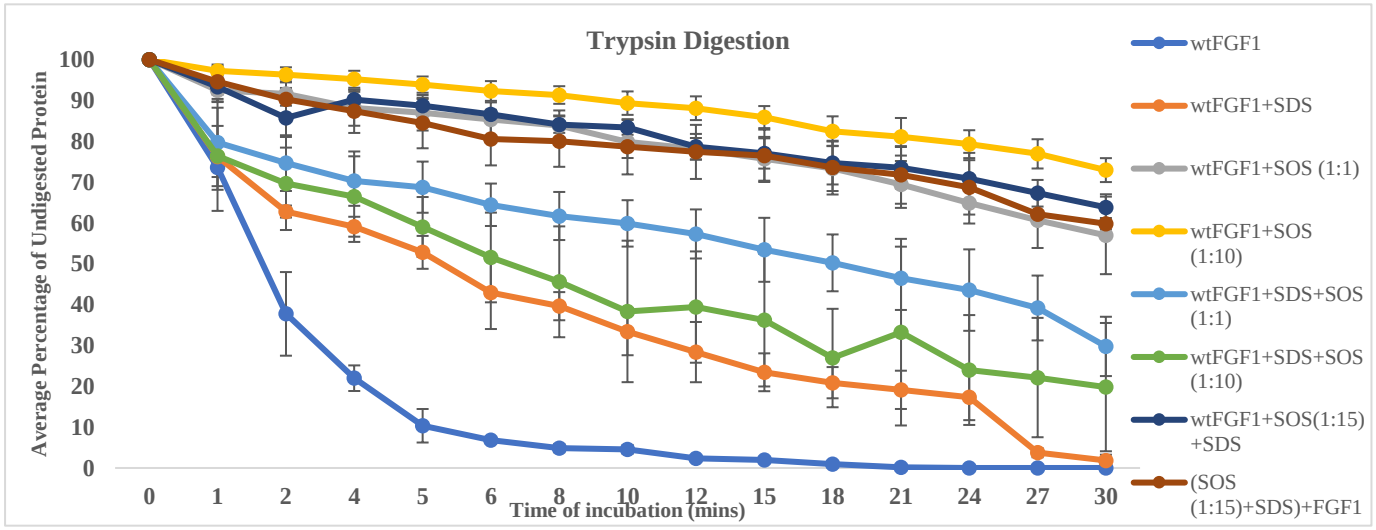

Figure 45 Compilation of time-dependent limited trypsin digestion.

e) SDS Binding-site in FGF-1

The basic of the mass spectrometry (MS) is the conversion of the molecules to gaseous ions in the ion source[85]. Then, separation is based on their mass-to-charge ratios (m/z) in the mass analyzer[85]. MS has emerged as a highly sensitive technique for amyloid aggregation studies and provides new and complementary insights into the onset of amyloid fibrils, including oligomer characterization, aggregation mechanism investigation, and inhibitor screening[85]. Nevertheless, in general, mass spectrometric methods have a relatively low tolerance for salts, buffers, and other sample impurities[86]. This obstacle is overcome by the one feature of matrix-assisted laser desorption/ionization time-of-flight mass spectrometry (MALDI-TOF MS)[86]. Its ability to detect biomolecules in complex mixtures in the presence of large molar excesses of salts, buffers, and other species is the feature of MALDI-TOF that makes it a promising technique for mass spectrometric analysis of biological samples[86].

We performed MALDI-TOF mass spectrometry to analyze the tryptic fragment of the hFGF-1; SDS-induced amyloid-like fibrils in hFGF-1, and the presence of SOS; hFGF-1-SOS complex in the presence of 0.2mM SDS. The concentration of trypsin was 0.04mg/mL, and after the addition of trypsin, all samples were incubated for 30 minutes. Figure 46 and 47 show the tryptic fragment of the hFGF-1 only and hFGF-1 in the presence of SDS 0.2mM after 30 minutes, respectively. A comparison of the tryptic fragment from the two samples demonstrates that peptide fragment AILFLPLPVSSD with the m/z 1271.868 is missing in SDS-induced amyloid-fibrils. This finding suggests that this fragment is resistant to trypsin digestion. However, this tryptic fragment is not fused with other amino acid residues. This result is confirmed by the time-dependent limited trypsin digestion in which SDS-induced amyloid-like fibrils in hFGF-1 is resistant to proteolytic degradation.

Table 1 Mass to charge ratio (m/z) of tryptic fragments

Theoritical cleavage of hFGF-1 by trypsin (ExPASy)	m/z of hFGF-1	m/z of hFGF-1+ SDS 0.2mM	m/z of hFGF-1+SDS 0.2mM+SOS(1:1)	m/z of hFGF-1+SOS(1:1)+SDS 0.2mM
1379.6	733.353	733.289	733.345	863.483
1414.54	863.513	863.513	863.505	991.618
2244.49	991.651	991.608	991.637	1143.693
3482.79	1143.792	1143.792	1143.715	1180.687
1510.62	1271.868	1180.668	1180.705	1379.839
611.7	1379.886	1379.820	1271.862	1510.910
863.03	1180.720	1510.880	1379.873	1639.025
635.74	1510.950	1639	1328.872	2244.381
888.98	1639.061	2244.357	1414.924	2515.484
2525.02	2244.424	2515.456	1510.979	3481.482
	2515.550	3481.497	1534.037	
	3481.580		1639.062	
			2244.411	
			2515.525	
			3481.525	

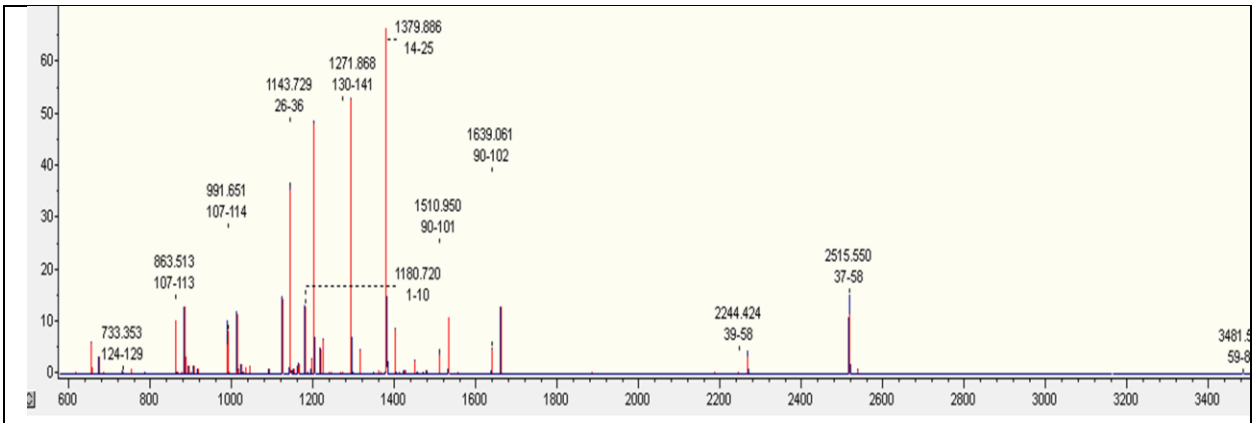

Figure 46 MALDI-TOF Mass Spectrometry Analysis of hFGF-1

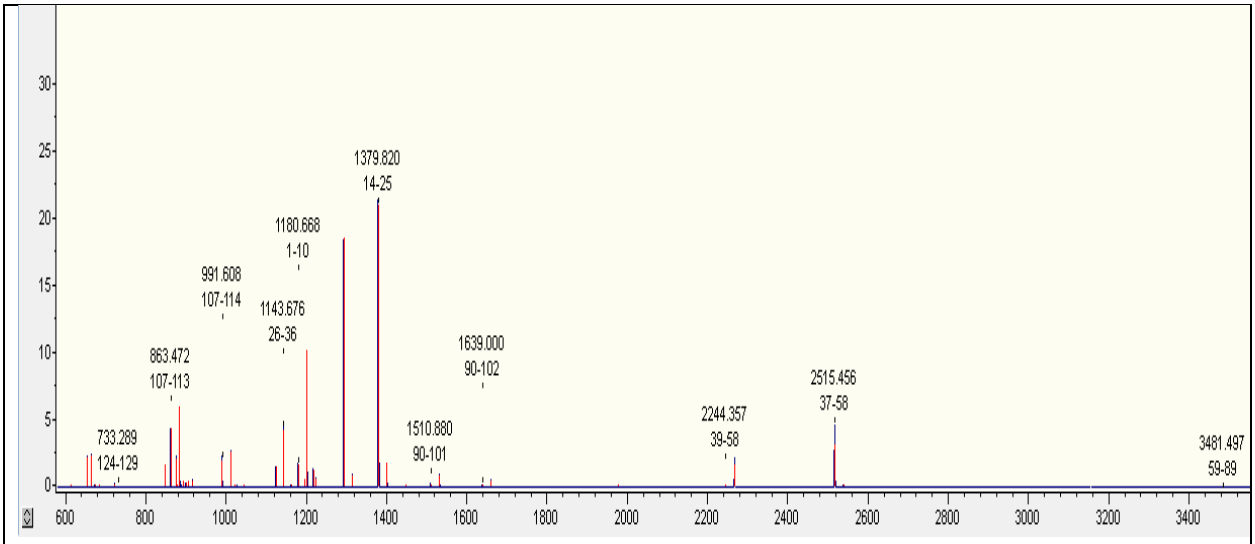

Figure 47 MALDI-TOF Mass Spectrometry Analysis of hFGF-1+SDS 0.2mM

Comparing the fragment of the fibrils to hFGF-1 in the presence of SDS 0.2mM and SOS (1:1) shows that all of the fragments of the fibrils are found in hFGF-1 in the presence of SDS 0.2mM and SOS (1:1). But there are three fragments that exist only in hFGF-1 in the presence of SDS 0.2mM and SOS (1:1), fragment with the m/z of 1271.862, 1328.872, and 1414.924. Fragment with the m/z 1271.862 corresponds to the AILFLPLPVSSD, which also finds in

hFGF-1 only. It suggests that SOS perturb the structure of the fibrils. Extrinsic, Intrinsic fluorescence and TEM results confirm this finding. TEM result indicates that SOS could destabilize the fibrillar assemblies of hFGF-1 induced by 0.2mM SDS. The extrinsic fluorescence result demonstrates the decrease in the fluorescence intensity at 485nm in the presence of SOS (decrease in aggregation). Moreover, intrinsic fluorescence shows that fibrils in the presence of different ratios of protein to SOS have a higher value of I_{305}/I_{350} compare in the absence of SOS. This indicates an alteration in the structure of the fibrils.

All of the fragments found in the fibrils also exist in the hFGF-1, SOS (1:1), and SDS 0.2mM, except one fragment with the m/z 733.289 (also found in hFGF-1). This indicates that this concentration is not optimum to protect the structure of the hFGF-1. The result from the intrinsic and extrinsic fluorescence also supports this finding, in the presence of SOS (1:1) the I_{305}/I_{350} shows the lowest value and the fluorescence intensity at 485 nm shows the highest value in comparison to other ratios of protein to SOS.

We could not get the signal for the sample containing SOS (1:10). Presumably, this ratio of hFGF-1 to SOS protects the structure of the hFGF-1 so that trypsin could not access and digest the protein. Intrinsic fluorescence shows that SOS (1:10) shows the higher value of I_{305}/I_{350} compare to the presence of SOS in a lower ratio. At the same time, the result of extrinsic fluorescence shows a significant decrease of fluorescence intensity at 485 nm in the presence of SOS (1:10).

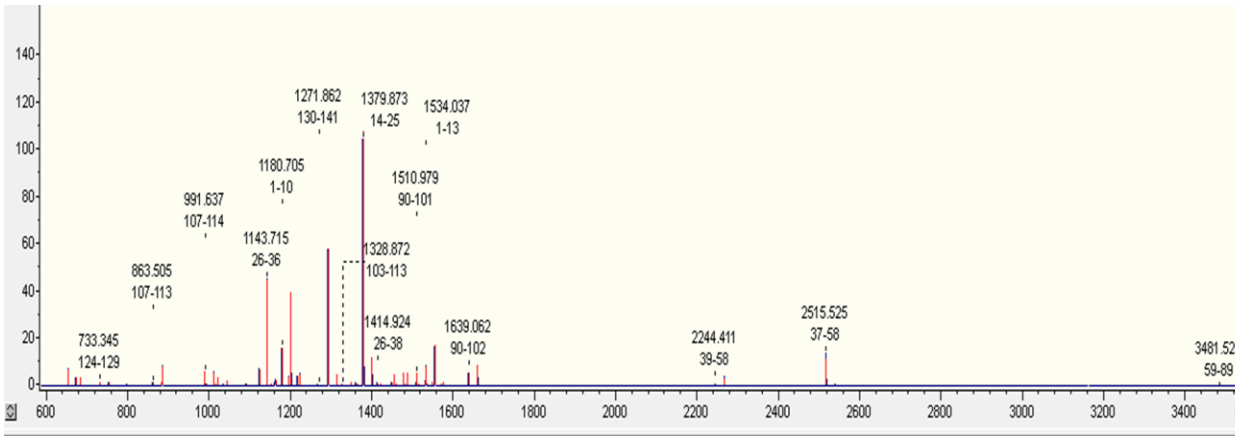

Figure 48 MALDI-TOF Mass Spectrometry Analysis of hFGF-1+0.2mM SDS+SOS (1:1)

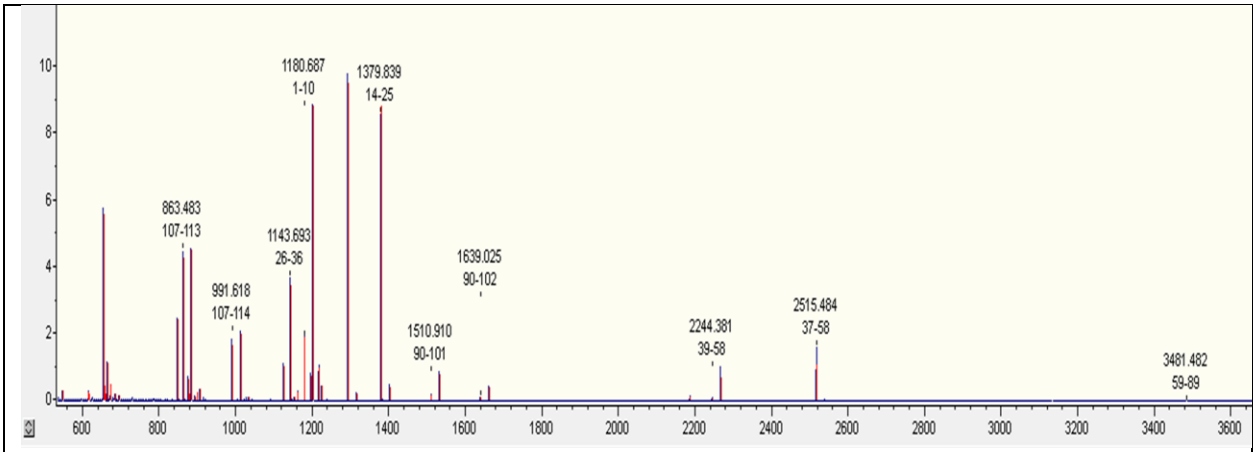

Figure 49 MALDI-TOF Mass Spectrometry Analysis of hFGF-1+SOS (1:1)+SDS 0.2mM

DISCUSSION

FGF-1 is known for its low stability and short half-life *in vivo*[87]. Almost 50% of the protein is in the unfolded state at physiological temperature. The unfolded state of the FGF-1 is known to be more susceptible to protease action[87-89]. SDS, an anionic detergent, resembles some characteristics of biological membranes and a good representation of anionic phospholipids[90]. The use of SDS as a fibrillar inducer is related to some reports in which lipid molecules presumably played roles in the conformational change of various amyloid precursor protein and the amyloid fibril formation in-vitro[91-93]. Electrostatic and hydrophobic interactions between

SDS and a protein can trigger protein conformational changes, both their secondary and tertiary structure[94].

Moreover, SDS triggers the formation of aggregates or amyloid-like fibrils in vitro in some proteins or peptides[95, 96]. Several investigations were attributed to the effect of SDS on protein amyloid aggregation, with two contrary effects, inhibition, or enhancer of amyloid formation; these effects are concentration dependent[90, 97-99]. The perturbation of protein structure by SDS involves two primary and distinct events, tertiary structure unfolding in the sub micellar and chain expansion in the micellar range of SDS concentrations[100]. The CMC for SDS is 7-8 mM in water but around 0.8-1 mM I PBS buffer[97]. Above its critical micelle concentration (CMC), SDS has been known to stabilize peptides in helical conformations[101, 102], whereas, below its CMC, SDS has been shown to stabilize β-strands[103, 104].

Pertinhez and coworkers (2002) reported that a high concentration of SDS (20mM) causes the formation of a stable α-helical structure of SCR3 peptide that does not convert into amyloid fibrils over the time of the investigation. Whereas, in the presence of sub-micellar (3mM) SDS, a large quantity of fibrillar structures was observed[96]. Another study, concentration of SDS above 1mM (above CMC) is found to increase α-helix content of β_2-microglobulin (β_2-m) to around 10%, while reducing β-sheet content to approximately 20%[90]. A structural investigation of the SDS-induced fibrillation of α-synuclein (αSN) showed that SDS at concentration 1.2-3mM could not form aggregation; it is found that SDS at a concentration of 0.3-1.2mM generated optimum aggregation at dip 1 (highest enthalpic changes associated with SDS binding)[97]. It is also found that the SDS molecules possess great potential to induce amyloid formation in twenty-five proteins including lysozyme and human serum albumin. This ability is observed when protein is in partially unfolded states (below two units of pI)[105].

In another study, thermally induced amyloid formation are found in *Notopthalmus viridescens* FGF-1 (nFGF-1). Maximum fibril formation is observed at 65℃. Thermal induced fibrils of nFGF-1 possess a typical "cross-β" structure with the β-strands perpendicular to the fibril axis. The coalescence of the protein (in the intermediate state (s)) through the solvent-exposed non-polar surface(s) is the mechanism behind the fibril formation[106].

The combined results of fluorescence spectroscopy, limited trypsin digestion, transmission electron microscope (TEM), and mass spectrometry suggest that 0.2mM is the optimum concentration of SDS to induce amyloid-like fibrils formation in hFGF-1. The presence of SOS in the fibrillar structure of hFGF-1 induced by the SDS cause disaggregation of the fibrillar structure. Furthermore, SOS seems to protect the structure of hFGF-1 so that trypsin cannot digest the protein, and SDS cannot perturb the tertiary structure of the protein. Upon binding to SOS, FGFs are protected against high temperatures and low pH[11]. SOS binds to a positively charged region of FGF-1. This region contains residues 112-127 where SOS mainly interacts with Lys112, Arg116, Lys118, and Arg122 (heparin-binding site). Binding of SOS and FGF-1 allows the neutralization of several positively charged residues that can destabilize the native structure of FGF-1 by electrostatic repulsion[67]. Stabilization of hFGF-1 by SOS presumably protects hFGF-1 from the denaturant activity of SDS at a certain level.

Stabilization of the heparin-binding pocket renders the ability of hFGF-1 to protect hFGF-1 and reduce the chance of amyloid fibrils formation. It has been known that under physiological conditions, proteins present in equilibrium between ensembles of unfolded states (U) and native states (N)[107]. Results obtained from this research suggest that the molecular mechanism in which SOS can protect and reduce the chance of fibrils formation is presumably through the stabilization of the native states of the hFGF-1 and also refolding unfolded states of

the protein at particular degree. SOS seems to push the equilibrium to the more native, folded state of the protein in the presence of 0.2mM SDS.

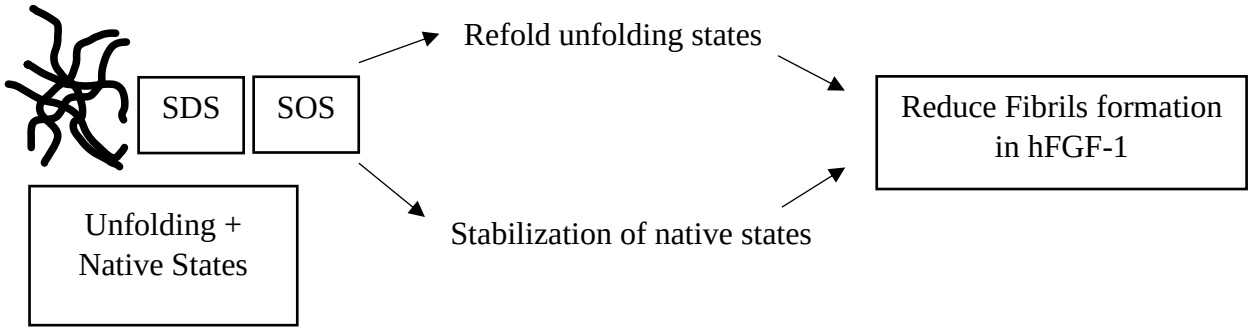

Figure 50 Molecular Mechanism of SOS in Protecting and Reducing Fibrils Formation in hFGF-1

Some previous studies link the presence of high levels of FGF-1 and the occurrence of Alzheimer's disease. The first study observed that astrocytes containing high levels of FGF-1 presented around senile plaques in seven Alzheimer's patients' postmortem brain tissue[6]. The examination was conducted by immunohistochemistry employing a specific antiserum against FGF-1[6]. The diagnosis of Alzheimer's disease was established in every case by the presence of a large amount of plaques and tangles[6]. Plaques were presumed due to the high binding affinity between FGF-1 and heparan sulfate proteoglycan[6]. This presumption is strengthened by the fact that the mitogenic activity of FGF-1 is increased more than 100-fold by heparin and heparin sulfate[6].

The result from in vivo observation showed that high levels of secreted FGF-1 upregulated apolipoprotein E (apoE) production in astrocytes of the brain injury lesion by autocrine mechanism[9]. Therefore, it was presumed that stress conditions (e.g., heat shock, oxidation, and long-term culture) trigger astrocytes to generate FGF-1 to induce the production of apoE-HDL (apolipoprotein E-high-density lipoproteins), an important compound for the healing process in the postinjury brain[9]. ApoE synthesis is triggered by FGF-1 via the PI3K/Akt (phosphoinositide

3-kinases/ protein kinase B) pathway rather than Ras/MEK/Erk (mitogen-activated protein kinase/ extracellular signal-regulated kinase) pathway [9].

Another study found that the level of FGF-1 in the cerebrospinal fluid and serum of thirty-two Alzheimer's patients were higher than those thirty-two patients without Alzheimer's disease (normal controls)[5]. Western blotting and enzyme-linked immunosorbent assay (ELISA) was carried out to measure the level of the FGF-1[5]. This study was based on the fact that FGF-1 is one of the most pivotal central nervous system (CNS) growth factors and a powerful mitogen[5]. Moreover, it was assumed that biochemical brain abnormalities could be manifested in cerebrospinal fluid (CSF) because of CSF proximity to the extracellular space of the brain [5]. It was found that FGF-1 plays an essential role in enhancing microglial and astrocyte-mediated neuroinflammation[10]. Neuroinflammation, the hallmark of Alzheimer's disease progression, can be a potential drug target in Alzheimer's drug development[10]. It can be pursued by blocking the expression and release of FGF-1 because inhibition of FGF-1 can prevent the expression of neuroinflammatory molecules[10].

It is imperative to conduct further research to unravel the roles of FGF-1 in AD, focusing on its potency to form amyloid-β confirmation to gain a detailed understanding of the pathological mechanism of the disease. A previous study indicates that FGF-1 plays a certain role in AD that can be a potential target therapy. Conducting in-vitro studies by using SDS as an amyloid fibril inducer of FGF-1 can be a preliminary step to understanding the significant role of FGF-1 in the pathophysiology of AD through the amyloid fibrils formation. Further development of in vitro studies into in vivo studies will broaden understandings towards this topic. Presumably, being able to simulate this process both in vitro and in vivo can aid future research

in exploring a new avenue of Alzheimer's drug development due to the nature of AD as a multifactorial neurodegenerative disorder.

CONCLUSIONS

The combined results of fluorescence spectroscopy, limited trypsin digestion, transmission electron microscope (TEM), and mass spectrometry from this study suggest that 0.2mM is the optimum concentration of SDS to induce amyloid-like fibrils formation in hFGF-1. The presence of SOS is found to protect hFGF-1 from fibrillation induced by SDS, reduce, and disaggregate fibrils formation in hFGF-1. Stabilization of the heparin-binding pocket renders the ability of hFGF-1 to protect and reduce the chance of amyloid fibrils formation induced by 0.2mM SDS.

FUTURE PERSPECTIVE

Based on the result of this research, we can develop a future study to engineer the heparin-binding pocket of hFGF-1 and comparing its stability. We found that *in vitro* condition, 0.2mM SDS can induce fibrils formation in hFGF-1. Moreover, we can examine the tendency of the hFGF-1 to form fibrils in physiological conditions by using lipid vesicle, designing molecules that have similar effects to SOS in stabilizing hFGF-1, and examining the toxicity of FGF-1 fibrils in the animal model.

REFERENCES

1. Invernizzi, G.; Papaleo, E.; Sabate, R.; Ventura, S., Protein aggregation: Mechanisms and functional consequences. *International Journal of Biochemistry & Cell Biology* **2012,** *44* (9), 1541-1554.
2. Chiti, F.; Dobson, C. M., Protein misfolding, functional amyloid, and human disease. In *Annual Review of Biochemistry*, Annual Reviews: Palo Alto, 2006; Vol. 75, pp 333-366.
3. Dobson, C. M., Protein folding and misfolding. *Nature* **2003,** *426* (6968), 884-890.
4. Panza, F.; Lozupone, M.; Logroscino, G.; Imbimbo, B. P., A critical appraisal of amyloid-beta targeting therapies for Alzheimer disease. *Nature Reviews Neurology* **2019,** *15* (2), 73-88.
5. Mashayekhi, F.; Hadavi, M.; Vaziri, H. R.; Naji, M., Increased acidic fibroblast growth factor concentrations in the serum and cerebrospinal fluid of patients with Alzheimer's disease. *Journal of Clinical Neuroscience* **2010,** *17* (3), 357-359.
6. Tooyama, I.; Akiyama, H.; McGeer, P. L.; Hara, Y.; Yasuhara, O.; Kimura, H., acidic Fibroblast growth factor-like immunoreactivity in brain of alzheimer patients. *Neuroscience Letters* **1991,** *121* (1-2), 155-158.
7. Wong, P.; Hampton, B.; Szylobryt, E.; Gallagher, A. M.; Jaye, M.; Burgess, W. H., Analysis of putative heparin-binding domains of fibroblast growth factor-1. Using site-directed mutagenesis and peptide analogues. *J Biol Chem* **1995,** *270* (43), 25805-11.
8. Pineda-Lucena, A.; Núñez De Castro, I.; Lozano, R. M.; Muñoz-Willery, I.; Zazo, M.; Giménez-Gallego, G., Effect of low pH and heparin on the structure of acidic fibroblast growth factor. *Eur J Biochem* **1994,** *222* (2), 425-31.
9. Ito, J.; Nagayasu, Y.; Lu, R.; Kheirollah, A.; Hayashi, M.; Yokoyama, S., Astrocytes produce and secrete FGF-1, which promotes the production of apoE-HDL in a manner of autocrine action. *Journal of Lipid Research* **2005,** *46* (4), 679-686.
10. Lee, M.; Kang, Y.; Suk, K.; Schwab, C.; Yu, S.; McGeer, P. L., Acidic Fibroblast Growth Factor (FGF) Potentiates Glial-mediated Neurotoxicity by Activating FGFR2 IIIb Protein. *Journal of Biological Chemistry* **2011,** *286* (48), 41230-41245.
11. Yeh, B. K.; Eliseenkova, A. V.; Plotnikov, A. N.; Green, D.; Pinnell, J.; Polat, T.; Gritli-Linde, A.; Linhardt, R. J.; Mohammadi, M., Structural basis for activation of fibroblast growth factor signaling by sucrose octasulfate. *Molecular and cellular biology* **2002,** *22* (20), 7184-7192.
12. Blaber, M.; DiSalvo, J.; Thomas, K. A., X-ray crystal structure of human acidic fibroblast growth factor. *Biochemistry* **1996,** *35* (7), 2086-94.
13. Braakman, I.; Hebert, D. N., Protein folding in the endoplasmic reticulum. *Cold Spring Harbor perspectives in biology* **2013,** *5* (5), a013201-a013201.
14. Ellis, R. J.; van der Vies, S. M., Molecular chaperones. *Annu Rev Biochem* **1991,** *60*, 321-47.

15. Wallis, K.; Freedman, R., Assisting Oxidative Protein Folding: How Do Protein Disulphide-Isomerases Couple Conformational and Chemical Processes in Protein Folding? *Topics in current chemistry* **2011,** *328*.

16. Braakman, I.; Bulleid, N. J., Protein Folding and Modification in the Mammalian Endoplasmic Reticulum. *Annual Review of Biochemistry* **2011,** *80* (1), 71-99.

17. Ballard, C.; Gauthier, S.; Corbett, A.; Brayne, C.; Aarsland, D.; Jones, E., Alzheimer's disease. *Lancet* **2011,** *377* (9770), 1019-1031.

18. Roberts, B. R.; Ryan, T. M.; Bush, A. I.; Masters, C. L.; Duce, J. A., The role of metallobiology and amyloid-ss peptides in Alzheimer's disease. *Journal of Neurochemistry* **2012,** *120*, 149-166.

19. Kumar, S.; Rezaei-Ghaleh, N.; Terwel, D.; Thal, D. R.; Richard, M.; Hoch, M.; Mc Donald, J. M.; Wullnner, U.; Glebov, K.; Heneka, M. T.; Walsh, D. M.; Zweckstetter, M.; Walter, J., Extracellular phosphorylation of the amyloid beta-peptide promotes formation of toxic aggregates during the pathogenesis of Alzheimer's disease. *Embo Journal* **2011,** *30* (11), 2255-2265.

20. Liu, B.; Moloney, A.; Meehan, S.; Morris, K.; Thomas, S. E.; Serpell, L. C.; Hider, R.; Marciniak, S. J.; Lomas, D. A.; Crowther, D. C., Iron Promotes the Toxicity of Amyloid beta Peptide by Impeding Its Ordered Aggregation. *Journal of Biological Chemistry* **2011,** *286* (6), 4248-4256.

21. Opazo, C.; Huang, X. D.; Cherny, R. A.; Moir, R. D.; Roher, A. E.; White, A. R.; Cappai, R.; Masters, C. L.; Tanzi, R. E.; Inestrosa, N. C.; Bush, A. I., Metalloenzyme-like activity of Alzheimer's disease beta-amyloid - Cu-dependent catalytic conversion of dopamine, cholesterol, and biological reducing agents to neurotoxic H2O2. *Journal of Biological Chemistry* **2002,** *277* (43), 40302-40308.

22. Greenwald, J.; Riek, R., Biology of Amyloid: Structure, Function, and Regulation. *Structure* **2010,** *18* (10), 1244-1260.

23. Salvatella, X., Structural aspects of amyloid formation. *Prog Mol Biol Transl Sci* **2013,** *117*, 73-101.

24. Bhak, G.; Choe, Y. J.; Paik, S. R., Mechanism of amyloidogenesis: nucleation-dependent fibrillation versus double-concerted fibrillation. *BMB Rep* **2009,** *42* (9), 541-51.

25. Chiti, F.; Dobson, C. M., Amyloid formation by globular proteins under native conditions. *Nature Chemical Biology* **2009,** *5* (1), 15-22.

26. Chandel, T. I.; Zaman, M.; Khan, M. V.; Ali, M.; Rabbani, G.; Ishtikhar, M.; Khan, R. H., A mechanistic insight into protein-ligand interaction, folding, misfolding, aggregation and inhibition of protein aggregates: An overview. *International Journal of Biological Macromolecules* **2018,** *106*, 1115-1129.

27. Giorgetti, S.; Greco, C.; Tortora, P.; Aprile, F. A., Targeting Amyloid Aggregation: An Overview of Strategies and Mechanisms. *International journal of molecular sciences* **2018,** *19* (9), 2677.

28. Stoilova, T.; Colombo, L.; Forloni, G.; Tagliavini, F.; Salmona, M., A New Face for Old Antibiotics: Tetracyclines in Treatment of Amyloidoses. *Journal of Medicinal Chemistry* **2013,** *56* (15), 5987-6006.

29. Perni, M.; Galvagnion, C.; Maltsev, A.; Meisl, G.; Müller, M. B. D.; Challa, P. K.; Kirkegaard, J. B.; Flagmeier, P.; Cohen, S. I. A.; Cascella, R.; Chen, S. W.; Limbocker, R.; Sormanni, P.; Heller, G. T.; Aprile, F. A.; Cremades, N.; Cecchi, C.; Chiti, F.; Nollen, E. A. A.; Knowles, T. P. J.; Vendruscolo, M.; Bax, A.; Zasloff, M.; Dobson, C. M., A natural product inhibits the initiation of α-synuclein aggregation and suppresses its toxicity. *Proceedings of the National Academy of Sciences of the United States of America* **2017,** *114* (6), E1009-E1017.

30. Perni, M.; Flagmeier, P.; Limbocker, R.; Cascella, R.; Aprile, F. A.; Galvagnion, C.; Heller, G. T.; Meisl, G.; Chen, S. W.; Kumita, J. R.; Challa, P. K.; Kirkegaard, J. B.; Cohen, S. I. A.; Mannini, B.; Barbut, D.; Nollen, E. A. A.; Cecchi, C.; Cremades, N.; Knowles, T. P. J.; Chiti, F.; Zasloff, M.; Vendruscolo, M.; Dobson, C. M., Multistep Inhibition of α-Synuclein Aggregation and Toxicity in Vitro and in Vivo by Trodusquemine. *ACS Chemical Biology* **2018,** *13* (8), 2308-2319.

31. Viet, M. H.; Ngo, S. T.; Lam, N. S.; Li, M. S., Inhibition of Aggregation of Amyloid Peptides by Beta-Sheet Breaker Peptides and Their Binding Affinity. *The Journal of Physical Chemistry B* **2011,** *115* (22), 7433-7446.

32. Soto, C.; Sigurdsson, E. M.; Morelli, L.; Asok Kumar, R.; Castaño, E. M.; Frangione, B., β-sheet breaker peptides inhibit fibrillogenesis in a rat brain model of amyloidosis: Implications for Alzheimer's therapy. *Nature Medicine* **1998,** *4* (7), 822-826.

33. Poduslo, J. F.; Curran, G. L.; Kumar, A.; Frangione, B.; Soto, C., Beta-sheet breaker peptide inhibitor of Alzheimer's amyloidogenesis with increased blood-brain barrier permeability and resistance to proteolytic degradation in plasma. *J Neurobiol* **1999,** *39* (3), 371-82.

34. Adessi, C.; Soto, C., Converting a peptide into a drug: strategies to improve stability and bioavailability. *Curr Med Chem* **2002,** *9* (9), 963-78.

35. Jha, A.; Kumar, M. G.; Gopi, H. N.; Paknikar, K. M., Inhibition of β-Amyloid Aggregation through a Designed β-Hairpin Peptide. *Langmuir* **2018,** *34* (4), 1591-1600.

36. Yang, J. E.; Rhoo, K. Y.; Lee, S.; Lee, J. T.; Park, J. H.; Bhak, G.; Paik, S. R., EGCG-mediated Protection of the Membrane Disruption and Cytotoxicity Caused by the 'Active Oligomer' of α-Synuclein. *Scientific Reports* **2017,** *7* (1), 17945.

37. Young, L. M.; Cao, P.; Raleigh, D. P.; Ashcroft, A. E.; Radford, S. E., Ion Mobility Spectrometry–Mass Spectrometry Defines the Oligomeric Intermediates in Amylin Amyloid Formation and the Mode of Action of Inhibitors. *Journal of the American Chemical Society* **2014,** *136* (2), 660-670.

38. Ehrnhoefer, D. E.; Bieschke, J.; Boeddrich, A.; Herbst, M.; Masino, L.; Lurz, R.; Engemann, S.; Pastore, A.; Wanker, E. E., EGCG redirects amyloidogenic polypeptides into unstructured, off-pathway oligomers. *Nature Structural & Molecular Biology* **2008,** *15* (6), 558-566.

39. Visentin, C.; Pellistri, F.; Natalello, A.; Vertemara, J.; Bonanomi, M.; Gatta, E.; Penco, A.; Relini, A.; De Gioia, L.; Airoldi, C.; Regonesi, M. E.; Tortora, P., Epigallocatechin-3-

gallate and related phenol compounds redirect the amyloidogenic aggregation pathway of ataxin-3 towards non-toxic aggregates and prevent toxicity in neural cells and Caenorhabditis elegans animal model. *Hum Mol Genet* **2017,** *26* (17), 3271-3284.

40. Mo, Y.; Lei, J.; Sun, Y.; Zhang, Q.; Wei, G., Conformational Ensemble of hIAPP Dimer: Insight into the Molecular Mechanism by which a Green Tea Extract inhibits hIAPP Aggregation. *Sci Rep* **2016,** *6*, 33076.

41. Jia, Y.; Liu, Z.; Huo, X.; Wang, C.; Meng, Q.; Liu, Q.; Sun, H.; Sun, P.; Yang, X.; Shu, X.; Liu, K., Enhancement effect of resveratrol on the intestinal absorption of bestatin by regulating PEPT1, MDR1 and MRP2 in vivo and in vitro. *Int J Pharm* **2015,** *495* (1), 588-598.

42. Rane, J. S.; Bhaumik, P.; Panda, D., Curcumin Inhibits Tau Aggregation and Disintegrates Preformed Tau Filaments in vitro. *J Alzheimers Dis* **2017,** *60* (3), 999-1014.

43. Yang, F.; Lim, G.; Begum, A.; Ubeda, O.; Simmons, M.; Ambegaokar, S.; Chen, P.; Kayed, R.; Glabe, C.; Frautschy, S.; Cole, G., Curcumin Inhibits Formation of Amyloid Oligomers and Fibrils, Binds Plaques, and Reduces Amyloid in Vivo. *The Journal of biological chemistry* **2005,** *280*, 5892-901.

44. Thapa, A.; Jett, S. D.; Chi, E. Y., Curcumin Attenuates Amyloid-β Aggregate Toxicity and Modulates Amyloid-β Aggregation Pathway. *ACS Chemical Neuroscience* **2016,** *7* (1), 56-68.

45. Ahsan, N.; Mishra, S.; Jain, M. K.; Surolia, A.; Gupta, S., Curcumin Pyrazole and its derivative (N-(3-Nitrophenylpyrazole) Curcumin inhibit aggregation, disrupt fibrils and modulate toxicity of Wild type and Mutant α-Synuclein. *Scientific Reports* **2015,** *5* (1), 9862.

46. Debnath, K.; Pradhan, N.; Singh, B. K.; Jana, N. R., Poly(trehalose) Nanoparticles Prevent Amyloid Aggregation and Suppress Polyglutamine Aggregation in a Huntington's Disease Model Mouse. *ACS Appl Mater Interfaces* **2017,** *9* (28), 24126-24139.

47. Hsieh, S.; Chang, C. W.; Chou, H. H., Gold nanoparticles as amyloid-like fibrillogenesis inhibitors. *Colloids Surf B Biointerfaces* **2013,** *112*, 525-9.

48. Liao, Y. H.; Chang, Y. J.; Yoshiike, Y.; Chang, Y. C.; Chen, Y. R., Negatively charged gold nanoparticles inhibit Alzheimer's amyloid-β fibrillization, induce fibril dissociation, and mitigate neurotoxicity. *Small* **2012,** *8* (23), 3631-9.

49. Wang, M.; Kakinen, A.; Pilkington, E. H.; Davis, T. P.; Ke, P. C., Differential effects of silver and iron oxide nanoparticles on IAPP amyloid aggregation. *Biomater Sci* **2017,** *5* (3), 485-493.

50. Yun, Y. R.; Won, J. E.; Jeon, E.; Lee, S.; Kang, W.; Jo, H.; Jang, J. H.; Shin, U. S.; Kim, H. W., Fibroblast growth factors: biology, function, and application for tissue regeneration. *J Tissue Eng* **2010,** *2010*, 218142.

51. Turner, N.; Grose, R., Fibroblast growth factor signalling: from development to cancer. *Nature Reviews Cancer* **2010,** *10* (2), 116-129.

52. Itoh, N., The Fgf families in humans, mice, and zebrafish: Their evolutional processes and roles in development, metabolism, and disease. *Biological & Pharmaceutical Bulletin* **2007,** *30* (10), 1819-1825.

53. Eswarakumar, V. P.; Lax, I.; Schlessinger, J., Cellular signaling by fibroblast growth factor receptors. *Cytokine Growth Factor Rev* **2005,** *16* (2), 139-49.

54. Edward Conrad, H., Chapter 9 - Fibroblast Growth Factors. In *Heparin-Binding Proteins*, Edward Conrad, H., Ed. Academic Press: San Diego, 1998; pp 301-III.

55. Bradshaw, R. A.; Dennis, E. A., Chapter 1 - Cell Signaling: Yesterday, Today, and Tomorrow. In *Handbook of Cell Signaling (Second Edition)*, Bradshaw, R. A.; Dennis, E. A., Eds. Academic Press: San Diego, 2010; pp 1-4.

56. Ornitz, D. M.; Xu, J.; Colvin, J. S.; McEwen, D. G.; MacArthur, C. A.; Coulier, F.; Gao, G.; Goldfarb, M., Receptor specificity of the fibroblast growth factor family. *J Biol Chem* **1996,** *271* (25), 15292-7.

57. Zhang, X.; Ibrahimi, O. A.; Olsen, S. K.; Umemori, H.; Mohammadi, M.; Ornitz, D. M., Receptor specificity of the fibroblast growth factor family. The complete mammalian FGF family. *J Biol Chem* **2006,** *281* (23), 15694-700.

58. Beenken, A.; Eliseenkova, A. V.; Ibrahimi, O. A.; Olsen, S. K.; Mohammadi, M., Plasticity in interactions of fibroblast growth factor 1 (FGF-1) N terminus with FGF receptors underlies promiscuity of FGF-1. *J Biol Chem* **2012,** *287* (5), 3067-78.

59. Murzin, A. G.; Lesk, A. M.; Chothia, C., beta-Trefoil fold. Patterns of structure and sequence in the Kunitz inhibitors interleukins-1 beta and 1 alpha and fibroblast growth factors. *J Mol Biol* **1992,** *223* (2), 531-43.

60. McLachlan, A. D., Three-fold structural pattern in the soybean trypsin inhibitor (Kunitz). *J Mol Biol* **1979,** *133* (4), 557-63.

61. Angalakurthi, S. K.; Tenorio, C. A.; Blaber, M.; Middaugh, C. R., Investigating the dynamics and polyanion binding sites of fibroblast growth factor-1 using hydrogen-deuterium exchange mass spectrometry. *Protein Sci* **2018,** *27* (6), 1068-1082.

62. Canales, A.; Lozano, R.; López-Méndez, B.; Angulo, J.; Ojeda, R.; Nieto, P. M.; Martín-Lomas, M.; Giménez-Gallego, G.; Jiménez-Barbero, J., Solution NMR structure of a human FGF-1 monomer, activated by a hexasaccharide heparin-analogue. *Febs j* **2006,** *273* (20), 4716-27.

63. Volkin, D. B.; Tsai, P. K.; Dabora, J. M.; Gress, J. O.; Burke, C. J.; Linhardt, R. J.; Middaugh, C. R., Physical stabilization of acidic fibroblast growth factor by polyanions. *Arch Biochem Biophys* **1993,** *300* (1), 30-41.

64. Pellegrini, L.; Burke, D. F.; von Delft, F.; Mulloy, B.; Blundell, T. L., Crystal structure of fibroblast growth factor receptor ectodomain bound to ligand and heparin. *Nature* **2000,** *407* (6807), 1029-1034.

65. DiGabriele, A. D.; Lax, I.; Chen, D. I.; Svahn, C. M.; Jaye, M.; Schlessinger, J.; Hendrickson, W. A., Structure of a heparin-linked biologically active dimer of fibroblast growth factor. *Nature* **1998,** *393* (6687), 812-817.

66. Raman, R.; Venkataraman, G.; Ernst, S.; Sasisekharan, V.; Sasisekharan, R., Structural specificity of heparin binding in the fibroblast growth factor family of proteins. *Proc Natl Acad Sci U S A* **2003,** *100* (5), 2357-62.

67. Zhu, X.; Hsu, B. T.; Rees, D. C., Structural studies of the binding of the anti-ulcer drug sucrose octasulfate to acidic fibroblast growth factor. *Structure* **1993,** *1* (1), 27-34.

68. Correia, J. J.; Detrich, H. W., Preface. In *Methods in Cell Biology*, Academic Press: 2008; Vol. 84, pp XIX-XXII.

69. Rodger, A., Far UV Protein Circular Dichroism. In *Encyclopedia of Biophysics*, Roberts, G. C. K., Ed. Springer Berlin Heidelberg: Berlin, Heidelberg, 2013; pp 726-730.

70. Sauer, M.; Hofkens, J.; Enderlein, J., Handbook of Fluorescence Spectroscopy and Imaging: From Single Molecules to Ensembles. *Handbook of Fluorescence Spectroscopy and Imaging: From Single Molecules to Ensembles* **2011**.

71. Shanker, N.; Bane, S. L., Basic Aspects of Absorption and Fluorescence Spectroscopy and Resonance Energy Transfer Methods. In *Methods in Cell Biology*, Academic Press: 2008; Vol. 84, pp 213-242.

72. Hawe, A.; Sutter, M.; Jiskoot, W., Extrinsic fluorescent dyes as tools for protein characterization. *Pharmaceutical research* **2008,** *25* (7), 1487-1499.

73. Ladokhin, A., Fluorescence Spectroscopy in Peptide and Protein Analysis. 2006.

74. Biancalana, M.; Koide, S., Molecular mechanism of Thioflavin-T binding to amyloid fibrils. *Biochimica et biophysica acta* **2010,** *1804* (7), 1405-1412.

75. Alsenaidy, M. A.; Wang, T. T.; Kim, J. H.; Joshi, S. B.; Lee, J.; Blaber, M.; Volkin, D. B.; Middaugh, C. R., An empirical phase diagram approach to investigate conformational stability of "second-generation" functional mutants of acidic fibroblast growth factor-1. *Protein Science* **2012,** *21* (3), 418-432.

76. Xia, X.; Kumru, O. S.; Blaber, S. I.; Middaugh, C. R.; Li, L.; Ornitz, D. M.; Sutherland, M. A.; Tenorio, C. A.; Blaber, M., Engineering a Cysteine-Free Form of Human Fibroblast Growth Factor-1 for "Second Generation" Therapeutic Application. *Journal of Pharmaceutical Sciences* **2016,** *105* (4), 1444-1453.

77. Copeland, R. A.; Ji, H.; Halfpenny, A. J.; Williams, R. W.; Thompson, K. C.; Herber, W. K.; Thomas, K. A.; Bruner, M. W.; Ryan, J. A.; Marquis-Omer, D.; et al., The structure of human acidic fibroblast growth factor and its interaction with heparin. *Arch Biochem Biophys* **1991,** *289* (1), 53-61.

78. Srisailam, S.; Kumar, T. K. S.; Rajalingam, D.; Kathir, K. M.; Sheu, H. S.; Jan, F. J.; Chao, P. C.; Yu, C., Amyloid-like Fibril Formation in an All -Barrel Protein: PARTIALLY STRUCTURED INTERMEDIATE STATE(S) IS A PRECURSOR FOR FIBRIL FORMATION. **2003,** *278* (20), 17701-17709.

79. Arunkumar, A. I.; Kumar, T. K. S.; Kathir, K. M.; Srisailam, S.; Wang, H.-M.; Leena, P. S. T.; Chi, Y.-H.; Chen, H.-C.; Wu, C.-H.; Wu, R.-T.; Chang, G.-G.; Chiu, I.-M.; Yu, C., Oligomerization of acidic fibroblast growth factor is not a prerequisite for its cell proliferation activity. *Protein science : a publication of the Protein Society* **2002,** *11* (5), 1050-1061.

80. Srisailam, S.; Kumar, T. K.; Rajalingam, D.; Kathir, K. M.; Sheu, H. S.; Jan, F. J.; Chao, P. C.; Yu, C., Amyloid-like fibril formation in an all beta-barrel protein. Partially structured

intermediate state(s) is a precursor for fibril formation. *J Biol Chem* **2003,** *278* (20), 17701-9.

81. An, T.-T.; Feng, S.; Zeng, C.-M., Oxidized epigallocatechin gallate inhibited lysozyme fibrillation more strongly than the native form. *Redox Biology* **2017,** *11*, 315-321.
82. Kheterpal, I.; Williams, A.; Murphy, C.; Bledsoe, B.; Wetzel, R., Structural Features of the Aβ Amyloid Fibril Elucidated by Limited Proteolysis†. *Biochemistry* **2001,** *40* (39), 11757-11767.
83. Samuel, D.; Kumar, T. K.; Srimathi, T.; Hsieh, H.; Yu, C., Identification and characterization of an equilibrium intermediate in the unfolding pathway of an all beta-barrel protein. *J Biol Chem* **2000,** *275* (45), 34968-75.
84. Fontana, A.; de Laureto, P. P.; Spolaore, B.; Frare, E.; Picotti, P.; Zambonin, M., Probing protein structure by limited proteolysis. *Acta biochimica Polonica* **2004,** *51* (2), 299-321.
85. Hu, J.; Zheng, Q., Applications of Mass Spectrometry in the Onset of Amyloid Fibril Formation: Focus on the Analysis of Early-Stage Oligomers. *Frontiers in Chemistry* **2020,** *8*, 324.
86. Bergquist, J.; Andersen, O.; Westman, A., Rapid method to characterize mutations in transthyretin in cerebrospinal fluid from familial amyloidotic polyneuropathy patients by use of matrix-assisted laser desorption/ionization time-of-flight mass spectrometry. *Clin Chem* **2000,** *46* (9), 1293-300.
87. Culajay, J. F.; Blaber, S. I.; Khurana, A.; Blaber, M., Thermodynamic Characterization of Mutants of Human Fibroblast Growth Factor 1 with an Increased Physiological Half-Life †. **2000,** *39* (24), 7153-7158.
88. Hubbard, S. J., The structural aspects of limited proteolysis of native proteins. *Biochim Biophys Acta* **1998,** *1382* (2), 191-206.
89. Buczek, O.; Krowarsch, D.; Otlewski, J., Thermodynamics of single peptide bond cleavage in bovine pancreatic trypsin inhibitor (BPTI). *Protein science : a publication of the Protein Society* **2002,** *11* (4), 924-932.
90. Yamamoto, S.; Hasegawa, K.; Yamaguchi, I.; Tsutsumi, S.; Kardos, J.; Goto, Y.; Gejyo, F.; Naiki, H., Low Concentrations of Sodium Dodecyl Sulfate Induce the Extension of β2-Microglobulin-Related Amyloid Fibrils at a Neutral pH. *Biochemistry* **2004,** *43* (34), 11075-11082.
91. Andreola, A.; Bellotti, V.; Giorgetti, S.; Mangione, P. P.; Obici, L.; Stoppini, M.; Torres, J.; Monzani, E.; Merlini, G.; Sunde, M., Conformational Switching and Fibrillogenesis in the Amyloidogenic Fragment of Apolipoprotein A-I. *The Journal of biological chemistry* **2003,** *278*, 2444-51.
92. Morillas, M.; Swietnicki, W.; Gambetti, P.; Surewicz, W. K., Membrane environment alters the conformational structure of the recombinant human prion protein. *J Biol Chem* **1999,** *274* (52), 36859-65.
93. Ji, S.-R.; wu, y.; Sui, S.-f., Cholesterol Is an Important Factor Affecting the Membrane Insertion of -Amyloid Peptide (A 1-40), Which May Potentially Inhibit the Fibril Formation. *The Journal of biological chemistry* **2002,** *277*, 6273-9.

94. Gelamo, E. L.; Silva, C. H.; Imasato, H.; Tabak, M., Interaction of bovine (BSA) and human (HSA) serum albumins with ionic surfactants: spectroscopy and modelling. *Biochim Biophys Acta* **2002,** *1594* (1), 84-99.

95. Hagihara, Y.; Hong, D. P.; Hoshino, M.; Enjyoji, K.; Kato, H.; Goto, Y., Aggregation of beta(2)-glycoprotein I induced by sodium lauryl sulfate and lysophospholipids. *Biochemistry* **2002,** *41* (3), 1020-6.

96. Pertinhez, T. A.; Bouchard, M.; Smith, R. A. G.; Dobson, C. M.; Smith, L. J., Stimulation and inhibition of fibril formation by a peptide in the presence of different concentrations of SDS. *Febs Letters* **2002,** *529* (2-3), 193-197.

97. Giehm, L.; Oliveira, C. L. P.; Christiansen, G.; Pedersen, J. S.; Otzen, D. E., SDS-Induced Fibrillation of α-Synuclein: An Alternative Fibrillation Pathway. *Journal of Molecular Biology* **2010,** *401* (1), 115-133.

98. Rangachari, V.; Reed, D. K.; Moore, B. D.; Rosenberry, T. L., Secondary Structure and Interfacial Aggregation of Amyloid-β(1−40) on Sodium Dodecyl Sulfate Micelles. *Biochemistry* **2006,** *45* (28), 8639-8648.

99. Movaghati, S.; Moosavi-Movahedi, A. A.; Khodagholi, F.; Digaleh, H.; Kachooei, E.; Sheibani, N., Sodium dodecyl sulphate modulates the fibrillation of human serum albumin in a dose-dependent manner and impacts the PC12 cells retraction. *Colloids Surf B Biointerfaces* **2014,** *122*, 341-349.

100. Bhuyan, A. K., On the mechanism of SDS-induced protein denaturation. *Biopolymers* **2010,** *93* (2), 186-199.

101. Mammi, S.; Peggion, E., Conformational studies of human [15-2-aminohexanoic acid]little gastrin in sodium dodecyl sulfate micelles by 1H NMR. *Biochemistry* **1990,** *29* (22), 5265-9.

102. Rizo, J.; Blanco, F. J.; Kobe, B.; Bruch, M. D.; Gierasch, L. M., Conformational behavior of Escherichia coli OmpA signal peptides in membrane mimetic environments. *Biochemistry* **1993,** *32* (18), 4881-94.

103. Zhong, L.; Johnson, W. C., Jr., Environment affects amino acid preference for secondary structure. *Proc Natl Acad Sci U S A* **1992,** *89* (10), 4462-5.

104. Waterhous, D. V.; Johnson, W. C., Jr., Importance of environment in determining secondary structure in proteins. *Biochemistry* **1994,** *33* (8), 2121-8.

105. Khan, J. M.; Qadeer, A.; Chaturvedi, S. K.; Ahmad, E.; Rehman, S. A. A.; Gourinath, S.; Khan, R. H., SDS can be utilized as an amyloid inducer: a case study on diverse proteins. *PloS one* **2012,** *7* (1), e29694-e29694.

106. Srisailam, S.; Wang, H.-M.; Kumar, T. K. S.; Rajalingam, D.; Sivaraja, V.; Sheu, H.-S.; Chang, Y.-C.; Yu, C., Amyloid-like Fibril Formation in an All β-Barrel Protein Involves the Formation of Partially Structured Intermediate(s). *Journal of Biological Chemistry* **2002,** *277* (21), 19027-19036.

107. Walters, J.; Milam, S. L.; Clark, A. C., Chapter 1 Practical Approaches to Protein Folding and Assembly. Elsevier: 2009; pp 1-39.